Electronic Motion in Molecular Systems: From the Hydrogen Molecular Ion to Nanostructures

Inaugural-Dissertation

to obtain the academic degree
Doctor rerum naturalium (Dr. rer. nat.)

submitted to
the Department of Biology, Chemistry and Pharmacy
of Freie Universität Berlin

by

Vincent Pohl

from Eisenhüttenstadt

2017

This work was prepared under supervision of

Jean Christophe Tremblay, Ph.D. (Freie Universität Berlin)

from

October 2013 until September 2017

1st Reviewer	Jean Christophe Tremblay, Ph.D.
2nd Reviewer	Prof. Dr. Beate Paulus
Date of Defense	November 1st, 2017

Abstract

The analysis and visualization of electron dynamics in molecular systems represents an effective means to gain deeper understanding of various physical and chemical processes. For this purpose, this theoretical-chemical dissertation aims at the development of general analysis tools (DETCI@ORBKIT) and new theoretical methods ("Born-Oppenheimer Broken Symmetry" ansatz), focusing on the different components of the electronic continuity equation. This fundamental relation connects the electron density with the electronic flux density, or electronic current density. While the former is a scalar field, which defines the probability distribution of the electrons, the latter is a vector field describing the instantaneous and spatially resolved flow of electrons. The robustness and scalability of the developed methodological framework is first benchmarked, before it is subsequently applied to various fields.

In chemistry, curved arrows are drawn at Lewis structures to symbolize the electron movement during chemical reactions. In the first application, this simple model is elucidated by means of quantum dynamics exemplary for the benzene molecule. For this purpose, different localized electronic superposition states are prepared by laser excitation initiating charge migration in the attosecond time regime. The analysis of the time evolution of the electron density reveals that, in the investigated cases, the electrons follow a pincer-type mechanism and that, in contrast to the predictions by the simple traditional model, a very small number of electrons is transported. Interestingly, the laser preparation phase is observed to play an important role in the patterns of charge migration.

The last part of this dissertation is devoted to electron dynamics in a graphene-based molecular nanojunction. By applying dissipative quantum dynamics, it is demonstrated that this nanostructure can be reliably switched by a static electric field in the spirit of a traditional field effect transistor. The subsequent investigation of the electronic flux density for both conformers yields an intuitive picture of the charge migration mechanism and reveals a possible route to optimize the structure of the nanojunction.

The main conclusions of my doctoral studies can be summarized as follows: While the analysis of the electron density allows quantitative statements about reaction mechanisms, the electronic flux density gives a direct and intuitive insight into the exact course of chemical reactions. The gained dynamical information not only significantly contributes to the understanding of chemical mechanisms, but can also help to optimize the functionality of the devices under investigation.

Kurzzusammenfassung

Die Analyse und Visualisierung von Elektronendynamik in molekularen Systemen stellt ein effektives Mittel dar, um ein tiefer gehendes Verständnis über verschiedenste physikalische und chemische Prozesse zu gewinnen. Um dies zu ermöglichen, werden in dieser theoretisch-chemischen Doktorarbeit allgemeine Analysewerkzeuge (DETCI@ORBKIT) und neue theoretische Methoden („Born-Oppenheimer Broken Symmetry“ Ansatz) erarbeitet. Dabei wird der Schwerpunkt auf die verschiedenen Komponenten der elektronischen Kontinuitätsgleichung gelegt. Diese fundamentale Gleichung verbindet das Skalarfeld der Elektronendichte, die die Aufenthaltswahrscheinlichkeit der Elektronen definiert, mit dem Vektorfeld der Elektronenflussdichte oder Elektronenstromdichte, welche den instantanen und ortsaufgelösten Elektronenfluss beschreibt. Der entwickelte methodische Rahmen wird zunächst auf seine Robustheit und Skalierbarkeit hin untersucht, bevor er anschließend produktiv in verschiedenen Bereichen eingesetzt wird.

In der Chemie werden gebogenen Pfeile an Lewisstrukturen skizziert, um die Elektronenbewegung während chemischer Reaktionen zu symbolisieren. Im ersten Anwendungsbereich wird dieses einfache Modell mit quantendynamischen Mitteln am Beispiel des Benzolmoleküls näher beleuchtet. Mittels Laseranregung werden hierfür zunächst verschiedene lokalisierte elektronische Superpositionszustände erzeugt, was jeweils eine Ladungsmigration im Attosekundenbereich zur Folge hat. Analysen der Dynamik der Elektronendichte verdeutlichen, dass die Elektronen in den untersuchten Fällen einem zangenartigen Mechanismus folgen und dass wesentlich weniger Elektronen fließen als durch das einfache Modell vorhergesagt. Interessanterweise, wird beobachtet, dass die Laserpräparationsphase einen großen Einfluss auf die Flussmuster während der Ladungsmigration haben kann.

Der letzte Teil dieser Dissertation widmet sich der Elektronendynamik in einem graphenbasierten molekularen Nanoschalter. Zunächst wird mittels dissipativer Quantendynamik demonstriert, dass die Nanostruktur ähnlich eines traditionellen Feldeffekttransistors durch ein statisches elektrisches Feld zuverlässig geschaltet werden kann. Die nachfolgende Untersuchung der Elektronenflussdichte in beiden Konformeren zeigt anschaulich den Ladungsmigrationsmechanismus und offenbart einen möglichen Optimierungsweg hinsichtlich der Struktur des Nanoschalters.

Die Hauptaussagen meines Promotionsstudiums lassen sich folgendermaßen zusammenfassen: Während die Analyse der Elektronendichte quantitative Aussagen über Reaktionsmechanismen erlaubt, gibt die Elektronenflussdichte einen direkten und intuitiven Einblick in deren genaue Abläufe. Die gewonnenen dynamischen Informationen tragen nicht nur signifikant zum Verständnis der Mechanismen bei, sondern können auch dabei helfen die Funktionalität der untersuchten Geräte zu optimieren.

Contents

List of Publications

Charge Migration

Paper A1 G. Hermann, C. Liu, J. Manz, B. Paulus, J. F. Pérez-Torres, V. Pohl, and J. C. Tremblay
"Multidirectional Angular Electronic Flux during Adiabatic Attosecond Charge Migration in Excited Benzene"
J. Phys. Chem. A **120**, 5360–5369 (2016)
DOI: 10.1021/acs.jpca.6b01948

Paper A2 G. Hermann, C. Liu, J. Manz, B. Paulus, V. Pohl, and J. C. Tremblay
"Attosecond Angular Flux of Partial Charges on the Carbon Atoms of Benzene in Non-Aromatic Excited State"
Chem. Phys. Lett. **683**, 553–558 (2017)
DOI: 10.1016/j.cplett.2017.01.030

Paper A3 D. Jia, J. Manz, B. Paulus, V. Pohl, J. C. Tremblay, and Y. Yang
"Quantum Control of Electronic Fluxes during Adiabatic Attosecond Charge Migration in Degenerate Superposition States of Benzene"
Chem. Phys. **482**, 146–159 (2017)
DOI: 10.1016/j.chemphys.2016.09.021

Electronic Flux Density

Paper B1 V. Pohl, G. Hermann, and J. C. Tremblay
"An Open-Source Framework for Analyzing N-Electron Dynamics. I. Multideterminantal Wave Functions"
J. Comput. Chem. **38**, 1515–1527 (2017)
DOI: 10.1002/jcc.24792

Paper B2 G. Hermann, V. Pohl, and J. C. Tremblay

"An Open-Source Framework for Analyzing N-Electron Dynamics. II. Hybrid Density Functional Theory/Configuration Interaction Methodology"

J. Comput. Chem. **38**, 2378–2387 (2017)

DOI: 10.1002/jcc.24896

Paper B3 V. Pohl and J. C. Tremblay

"Adiabatic Electronic Flux Density: A Born-Oppenheimer Broken-Symmetry Ansatz"

Phys. Rev. A **93**, 012504 (2016)

DOI: 10.1103/PhysRevA.93.012504

Electron Dynamics in Nanojunctions

Paper C1 V. Pohl and J. C. Tremblay

"Field-Induced Conformational Change in a Single-Molecule-Graphene–Nanoribbon Junction: Effect of Vibrational Energy Redistribution"

J. Phys. Chem. C **120**, 28808–28819 (2016)

DOI: 10.1021/acs.jpcc.6b09682

Paper C2 V. Pohl, L. E. Marsoner Steinkasserer, and J. C. Tremblay

"Electronic Flux Density Maps Reveal Unique Current Patterns in a Single-Molecule-Graphene–Nanoribbon Junction"

arXiv preprint arXiv:1707.07635 (2017)

Additional Publications

Paper D1 G. Hermann, B. Paulus, J. F. Pérez-Torres, and V. Pohl

"Electronic and Nuclear Flux Densities in the H_2 Molecule"

Phys. Rev. A **89**, 052504 (2014)

DOI: 10.1103/physreva.89.052504

Paper D2 G. Hermann, V. Pohl, J. C. Tremblay, B. Paulus, H.-C. Hege, and A. Schild

"ORBKIT: A Modular Python Toolbox for Cross-Platform Postprocessing of Quantum Chemical Wavefunction Data"

J. Comput. Chem. **37**, 1511–1520 (2016)

DOI: 10.1002/jcc.24358

Chapter 1

Introduction

Electronic motion is ubiquitous in all areas of chemistry. The spectrum ranges from electrons, which are rearranged during simple chemical reactions, to electrons that are driven through molecular nano-junctions by chemical potentials. Understanding these transport processes can represent a keystone not only for the development of novel materials and molecular devices, but also for shedding light on the mechanisms of chemical reactions.

As an illustrative example, consider the curved arrows drawn at the Lewis structures of the reactants in chemical equations (see for example organic chemistry textbooks such as Refs. [1–4]). These arrows, which are familiar to every chemist, are usually intended to symbolize the motion of one or two valence electrons from one bond to another during a chemical reaction. But is there a relation between this very simplified picture and the actual electronic motion? Furthermore, if this is the case, how many electrons are transferred during this process?

The benzene molecule is predestined as a simple model system to study these questions. The six delocalized π-electrons of this highly symmetric molecule can be localized to resemble the typically sketched non-aromatic Kekulé structures (see Fig. 1.1a), and this initiates a charge migration process, where the electrons migrate from one Kekulé structure to the other. The localization of an oriented[5–11] benzene molecule can be achieved either by exciting the so-called Kekulé vibrational mode in the electronic ground state, as shown by Schild et al.,[12] or by an electronic excitation to a non-aromatic superposition state, as demonstrated by Ulusoy and Nest.[13] The ensuing charge carrier dynamics is either mediated by nuclear or electronic motion, respectively. To differentiate both phenomena, the former is commonly referred to as charge transfer, while the latter, usually much faster process is called charge migration.[14]

Regarding the first scenario, Schild et al.[12] were able to show that only 0.2 electrons are transferred

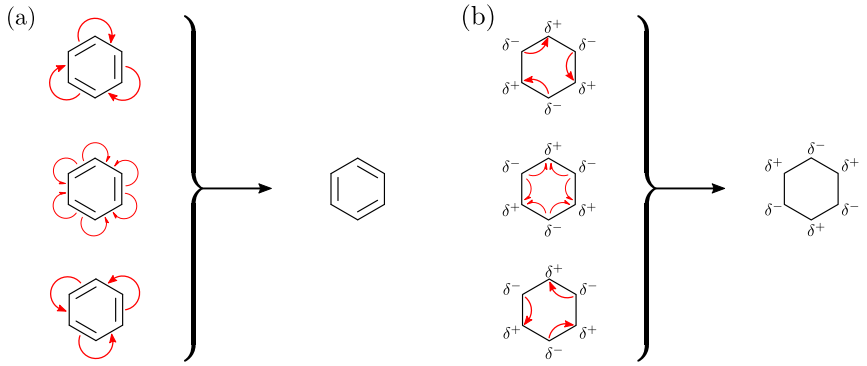

Figure 1.1: Lewis structures of the two non-aromatic superposition states of the benzene molecule investigated by Ulusoy and Nest.[13] (a) The partial localization of the electron density resembles the typically sketched Kekulé structures. (b) Negative and positive partial charges are found on alternating carbon atoms. The red arrows show the possible charge migration mechanisms: clockwise, pincer-type, or anti-clockwise motion (from top to down). In the simple traditional model, the harpoons (central rows) symbolize the motion of one and the arrows (upper and lower rows) correspond to the motion of two electrons. Thus, in this model, all six electrons participate in both scenario. The depictions are inspired from Refs. [13, 16].

during the femtosecond vibrational dynamics. This small fraction stands in stark contrast to the six electrons hypothesized by the simple traditional model sketched in Fig. 1.1a. Concerning the mechanism, they could show that, as expected, the π-electrons follow the nuclei. Note that this approach to charge transfer processes has been applied to several similar systems (cf. Refs. [15–18]) with comparable outcomes.

Concerning the second scenario, charge migration processes in general attracted great amounts of experimental and theoretical interest in the recent years. The phenomenon has been first discussed purely hypothetically in 1944 by Eyring, Walter, and Kimball in their Quantum Chemistry textbook.[19] The first experimental evidences were found by Weinkauf and Schlag et al.[20–23] The subsequent theoretical development was pioneered by Levine and Remacle et al.,[24–26] Cederbaum et al.,[27–33] Bandrauk et al.,[34–36] Fujimura, Kono and Lin et al.,[37–39] and other groups.[40–44] Recent developments in attosecond laser technology, which allow to indirectly monitor electron dynamics on its natural timescale,[45–55] have enabled the first experimental observation and control of the attosecond charge migration in ionized iodoacetylene.[56]

The charge migration involving a non-aromatic electronic superposition state in the benzene molecule (second scenario) was first studied by Ulusoy and Nest.[13] They modeled a sequence of laser pulses in order to prepare a superposition state of the electronic ground and the first excited state. After its preparation, the system undergoes a Rabi-type electronic charge migration between the two Kekulé structures in the attosecond time domain. As sketched in Fig. 1.1a, the charge migration could either proceed clockwise, anti-clockwise, or via a pincer-type motion. The latter is the one proposed in Ref. [13]. **Paper A1** is supposed to validate this assumption by modeling this process in real space

and real time. The number of electrons participating in this charge migration process is quantified by applying methods originally derived for concerted electronic and nuclear fluxes during coherent tunneling (see Ref. [18]). **Paper A2** focuses on an equivalent analysis for another non-aromatic electronic superposition state considered in Ref. [13]. This specific superposition state generates negative and positive partial charges on alternating carbon atoms as sketched in Fig. 1.1b. Here, no mechanism was proposed so far.

Even the simple benzene model system offers very rich possibilities to initiate charge migration. In **Paper A3**, this is used to investigate the possibility of quantum control of the charge migration mechanism in degenerate superposition states of benzene. By varying exclusively the polarization of the laser field, different degenerate superposition states of benzene are excited and the effect on the charge migration mechanism is investigated.

The studies in the **Papers A1–A3** focus on the analysis of the dynamics of the electronic probability density and derived quantities. Although this is a powerful procedure allowing for quantitative statements, it requires an intricate analysis to unravel mechanistic details. However, if the probability density is interpreted as a probability fluid, another very insightful, complementary quantity can be derived: the electronic probability flux density, or local electronic current density. This quantity describes the spatially resolved instantaneous flow of electrons and allows for a very intuitive interpretation of the mechanisms of charge migration at a single glance. Although the electronic flux density can be derived straightforwardly for a general multi-determinantal wave packet, to the best of our knowledge no post-processing program is capable of computing it. In **Paper B1**, we derive the required formulas and develop detCI@ORBKIT — an open-source framework to analyze and visualize N-electron dynamics. This computational project follows the open-source molecular modeling philosophy[57] and is an extension to ORBKIT,[D2] our recently published open-source Python library for post-processing single-determinantal wave function data from output files of quantum chemistry programs. The new program detCI@ORBKIT extends this functionality to multi-determinantal configuration interaction wave functions and allows for the computation of expectation values of several one-electron operators. Besides the implementation details, **Paper B1** focuses on the robustness and convergence properties of the electronic flux density with respect to the quantum chemical level of theory and the basis set. As the system size increases, the computational effort of high-level quantum chemistry calculations rapidly becomes prohibitively large. Therefore, **Paper B2** supplements the framework of detCI@ORBKIT with a hybrid density functional theory/configuration interaction methodology. The quality and scalability of this novel non-variational hybrid approach is studied for the quantum dynamics in two exemplary scenarios: a state selective excitation of a diatomic molecule and a broadband excitation of

a medium-sized organic dye.

Consider charge transfer processes in the electronic ground state, i.e., electron dynamics driven by nuclear vibrational dynamics. If an attempt is made to compute the electronic flux density for this scenario, it vanishes as soon as the clamped nuclei approximation is applied. This approximation lays the foundation to the Born-Oppenheimer approximation, which is the cornerstone of modern quantum chemistry. Since avoiding the use of the Born-Oppenheimer approximation is only computationally tractable for very small systems, e.g., H_2^+,[58–63] H_2,[64–67] and H_2D^+,[68,69] approximations become inevitable. A few approaches with various drawbacks have been proposed to overcome this problem. The semi-classical coupled channels theory[70–72, D1] and its generalization[73] by Diestler and coworkers correlates the gross atomic density with the nuclear flux density and thereby constrains the electronic flux density to strictly follow the nuclear motion. The so-called time-shift flux of Okuyama and Takatsuka[74] introduces a time delay into the wave function yielding a non-vanishing but complex-valued electronic flux density. The ansatz to reduce the complete Schrödinger equation as proposed by Manz et al.[18] is only capable of providing information about a single component of the flux density in the average field of the others. Besides, different perturbative approaches have been proposed involving the influence of electronically excited states,[75–78] but those depart from the Born-Oppenheimer picture. In **Paper B3**, we pursue another strategy to obtain the electronic flux density within the framework of the Born-Oppenheimer approximation. Our Born-Oppenheimer broken symmetry (BOBS) ansatz correlates the electronic with the nuclear motion by translating the density pairwise anti-symmetrically within the nuclear configuration space. Requiring only knowledge of the ground state nuclear quantum dynamics and static ground state electronic quantities that are readily accessible with ORBKIT[D2] from the standard output of quantum chemical programs, this approach yields a non-vanishing electronic flux density which can be forced to approximately fulfill the electronic continuity equation. In **Paper B3**, the robustness and general applicability of the BOBS ansatz are investigated for the hydrogen molecular ion vibrating in its electronic ground state. The results are then benchmarked against non-Born-Oppenheimer results that are available for this particular scenario.[63]

In summary, the **Papers B1–B3** establish a reliable framework for the visualization and analysis for charge migration and charge transport processes. The general applicability of this toolset can be exploited to investigate electron dynamics not only in small but also in much larger systems, such as those encountered in molecular electronics.

The research field of molecular electronics (cf., e.g., Refs. [79–81] and references therein) addresses the design of electronic components, where the functional unit is built up from a single molecule. Exam-

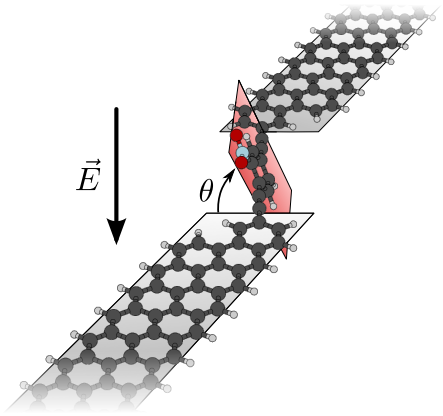

Figure 1.2: Cartoon of the molecular junction proposed by Agapito and Cheng[134] which consists of nitro-substituted oligo-(phenylene ethynylene) covalently bound to graphene nanoribbon leads (OPE-GNR). In Paper C1, we demonstrate that the conductivity of this device can be switched in the spirit of a traditional field effect transistor, i.e., by applying an external static electric field $\vec{E}$.

ples include wires,[82,83] rectifiers,[84–94] LEDs,[95–98] transistors,[99–120] and other electronics.[121–124] Transistors are of particular interest, since these components represent the central switching units in modern electronics. A wide variety of systems have been proposed and investigated for this particular application (cf., e.g., Ref. [125–128] and references therein). Recently, the first experimental demonstration of a light-induced graphene based molecular switch working at room temperature was presented by Jia et al.[129] Here, the well-known switching behavior of diarylethenes (cf., e.g., Ref. [130] and references therein) was exploited, and a representative of this class of molecules was bound covalently between two graphene tips. Graphene tips and related graphene-based nanostructures such as carbon nanotubes and graphene nanoribbons (GNRs) are predestined as contact materials,[131] since they are virtually one-dimensional, show unique electronic transport properties even at room temperature,[132,133] and can bind covalently to organic molecules, which potentially enhances their conductance properties.

For this endeavor, oligo-(phenylene ethynylene)s (OPEs) which attracted attention especially as molecular wires (cf., e.g., Ref. [82] and references therein) have interesting electrochemical properties. When they are inserted into a host n-alkanethiolate self-assembled monolayer on a gold surface, they exhibit stochastic conductance switching in STM experiments.[135–139] Based on (from the present point of view) outdated mechanistic interpretations of this phenomenon (for an assessment of the different proposed mechanisms, see Ref. [128]), Agapito and Cheng[134] designed a molecular junction, where nitro-substituted OPE is covalently bound to graphene nanoribbon leads (OPE-GNR), see Fig. 1.2. They applied the non-equilibrium Green's function formalism to demonstrate that this nanojunction can be found in two distinct conformers, which differ significantly in their conductance. In **Paper C1**,

we model the reaction path between both conformers and show that this system can be switched in the spirit of a traditional field effect transistor, i.e., by applying an external static electric field in top gate position. We apply dissipative quantum dynamics to model the complete switching cycle and show that the energetically unfavored less conducting conformer can be readily accessed.

In reference to the ground-breaking experimental work by Jia et al,[129] C. D. Frisbie highlighted in a perspective article[140] the necessity of the precise knowledge of the electron flow mechanism through the device as the key aspect for the design of more efficient molecular junctions. In **Paper C2**, we take up this challenge and develop a novel computational procedure to visualize spatially-resolved electron transport through single-molecule-graphene-nanoribbon junctions. The foundation of our approach is the driven Liouville-von Neumann (DLvN) formalism for time-dependent electronic transport calculations.[141–149] The transparent DLvN formalism allows us to directly access the density matrix of the molecular junction, and thus, to reconstruct the time-dependent local electronic current density allowing for a detailed mechanistic investigation. As a realistic test case, we investigate in detail the electronic current dynamics in both conformers of the OPE-GNR nanojunction (cf. **Paper C1**).

This dissertation is structured as follows. The chapter Theoretical Background gives a brief introduction to the basic quantum mechanical concepts used in this thesis. Because of the diversity of the time-independent and time-dependent phenomena studied, this chapter covers a wide range of quantum chemical and quantum dynamical methods, and I try to present a compact derivation revealing the connections between all these methods. The chapter Publications contains all the papers that have been published as part of my doctoral studies. Here, the contributions by the individual authors are clearly outlined. Finally, the central findings of all publications are summarized and put into context in the chapter Summary.

Chapter 2

Theoretical Background

The subsequent chapter should serve as an overview for the theoretical framework behind this thesis. The methods and underlying basic quantum mechanical concepts, which are necessary to understand the publications arisen from this dissertation, will be established and explained. No claims to completeness are raised, and it is assumed that the reader is familiar with the basic concepts of quantum chemistry. The underlying literature is marked as a citation in the heading of each chapter.

2.1 The Time-Dependent Schrödinger Equation [150,151]

Neglecting relativistic effects, the state of a molecular system evolves according to the time-dependent Schrödinger equation[152]

$$\imath\hbar\frac{\partial}{\partial t}\left|\Phi_{\mathrm{tot}}(t)\right\rangle = \left(\hat{H}_{\mathrm{mol}}(\boldsymbol{r},\boldsymbol{R}) + \hat{V}_{\mathrm{int}}(\boldsymbol{r},\boldsymbol{R},t)\right)\left|\Phi_{\mathrm{tot}}(t)\right\rangle, \tag{2.1}$$

where $\hbar$ is the reduced Planck constant, and t stands for the time. The spatial coordinates of the N electrons and M nuclei are labeled $\boldsymbol{r} = \{\vec{r}_k\}_{k=1}^{N}$ and $\boldsymbol{R} = \{\vec{R}_A\}_{A=1}^{M}$, respectively. The total molecular wave function $\left|\Phi_{\mathrm{tot}}(t)\right\rangle$ depends on the time, the $4N$ electronic, and $4M$ nuclear spatial and spin coordinates. Note that the nuclear spin will be ignored throughout this work. The time-dependent interaction operator $\hat{V}_{\mathrm{int}}(\boldsymbol{r},\boldsymbol{R},t)$ incorporates effects such as the interaction with an external electric field, which in the semi-classical dipole approximation is given by $\hat{V}_{\mathrm{int}}(\boldsymbol{r},\boldsymbol{R},t) = -\hat{\mu}(\boldsymbol{r},\boldsymbol{R})\cdot\vec{F}(t)$ with the dipole operator $\hat{\mu}(\boldsymbol{r},\boldsymbol{R})$ and the electric field operator $\vec{F}(t)$. The field-free Hamiltonian $\hat{H}_{\mathrm{mol}}(\boldsymbol{r},\boldsymbol{R})$ has no explicit time-dependence. It describes all interaction within the molecular framework and reads

in the laboratory frame of reference

$$\begin{aligned}\hat{H}_{\mathrm{mol}}(\boldsymbol{r},\boldsymbol{R}) &= \hat{T}_{\mathrm{nuc}}(\boldsymbol{R}) + \hat{H}_{\mathrm{el}}(\boldsymbol{r},\boldsymbol{R}) \\ &= -\sum_{A}^{M} \frac{\hbar^2}{2M_A}\nabla^2_{\vec{R}_A} + \hat{H}_{\mathrm{el}}(\boldsymbol{r},\boldsymbol{R})\end{aligned} \tag{2.2}$$

with the nuclear kinetic energy operator $\hat{T}_{\mathrm{nuc}}(\boldsymbol{R})$. Here, M_A is the mass of the A^{th} nucleus, and $\vec{\nabla}_{\vec{R}_A}$ is the spatial gradient with respect to the Cartesian coordinates of this nucleus. The second term of Eq. (2.2) is usually referred to as the electronic Hamiltonian,

$$\begin{aligned}\hat{H}_{\mathrm{el}}(\boldsymbol{r},\boldsymbol{R}) &= \hat{T}_{\mathrm{el}}(\boldsymbol{r}) + \hat{V}_{\mathrm{coul}}(\boldsymbol{r},\boldsymbol{R}) \\ &= -\sum_{k}^{N} \frac{\hbar^2}{2m_e}\nabla^2_{\vec{r}_k} + \hat{V}_{\mathrm{coul}}(\boldsymbol{r},\boldsymbol{R}),\end{aligned} \tag{2.3}$$

and is composed of the kinetic energy operator for the electrons $\hat{T}_{\mathrm{el}}(\boldsymbol{r})$ and all intra-molecular Coulomb interactions

$$\hat{V}_{\mathrm{coul}}(\boldsymbol{r},\boldsymbol{R}) = \sum_{A}^{M}\sum_{B>A}^{M} \frac{Z_A Z_B e^2}{4\pi\epsilon_0\left|\vec{R}_A - \vec{R}_B\right|} - \sum_{k}^{N}\sum_{A}^{M} \frac{Z_A e^2}{4\pi\epsilon_0\left|\vec{r}_k - \vec{R}_A\right|} + \sum_{k}^{N}\sum_{k'>k}^{N} \frac{e^2}{4\pi\epsilon_0\left|\vec{r}_k - \vec{r}_{k'}\right|}, \tag{2.4}$$

where the first term corresponds to the internuclear repulsion, the second term is the electron-nuclear attraction, and the last represents the electron-electron repulsion. Further, m_e is the electron rest mass, e the elementary charge, ϵ_0 the vacuum permittivity, and $\vec{\nabla}_{\vec{r}_k}$ is the spatial gradient with respect to the Cartesian coordinates of electron k.

The great difference between the masses of electrons and nuclei justifies the assumption that the electrons are moving much faster than the nuclei. Consequently, from the nuclear point of view, the electrons adjust instantaneously to the nuclear motion, and from the electronic point of view, the nuclei are fixed in space. Within this clamped nuclei approximation, stationary solutions of the electronic problem can be obtained by solving the time-independent electronic Schrödinger equation parametrically for a given nuclear configuration

$$\hat{H}_{\mathrm{el}}(\boldsymbol{r};\boldsymbol{R})\left|\Psi^{(\lambda)}\right\rangle = E^{(\lambda)}_{\mathrm{el}}(\boldsymbol{R})\left|\Psi^{(\lambda)}\right\rangle, \tag{2.5}$$

where the parametric dependence on $\boldsymbol{R}$ is symbolized by a semicolon. Here, $\left|\Psi^{(\lambda)}\right\rangle$ is the stationary electronic wave function of the electronic state λ for the nuclear configuration $\boldsymbol{R}$, and $E^{(\lambda)}_{\mathrm{el}}(\boldsymbol{R})$ is the associated electronic energy, which is called potential energy surface.

As the electronic wave functions form a complete set, the total molecular wave function may be

expanded as a linear combination of these basis functions

$$\left|\Phi_{\mathrm{tot}}(t)\right\rangle = \sum_{\lambda} \left|\Psi^{(\lambda)}\right\rangle \left|\chi^{(\lambda)}(t)\right\rangle, \tag{2.6}$$

where the expansion coefficients $\left|\chi^{(\lambda)}(t)\right\rangle$ depend on the time and the nuclear coordinates and are usually referred to as nuclear wave functions. Eq. (2.6), known as the general Born-Huang ansatz, is exact as long as the summation is not truncated. When inserting this ansatz into the time-dependent Schrödinger equation, cf. Eq. (2.1), and integrating over the electronic wave functions, i.e., left-multiplying by $\left\langle\Psi^{(\lambda)}\right|$, we arrive at the equations of motion for the nuclei

$$\imath\hbar\frac{\partial}{\partial t}\left|\chi^{(\lambda)}(t)\right\rangle = \left[\hat{T}_{\mathrm{nuc}}(\boldsymbol{R}) + E^{(\lambda)}_{\mathrm{el}}(\boldsymbol{R}) + \left(\sum_{\nu}\Lambda_{\lambda\nu}(\boldsymbol{R})\right) + \hat{V}_{\mathrm{int}}(\boldsymbol{R},t)\right]\left|\chi^{(\lambda)}(t)\right\rangle, \tag{2.7}$$

Here, the non-adiabatic or kinetic coupling terms are given by

$$\Lambda_{\lambda\nu}(\boldsymbol{R}) = -\sum_{A}^{M}\frac{\hbar^2}{2M_A}\left[2\vec{\Lambda}^{(1)}_{\lambda\nu,\vec{R}_A}(\boldsymbol{R})\cdot\vec{\nabla}_{\vec{R}_A} + \Lambda^{(2)}_{\lambda\nu,\vec{R}_A}(\boldsymbol{R})\right]. \tag{2.8}$$

where the first-order coupling terms $\vec{\Lambda}^{(1)}_{\lambda\nu,\vec{R}_A}(\boldsymbol{R}) = \left\langle\Psi^{(\lambda)}\right|\vec{\nabla}_{\vec{R}_A}\left|\Psi^{(\nu)}\right\rangle$ are vector quantities and the second-order coupling terms $\Lambda^{(2)}_{\lambda\nu,\vec{R}_A}(\boldsymbol{R})$ are scalar functions. As a convention, here and in the following, the Dirac notation of the inner product $\left\langle\Psi^{(\lambda)}\middle|\Psi^{(\nu)}\right\rangle$ indicates an integration over the electronic coordinates $\boldsymbol{r}$ only, while $\left\langle\chi^{(\lambda)}(t)\middle|\chi^{(\nu)}(t)\right\rangle$ refers to an integration over the nuclear coordinate space $\boldsymbol{R}$. Strictly speaking, the notation in Eq. (2.6) is not accurate, since it is a not direct product basis. Nonetheless, this issue can be circumvented by respecting the order of the integrals. Neglecting the non-adiabatic coupling terms, i.e., uncoupling the electronic states for the field-free Hamiltonian, yields the Born-Oppenheimer approximation.[151]

2.2 The Solution of the Time-Independent Electronic Schrödinger Equation [150]

Despite the simplifications achieved by the clamped-nuclei approximation and the associated Born-Oppenheimer approximation, the electronic problem, cf. Eq. (2.5), is still not solvable exactly for most systems. Thus, further approximations need to be applied. One famous approximation to access the electronic ground state ($\lambda = 0$) is to assume that the electrons can be treated independently from each other, experiencing the interactions with the remaining electrons only via an effective potential $\hat{v}_{\text{eff}}(\vec{r}_k; \boldsymbol{R})$. Within this mean-field method, the electronic Hamiltonian takes the form

$$\hat{H}_{\text{el}}(\boldsymbol{r}; \boldsymbol{R}) = \sum_{k}^{N} \left(-\frac{\hbar^2}{2m_e} \nabla^2_{\vec{r}_k} + \hat{v}_{\text{eff}}(\vec{r}_k; \boldsymbol{R}) \right) + \hat{V}_{\text{nuc-nuc}}(\boldsymbol{R}), \tag{2.9}$$

where the internuclear repulsion $\hat{V}_{\text{nuc-nuc}}(\boldsymbol{R})$ acts only as a constant factor, and the time-independent electronic Schrödinger equation can be recast from an N-electron problem to N one-electron problems,

$$\left(-\frac{\hbar^2}{2m_e} \nabla^2_{\vec{r}_k} + \hat{v}_{\text{eff}}(\vec{r}_k; \boldsymbol{R}) \right) \big|\psi_a\big\rangle = \varepsilon_a(\boldsymbol{R}) \big|\psi_a\big\rangle, \tag{2.10}$$

which hugely simplifies the eigenvalue problem. The one-electron wave functions $\big|\psi_a\big\rangle$ are called molecular spin orbitals, and the associated eigenenergies $\varepsilon_a(\boldsymbol{R})$ are denoted as molecular orbital energies. Due to the fact that the mean-field electronic Hamiltonian is a sum of single-particle Hamiltonians, the corresponding total molecular wave function $\big|\Psi^{(0)}_{\text{HF}}\big\rangle$ can be formulated as a product of molecular spin orbitals. Since $\big|\Psi^{(0)}_{\text{HF}}\big\rangle$ is further required to be antisymmetric with respect to the exchange of two electrons, the molecular spin orbitals can be arranged in the form of a Slater determinant

$$\begin{aligned} \Psi^{(0)}_{\text{HF}}(\boldsymbol{x}; \boldsymbol{R}) &= \frac{1}{\sqrt{N!}} \begin{vmatrix} \psi_a(\vec{x}_1; \boldsymbol{R}) & \psi_a(\vec{x}_2; \boldsymbol{R}) & \dots & \psi_a(\vec{x}_N; \boldsymbol{R}) \\ \psi_b(\vec{x}_1; \boldsymbol{R}) & \psi_b(\vec{x}_2; \boldsymbol{R}) & \dots & \psi_b(\vec{x}_N; \boldsymbol{R}) \\ \vdots & \vdots & \ddots & \vdots \\ \psi_c(\vec{x}_1; \boldsymbol{R}) & \psi_c(\vec{x}_2; \boldsymbol{R}) & \dots & \psi_c(\vec{x}_N; \boldsymbol{R}) \end{vmatrix} \\ &\equiv \big|\psi_a \psi_b \dots \psi_c\big\rangle \end{aligned} \tag{2.11}$$

where $\psi_a(\vec{x}_k; \boldsymbol{R})$ is the a^{th} spin orbital occupied by electron k with its spatial and spin coordinates $\vec{x}_k \equiv \{\vec{r}_k, m_{\text{s},k}\}$. For a non-relativistic Hamiltonian, each spin orbital can be factorized into a spatial part, $\varphi_a(\vec{r}_k)$, denoted as spatial molecular orbital (MO) and a spin function, $\sigma(m_{\text{s},k})$, i.e.,

$$\psi_a(\vec{x}_k; \boldsymbol{R}) = \varphi_a(\vec{r}_k; \boldsymbol{R}) \sigma(m_{\text{s},k}) \tag{2.12}$$

with $\sigma(m_{\mathrm{s},k})$ being either spin-up (α) or spin-down (β). Note that for many purposes the spin part can be integrated out in order to get a spin-free representation of the wave function.

Typically for molecules, the MOs are expressed according to the MO-LCAO ansatz (molecular orbitals as linear combination of atomic orbitals), i.e., they are expanded using a finite set of atom-centered basis functions

$$\varphi_a(\vec{r}_k;\boldsymbol{R}) = \sum_{A}^{M} \sum_{i_A}^{n_{\mathrm{AO}}(A)} C_{i_A}^{(a)}(\boldsymbol{R})\, \phi_{i_A}(\vec{r}_k - \vec{R}_A), \tag{2.13}$$

where $C_{i_A}^{(a)}(\boldsymbol{R})$ is the $i_A{}^{th}$ expansion coefficient of MO a, and each nucleus A possesses $n_{\mathrm{AO}}(A)$ atomic orbitals (AOs), $\phi_{i_A}(\vec{r}_k - \vec{R}_A)$. These are, for practical purposes, often themselves expanded in terms of Gaussian functions. For more details on basis functions, the reader is referred to, e.g., Ref. [153].

2.2.1 The Hartree-Fock Method [150,153]

When the Slater determinant wave function ansatz of Eq. (2.11) is inserted into the time-independent electronic Schrödinger equation, cf. Eq. (2.5), the one-electron eigenvalue equations as required by Eq. (2.10) can be obtained, leading to the Hartree-Fock equations

$$\begin{aligned} \hat{F}(\vec{r}_k;\boldsymbol{R})\, \psi_a^{\mathrm{HF}}(\vec{x}_k;\boldsymbol{R}) &= \left[\hat{h}(\vec{r}_k;\boldsymbol{R}) + \sum_{b}^{N} \Big(\hat{J}_b(\vec{r}_k;\boldsymbol{R}) - \hat{K}_b(\vec{r}_k;\boldsymbol{R})\Big)\right] \psi_a^{\mathrm{HF}}(\vec{x}_k;\boldsymbol{R}) \\ &= \varepsilon_a^{\mathrm{HF}}(\boldsymbol{R})\, \psi_a^{\mathrm{HF}}(\vec{x}_k;\boldsymbol{R}). \end{aligned} \tag{2.14}$$

Here, the electronic kinetic energy and the electron-nuclear attraction are described by the single particle operators

$$\hat{h}(\vec{r}_k;\boldsymbol{R})\, \psi_a^{\mathrm{HF}}(\vec{x}_k;\boldsymbol{R}) = \left[-\frac{\hbar^2}{2m_e}\nabla_{\vec{r}_k}^2 - \sum_{A}^{M} \frac{Z_A e^2}{4\pi\epsilon_0 |\vec{r}_k - \vec{R}_A|}\right] \psi_a^{\mathrm{HF}}(\vec{x}_k;\boldsymbol{R}) \tag{2.15}$$

and the electron-electron interactions are encoded in the Coulomb and the exchange operators

$$\hat{J}_b(\vec{r}_k;\boldsymbol{R})\, \psi_a^{\mathrm{HF}}(\vec{x}_k;\boldsymbol{R}) = \left[\int \mathrm{d}\vec{x}_{k'}\, \Big(\psi_b^{\mathrm{HF}}(\vec{x}_{k'};\boldsymbol{R})\Big)^{\dagger} \frac{e^2}{4\pi\epsilon_0 |\vec{r}_k - \vec{r}_{k'}|} \psi_b^{\mathrm{HF}}(\vec{x}_{k'};\boldsymbol{R})\right] \psi_a^{\mathrm{HF}}(\vec{x}_k;\boldsymbol{R}) \tag{2.16}$$

$$\hat{K}_b(\vec{r}_k;\boldsymbol{R})\, \psi_a^{\mathrm{HF}}(\vec{x}_k;\boldsymbol{R}) = \left[\int \mathrm{d}\vec{x}_{k'}\, \Big(\psi_b^{\mathrm{HF}}(\vec{x}_{k'};\boldsymbol{R})\Big)^{\dagger} \frac{e^2}{4\pi\epsilon_0 |\vec{r}_k - \vec{r}_{k'}|} \psi_a^{\mathrm{HF}}(\vec{x}_{k'};\boldsymbol{R})\right] \psi_b^{\mathrm{HF}}(\vec{x}_k;\boldsymbol{R}). \tag{2.17}$$

As the Coulomb and the exchange operators depend on the molecular spin orbitals, the Hartree-Fock equations cannot be solved directly. But since the exact energy is a lower bound to the expectation

value of the Hamiltonian with any trial wave function $\left|\tilde{\Psi}\right\rangle$ according to the variational principle,

$$E_{\mathrm{el}}^{(0)}(\boldsymbol{R}) \leq \frac{\left\langle\tilde{\Psi}\middle|\hat{H}_{\mathrm{el}}(\boldsymbol{r};\boldsymbol{R})\middle|\tilde{\Psi}\right\rangle}{\left\langle\tilde{\Psi}\middle|\tilde{\Psi}\right\rangle}, \tag{2.18}$$

the eigenvalue problem can be solved iteratively by varying the MO coefficients, until the solution is converged. Within the MO-LCAO ansatz, this minimization procedure is equivalent to solving the so-called Hartree-Fock-Roothaan-Hall matrix equation[154,155]

$$\boldsymbol{FC} = \boldsymbol{SC}\boldsymbol{\varepsilon} \tag{2.19}$$

with the Fock matrix in the AO basis $\boldsymbol{F}^{(i,j)} = \left\langle\phi_i\middle|\hat{F}(\vec{r}_k;\boldsymbol{R})\middle|\phi_j\right\rangle$, the MO coefficient matrix $\boldsymbol{C}^{(i,a)} = C_i^{(a)}$, the AO overlap matrix $\boldsymbol{S}^{(i,j)} = \left\langle\phi_i\middle|\phi_j\right\rangle$, and the diagonal MO energy matrix $\boldsymbol{\varepsilon}^{(a,a)} = \varepsilon_a$. The benefit of this variant is that by construction all integrals have to be carried out only once over all atomic orbitals at the beginning of the computational scheme. The solution of Eq. (2.19) gives as many MOs as there are AO basis functions, and only the N lowest spin orbitals, denoted occupied spin orbitals, contribute to the total energy. The remaining are called unoccupied or virtual spin orbitals.

2.2.2 The Configuration Interaction Method [150,153]

The Hartree-Fock method yields the best solution obtainable with a single Slater determinant at a given basis set level. However, even in the complete basis set limit, the resulting Hartree-Fock energy is not the exact electronic ground state energy. The energy difference is known as correlation energy, and many so-called post-Hartree-Fock methods have been proposed to approach the exact limit.

The conceptually simplest post-Hartree-Fock method is the method of configuration interaction (CI). Here, the electronic wave function for an electronic state λ is expressed as a linear combination of N-electron trial wave functions

$$\left|\Psi_{\mathrm{CI}}^{(\lambda)}\right\rangle = D_0^{(\lambda)}\left|\Psi_{\mathrm{HF}}^{(0)}\right\rangle + \left(\frac{1}{1!}\right)^2 \sum_{ar} D_a^{r(\lambda)}\left|\Psi_{\mathrm{HF}}^{(0)}\right\rangle_a^r + \left(\frac{1}{2!}\right)^2 \sum_{abrs} D_{ab}^{rs(\lambda)}\left|\Psi_{\mathrm{HF}}^{(0)}\right\rangle_{ab}^{rs} + \dots \tag{2.20}$$

with the CI coefficients $D_{ab\dots}^{rs\dots(\lambda)}$, which can be optimized applying the variational principle. The trial wave functions are n-tuply excited Slater determinants $\left|\Psi_{\mathrm{HF}}^{(0)}\right\rangle_{ab\dots}^{rs\dots}$ which are constructed from the Hartree-Fock reference wave function $\left|\Psi_{\mathrm{HF}}^{(0)}\right\rangle$ by promoting electrons from occupied $\{a, b, \dots\}$ to unoccupied spin orbitals $\{r, s, \dots\}$. Note that CI coefficients can be constrained, such that the spin of the wave function is respected. In practice, this is done by constructing configuration state functions (CSF). If all possible excitations are included, the method is labeled full CI and is exact within the

chosen basis set. Due to the fact that the number of determinants scales factorially with the number of electrons and orbitals, full CI is only applicable to very small systems.

To reduce the computational effort, two different strategies can be pursued: On the one hand, the rank of excitation can be restricted, e.g., allowing only for singly excited (CI singles) or only for doubly excited determinants (CI doubles). On the other hand, the excitations can be restricted to a specific orbital space, the so-called active space. This restricted active space CI (RAS-CI) method can be further improved by additionally optimizing the MO coefficients to account for orbital relaxation. This procedure is known as the multi-configuration self-consistent field (MCSCF) method.[156] Usually all possible excitations within the active space are considered, leading to the complete active space self-consistent field (CASSCF) method. A main drawback of the MCSCF procedure is that the MOs within the active space are treated differently than the MOs outside this orbital space. To compensate for this unbalanced situation, the MCSCF wave function is often taken as reference for an additional multi-reference CI (MRCI) calculation, where the excited determinants are constructed from all determinants present in the MCSCF reference wave functions, i.e.,

$$\left|\Psi^{(\lambda)}_{\mathrm{MRCI}}\right\rangle = D^{(\lambda)}_0 \left|\Psi^{(\lambda)}_{\mathrm{MCSCF}}\right\rangle + \left(\frac{1}{1!}\right)^2 \sum_{ar} D^{r(\lambda)}_a \left|\Psi^{(\lambda)}_{\mathrm{MCSCF}}\right\rangle^r_a + \left(\frac{1}{2!}\right)^2 \sum_{abrs} D^{rs(\lambda)}_{ab} \left|\Psi^{(\lambda)}_{\mathrm{MCSCF}}\right\rangle^{rs}_{ab} + \dots . \tag{2.21}$$

The CI methodology allows for an accurate high-level treatment of the ground and the excited electronic states of small and medium sized molecules, but as the system size increases, the computational effort rapidly becomes prohibitively large.

2.2.3 The Density Functional Theory [153,157]

The density functional theory (DFT) circumvents the explicit treatment of the correlated N-electron wave function by mapping the multi-dimensional problem onto the three-dimensional ground state one-electron density, which is defined by

$$\begin{aligned} \rho^{(0)}_{\mathrm{el}}(\vec{r};\boldsymbol{R}) &= N \sum_{m_\mathrm{s}} \int\cdots\int \mathrm{d}\vec{x}_2 \cdots \mathrm{d}\vec{x}_N \; \left|\Psi^{(0)}(\{\vec{r}, m_\mathrm{s}\}, \vec{x}_2, \dots, \vec{x}_N; \boldsymbol{R})\right|^2 \\ &= \rho^{(0)}_{\mathrm{el},\alpha}(\vec{r};\boldsymbol{R}) + \rho^{(0)}_{\mathrm{el},\beta}(\vec{r};\boldsymbol{R}). \end{aligned} \tag{2.22}$$

Here, the all-electron density is integrated over the coordinates of all but one electron, yielding two spin densities, which are summed up in the second line of Eq. (2.22). The spatial coordinates of the remaining electron $\vec{r}$ are sometimes referred to as the observation point. For sake of clarity, the index of this electron is omitted, and the coordinate dependence and the superscript of $\rho^{(0)}_{\mathrm{el}}(\vec{r};\boldsymbol{R})$ will be dropped in the following, wherever possible.

According to the first Hohenberg-Kohn theorem,[158] the exact ground state energy for a non-degenerate ground state is uniquely defined by the one-electron density, i.e., the energy is a functional of the one-electron density and may be written as

$$E\big[\rho_{\mathrm{el}}\big] = V_{\text{nuc-nuc}} + T\big[\rho_{\mathrm{el}}\big] + V_{\text{el-nuc}}\big[\rho_{\mathrm{el}}\big] + J\big[\rho_{\mathrm{el}}\big] + E'_{\mathrm{xc}}\big[\rho_{\mathrm{el}}\big], \tag{2.23}$$

where the functional forms are only known for the constant nuclear repulsion $V_{\text{nuc-nuc}}$, the electron-nuclear attraction functional

$$V_{\text{el-nuc}}\big[\rho_{\mathrm{el}}\big] = -\sum_{A}^{M} \int \mathrm{d}\vec{r}\, \frac{Z_A e^2}{4\pi\epsilon_0 \big|\vec{r} - \vec{R}_A\big|} \rho_{\mathrm{el}}(\vec{r}; \boldsymbol{R}), \tag{2.24}$$

and the Coulomb functional

$$J\big[\rho_{\mathrm{el}}\big] = \frac{1}{2} \iint \mathrm{d}\vec{r}\mathrm{d}\vec{r}\,' \, \frac{e^2}{4\pi\epsilon_0 \big|\vec{r} - \vec{r}\,'\big|} \rho_{\mathrm{el}}(\vec{r}; \boldsymbol{R}) \rho_{\mathrm{el}}(\vec{r}\,'; \boldsymbol{R}). \tag{2.25}$$

The expressions for the kinetic energy functional $T\big[\rho_{\mathrm{el}}\big]$ and the exchange-correlation energy functional $E'_{\mathrm{xc}}\big[\rho_{\mathrm{el}}\big]$ are unknown. However, if they would be known, according to the second Hohenberg-Kohn theorem,[158] the exact ground energy could be obtained variationally, as $E\big[\rho_{\mathrm{el}}\big] \leq E\big[\tilde{\rho}_{\mathrm{el}}\big]$ for any trial density $\tilde{\rho}_{\mathrm{el}}$.

One approach to at least partially solve this issue, is the famous Kohn-Sham formulation of DFT (KS-DFT).[159] Here, the one-electron density is mapped onto the density of a fictious non-interacting system, which is fully described by a single Slater determinant $\Psi_{\mathrm{KS}}(\boldsymbol{x}; \boldsymbol{R})$ built up from so-called Kohn-Sham orbitals $\psi_a^{\mathrm{KS}}(\{\vec{r}, m_{\mathrm{s}}\}; \boldsymbol{R})$. Consequently, the one-electron density can be written as a sum of single particle densities

$$\rho_{\mathrm{el}}(\vec{r}; \boldsymbol{R}) = \sum_{a}^{N} \sum_{m_{\mathrm{s}}} \big|\psi_a^{\mathrm{KS}}(\{\vec{r}, m_{\mathrm{s}}\}; \boldsymbol{R})\big|^2, \tag{2.26}$$

and the expression for the total energy can be reformulated as

$$E\big[\rho_{\mathrm{el}}\big] = T_{\mathrm{KS}}\big[\rho_{\mathrm{el}}\big] + V_{\text{nuc-nuc}} + V_{\text{el-nuc}}\big[\rho_{\mathrm{el}}\big] + J\big[\rho_{\mathrm{el}}\big] + E_{\mathrm{xc}}\big[\rho_{\mathrm{el}}\big], \tag{2.27}$$

where the expression for the non-interacting kinetic energy is naturally given by

$$T_{\mathrm{KS}}\big[\rho_{\mathrm{el}}\big] = -\frac{\hbar^2}{2m_e} \sum_{a}^{N} \big\langle \psi_a^{\mathrm{KS}} \big| \nabla_{\vec{r}}^2 \big| \psi_a^{\mathrm{KS}} \big\rangle. \tag{2.28}$$

The exchange-correlation energy functional $E_{\mathrm{xc}}\big[\rho_{\mathrm{el}}\big]$, which is the only unknown quantity in Eq. (2.27),

is augmented by the error in the kinetic energy, i.e., the fraction of the kinetic energy which is not covered by $T_{\mathrm{KS}}\left[\rho_{\mathrm{el}}\right]$,

$$E_{\mathrm{xc}}\left[\rho_{\mathrm{el}}\right] = E'_{\mathrm{xc}}\left[\rho_{\mathrm{el}}\right] + T\left[\rho_{\mathrm{el}}\right] - T_{\mathrm{KS}}\left[\rho_{\mathrm{el}}\right]. \tag{2.29}$$

This residual kinetic energy fraction is often ignored.[157]

Following the second Hohenberg-Kohn theorem, the single-particle Kohn-Sham equations

$$\left(-\frac{\hbar^2}{2m_e}\nabla^2_{\vec{r}} + \hat{v}_{\mathrm{eff}}(\vec{r};\boldsymbol{R})\right)\left|\psi^{\mathrm{KS}}_a\right\rangle = \varepsilon^{\mathrm{KS}}_a(\boldsymbol{R})\left|\psi^{\mathrm{KS}}_a\right\rangle, \tag{2.30}$$

which are of the same form as Eq. (2.10), can now be solved by variation of the electron density. Here, the effective potential operator is given by

$$\hat{v}_{\mathrm{eff}}(\vec{r};\boldsymbol{R}) = -\sum_A^M \frac{Z_A e^2}{4\pi\epsilon_0\left|\vec{r}-\vec{R}_A\right|} + \int \mathrm{d}\vec{r}\,' \, \frac{e^2\rho_{\mathrm{el}}(\vec{r}\,';\boldsymbol{R})}{4\pi\epsilon_0\left|\vec{r}-\vec{r}\,'\right|} + \hat{v}_{\mathrm{xc}}(\vec{r};\boldsymbol{R}), \tag{2.31}$$

where the first term is often referred to as external potential $\hat{v}_0(\vec{r};\boldsymbol{R})$. The exchange-correlation potential is the functional derivative of the exchange-correlation energy functional with respect to the electron density

$$\hat{v}_{\mathrm{xc}}(\vec{r};\boldsymbol{R}) = \frac{\delta E_{\mathrm{xc}}\left[\rho_{\mathrm{el}}\right]}{\delta\rho_{\mathrm{el}}(\vec{r};\boldsymbol{R})}. \tag{2.32}$$

Evidently, the Kohn-Sham equations are very similar to the Hartree-Fock equations. However, while the Hartree-Fock formalism is a mean-field approximation to the time-independent electronic Schrödinger equation, the Kohn-Sham formalism represents an exact recast of the N-electron problem to N one-electron problems, provided that the exchange-correlation potential would be known. Since this is not the case for almost all systems, approximations become inevitable.

The simplest approximation for the exchange-correlation energy is the local density approximation (LDA). Here, the electron density is locally treated as a homogeneous electron gas of the same density, for which the exchange energy $E_{\mathrm{x}}\left[\rho_{\mathrm{el}}\right]$ is known analytically[160,161] , and the respective correlation energy $E_{\mathrm{c}}\left[\rho_{\mathrm{el}}\right]$ can be fitted[162–164] to accurate quantum Monte Carlo simulations.[165] Accordingly, the LDA exchange-correlation energy functional is given by

$$E^{\mathrm{LDA}}_{\mathrm{xc}}\left[\rho_{\mathrm{el}}\right] = \int \mathrm{d}\vec{r}\;\rho_{\mathrm{el}}(\vec{r};\boldsymbol{R})\varepsilon^{\mathrm{LDA}}_{\mathrm{xc}}\left[\rho_{\mathrm{el}}\right]. \tag{2.33}$$

where $\varepsilon^{\mathrm{LDA}}_{\mathrm{xc}}\left[\rho_{\mathrm{el}}\right]$ is the exchange-correlation energy of the homogeneous electron gas of electron density ρ_{el}.

Clearly, for molecular systems, a slowly varying homogeneous electron gas is a rather poor approxi-

mation to the electron density. To this end, a local dependence on the gradient of the electron density can be added to the exchange-correlation energy functional to allow for the description of a more non-uniform electron distribution. This leads to the generalized gradient approximation (GGA) with

$$E_{\mathrm{xc}}^{\mathrm{GGA}}\left[\rho_{\mathrm{el}}\right] = \int \mathrm{d}\vec{r}\; \rho_{\mathrm{el}}(\vec{r};\boldsymbol{R})\varepsilon_{\mathrm{xc}}^{\mathrm{GGA}}\left[\rho_{\mathrm{el}}, \nabla\rho_{\mathrm{el}}\right]. \tag{2.34}$$

A variety of GGA functionals has been proposed over the years varying in quality and general applicability. Popular GGA functionals are PW91[166] or PBE[167] .

In order to further improve the results, the exchange-correlation energy expression can be supplemented by a fraction ζ of exact exchange $K\left[\{\psi_a^{\mathrm{KS}}\}\right]$, i.e., the exchange energy obtained within the Hartree-Fock formalism using Kohn-Sham orbitals $\{\psi_a^{\mathrm{KS}}\}$,[168]

$$E_{\mathrm{xc}}^{\mathrm{hybrid}}\left[\rho_{\mathrm{el}}\right] = \zeta\left(K\left[\{\psi_a^{\mathrm{KS}}\}\right] - E_{\mathrm{x}}^{\mathrm{LDA/GGA}}\left[\rho_{\mathrm{el}}, \vec{\nabla}\rho_{\mathrm{el}}\right]\right) + E_{\mathrm{xc}}^{\mathrm{LDA/GGA}}\left[\rho_{\mathrm{el}}\right] \tag{2.35}$$

Although, this treatment is computationally considerably more expensive than for GGA functionals, it is in general substantially cheaper than a post-HF treatment and yields reliable results in many cases. Consequently, those hybrid functionals are widely used in computational chemistry. Prominent examples for hybrid functionals are B3LYP[169,170] and PBE0[171] .

2.2.4 The Time-Dependent Density Functional Theory [153,157,172–174]

The purpose of the subsequent section is to extend the ground state capabilities of density functional theory to the description of excited state properties by means of linear response time-dependent density functional theory (LR-TDDFT).

Consider a molecular system with clamped nuclei in its electronic ground state being perturbed by an external stimulus. The electron dynamics of this system is given by the time-dependent Schrödinger equation Eq. (2.1) with the interaction operator

$$\hat{V}_{\mathrm{int}}(\boldsymbol{r}, t; \boldsymbol{R}) = \hat{v}_1(\boldsymbol{r}, t; \boldsymbol{R}) \cdot \vartheta(t - t_0), \tag{2.36}$$

where the time-dependent perturbation $\hat{v}_1(\boldsymbol{r}, t; \boldsymbol{R})$ is switched on at $t = t_0$ by a Heavyside step function $\vartheta(t - t_0)$. The time-independent problem, i.e., $t \leq t_0$, is assumed to be solved.

Two theorems, namely the Runge-Gross and the van Leeuwen theorem, form the basis of the time-dependent density functional theory (TDDFT) allowing for the treatment of such problems within the framework of DFT. While the Runge-Gross theorem[175] extends the Hohenberg-Kohn theorem

to the time-dependent regime for a given initial state, the van Leeuwen theorem[176] can be seen as a time-dependent analogue to the Kohn-Sham ansatz, i.e., the time-dependent electron density of the interacting system evolving from an initial state can be mapped onto a fictious non-interacting system being driven by a time-dependent effective potential. This effective potential is not only a functional of the time-dependent electron density, but also a functional of the initial states of both, the interacting and the non-interacting system. However, due to the particular choice for the interaction operator, cf. Eq. (2.36), the system is in its ground state for $t \leq t_0$, and thus, the latter functional dependences vanish since the initial state is itself functional of the density.

Analogously to the time-independent case, the time-dependent electron density can now be expanded in terms of time-dependent Kohn-Sham (TDKS) orbitals

$$\rho_{\mathrm{el}}(\vec{r}, t; \boldsymbol{R}) = \sum_{a}^{N} \sum_{m_{\mathrm{s}}} \left| \psi_a^{\mathrm{TDKS}}(\{\vec{r}, m_{\mathrm{s}}\}, t; \boldsymbol{R}) \right|^2, \tag{2.37}$$

which are described by the TDKS equations

$$\imath\hbar \frac{\partial}{\partial t} \left| \psi_a^{\mathrm{TDKS}}(t) \right\rangle = \left(-\frac{\hbar^2}{2m_e} \nabla_{\vec{r}}^2 + \hat{v}_{\mathrm{eff}}(\vec{r}, t; \boldsymbol{R}) \right) \left| \psi_a^{\mathrm{TDKS}}(t) \right\rangle \tag{2.38}$$

with the initial condition $\left| \psi_a^{\mathrm{TDKS}}(t = t_0) \right\rangle = \left| \psi_a^{\mathrm{KS}} \right\rangle$ and the time-dependent effective potential

$$\hat{v}_{\mathrm{eff}}(\vec{r}, t; \boldsymbol{R}) = \hat{v}(\vec{r}, t; \boldsymbol{R}) + \int \mathrm{d}\vec{r}\,' \, \frac{e^2 \rho_{\mathrm{el}}(\vec{r}\,', t; \boldsymbol{R})}{4\pi\epsilon_0 \left| \vec{r} - \vec{r}\,' \right|} + \hat{v}_{\mathrm{xc}}(\vec{r}, t; \boldsymbol{R}). \tag{2.39}$$

The time-dependent external potential is given as

$$\begin{aligned} \hat{v}(\vec{r}, t; \boldsymbol{R}) &= \hat{v}_0(\vec{r}; \boldsymbol{R}) + \hat{v}_1(\boldsymbol{r}, t; \boldsymbol{R}) \cdot \vartheta(t - t_0) \\ &= -\sum_{A}^{M} \frac{Z_A e^2}{4\pi\epsilon_0 \left| \vec{r} - \vec{R}_A \right|} + \hat{v}_1(\boldsymbol{r}, t; \boldsymbol{R}) \cdot \vartheta(t - t_0) \end{aligned} \tag{2.40}$$

with the unperturbed external potential $\hat{v}_0(\vec{r}; \boldsymbol{R})$. Notice that the time-dependent exchange-correlation potential $\hat{v}_{\mathrm{xc}}(\vec{r}, t; \boldsymbol{R})$ is causal and history-dependent. However, the treatment of the causality and history-dependence is usually avoided by introducing the so-called adiabatic approximation. Here, it is assumed that the density is slowly varying in time and that consequently, the time-dependent exchange-correlation potential becomes local in time. This allows us to employ the well-established framework of time-independent DFT functionals with the time-dependent density, i.e.,

$$\hat{v}_{\mathrm{xc}}(\vec{r}, t; \boldsymbol{R}) = \left. \frac{\delta E_{\mathrm{xc}}\left[\rho_{\mathrm{el}}\right]}{\delta \rho_{\mathrm{el}}(\vec{r}; \boldsymbol{R})} \right|_{\rho_{\mathrm{el}}(\vec{r}; \boldsymbol{R}) \to \rho_{\mathrm{el}}(\vec{r}, t; \boldsymbol{R})}. \tag{2.41}$$

The Linear-Response Time-Dependent Density Functional Theory [153,157,172–174]

Now, let the external stimulus be a weak uniform oscillating electric field in the semi-classical dipole approximation

$$\hat{v}_1(\boldsymbol{r}, t; \boldsymbol{R}) = -\hat{\mu}_{\mathrm{el}}(\boldsymbol{r}) \cdot F \cos(\omega t) \tag{2.42}$$

with the electronic dipole moment operator $\hat{\mu}_{\mathrm{el}}(\boldsymbol{r})$, the electric field strength F, and the field frequency ω. The density response induced by this perturbation can be expanded using a functional Taylor series expansion around $\hat{v}_0(\vec{r}; \boldsymbol{R})$[177]

$$\begin{aligned}\rho_{\mathrm{el}}(\vec{r}, t; \boldsymbol{R}) - \rho_{\mathrm{el}}[\hat{v}_0](\vec{r}, t; \boldsymbol{R}) = &\iint \mathrm{d}t' \, \mathrm{d}\vec{r}' \; \frac{\delta \rho_{\mathrm{el}}[\hat{v}_0](\vec{r}, t; \boldsymbol{R})}{\delta \, \hat{v}(\vec{r}', t'; \boldsymbol{R})} \hat{v}_1(\vec{r}', t'; \boldsymbol{R}) \\ + \frac{1}{2!} &\iiiint \mathrm{d}t' \mathrm{d}\vec{r}' \mathrm{d}t'' \, \mathrm{d}\vec{r}'' \; \frac{\delta^2 \rho_{\mathrm{el}}[\hat{v}_0](\vec{r}, t; \boldsymbol{R})}{\delta \, \hat{v}(\vec{r}', t'; \boldsymbol{R}) \delta \, \hat{v}(\vec{r}'', t''; \boldsymbol{R})} \hat{v}_1(\vec{r}', t'; \boldsymbol{R}) \hat{v}_1(\vec{r}'', t''; \boldsymbol{R}) + \dots\end{aligned} \tag{2.43}$$

where $\rho_{\mathrm{el},0}(\vec{r}; \boldsymbol{R}) = \rho_{\mathrm{el}}[\hat{v}_0](\vec{r}, t; \boldsymbol{R})$ is the unperturbed density, the first term on the right hand side corresponds to the linear response $\rho_{\mathrm{el},1}(\vec{r}, t; \boldsymbol{R})$, the second term to the quadratic (second-order) response $\rho_{\mathrm{el},2}(\vec{r}, t; \boldsymbol{R})$, etc. Here, we focus only on the linear density response, which can be rewritten as

$$\rho_{\mathrm{el},1}(\vec{r}, t; \boldsymbol{R}) = \iint \mathrm{d}t' \, \mathrm{d}\vec{r}' \; \boldsymbol{\chi}(\vec{r}, t, \vec{r}', t'; \boldsymbol{R}) \, \hat{v}_1(\vec{r}', t'; \boldsymbol{R}), \tag{2.44}$$

where the density-density response function is given by the functional derivative of the density with respect to the time-dependent external potential

$$\boldsymbol{\chi}(\vec{r}, t, \vec{r}', t'; \boldsymbol{R}) = \left. \frac{\delta \rho_{\mathrm{el}}[\hat{v}](\vec{r}, t; \boldsymbol{R})}{\delta \, \hat{v}(\vec{r}', t'; \boldsymbol{R})} \right|_{\hat{v}_0(\vec{r}; \boldsymbol{R})}. \tag{2.45}$$

The same linear density response as in Eq. (2.44) can be described within the framework of the non-interacting TDKS system, i.e.,

$$\rho_{\mathrm{el},1}(\vec{r}, t; \boldsymbol{R}) = \iint \mathrm{d}t' \, \mathrm{d}\vec{r}' \; \boldsymbol{\chi}_{\mathrm{eff}}(\vec{r}, t, \vec{r}', t'; \boldsymbol{R}) \, \hat{v}_{\mathrm{eff},1}(\vec{r}', t'; \boldsymbol{R}) \tag{2.46}$$

with the linearized effective potential

$$\hat{v}_{\mathrm{eff},1}(\vec{r}, t; \boldsymbol{R}) = \hat{v}_1(\vec{r}, t; \boldsymbol{R}) + \int \mathrm{d}\vec{r}' \; \frac{e^2 \rho_{\mathrm{el},1}(\vec{r}', t; \boldsymbol{R})}{4\pi\epsilon_0 \left| \vec{r} - \vec{r}' \right|} + \hat{v}_{\mathrm{xc},1}(\vec{r}, t; \boldsymbol{R}), \tag{2.47}$$

where the linearized exchange-correlation potential is given by

$$\hat{v}_{\mathrm{xc},1}(\vec{r}, t; \boldsymbol{R}) = \iint \mathrm{d}t' \, \mathrm{d}\vec{r}' \; \hat{f}_{\mathrm{xc}}(\vec{r}, t, \vec{r}', t'; \boldsymbol{R}) \, \rho_{\mathrm{el},1}(\vec{r}', t'; \boldsymbol{R}). \tag{2.48}$$

The time-dependent exchange-correlation kernel $\hat{f}_{\mathrm{xc}}(\vec{r},t,\vec{r}\,',t';\boldsymbol{R})$ is a crucial quantity for LR-TDDFT and is defined as the functional derivative of the exchange-correlation potential with respect to the density

$$\hat{f}_{\mathrm{xc}}(\vec{r},t,\vec{r}\,',t';\boldsymbol{R}) = \left.\frac{\delta\,\hat{v}_{\mathrm{xc}}[\rho_{\mathrm{el}}](\vec{r},t;\boldsymbol{R})}{\delta\rho_{\mathrm{el}}(\vec{r}\,',t';\boldsymbol{R})}\right|_{\rho_{\mathrm{el},0}(\vec{r};\boldsymbol{R})} . \tag{2.49}$$

Note that, as for the exchange-correlation potential, cf. Eq. (2.41), the exchange-correlation kernel becomes time-independent and real valued, within the commonly used adiabatic approximation.

In Fourier space, the non-interacting Kohn-Sham density-density response function, cf. Eq. (2.46), can be written explicitly in terms of unperturbed Kohn-Sham orbitals

$$\boldsymbol{\chi}_{\mathrm{eff}}(\vec{r},\vec{r}\,',\omega;\boldsymbol{R}) = \sum_{ar}\left[\frac{\rho^{\mathrm{KS}}_{ar}(\vec{r}\,';\boldsymbol{R})\rho^{\mathrm{KS}}_{ra}(\vec{r};\boldsymbol{R})}{\omega-\omega^{\mathrm{KS}}_{ar}+\imath\eta} - \frac{\rho^{\mathrm{KS}}_{ra}(\vec{r}\,';\boldsymbol{R})\rho^{\mathrm{KS}}_{ar}(\vec{r};\boldsymbol{R})}{\omega+\omega^{\mathrm{KS}}_{ar}+\imath\eta}\right] \tag{2.50}$$

Here and in the following, $\{a,b,\dots\}$ label occupied, $\{r,s,\dots\}$ unoccupied, and $\{p,q,\dots\}$ generic orbitals. In Eq. (2.50), $\rho^{\mathrm{KS}}_{pq}(\vec{r};\boldsymbol{R}) = \sum_{m_{\mathrm{s}}}\left(\psi^{\mathrm{KS}}_{q}(\{\vec{r},m_{\mathrm{s}}\};\boldsymbol{R})\right)^{\dagger}\psi^{\mathrm{KS}}_{p}(\{\vec{r},m_{\mathrm{s}}\};\boldsymbol{R})$ is the transition density from orbital p to orbital q, $\omega^{\mathrm{KS}}_{pq}(\boldsymbol{R}) = [\varepsilon^{\mathrm{KS}}_{q}(\boldsymbol{R}) - \varepsilon^{\mathrm{KS}}_{p}(\boldsymbol{R})]/\hbar$ is the respective transition frequency, and η is an infinitesimally small positive number.

Collecting and Fourier transforming the results obtained above, cf. Eqs. (2.44–2.50), yields after some algebra a Dyson-type equation,

$$\begin{aligned}\boldsymbol{\chi}(\vec{r},\vec{r}\,',\omega;\boldsymbol{R}) &= \boldsymbol{\chi}_{\mathrm{eff}}(\vec{r},\vec{r}\,',\omega;\boldsymbol{R}) \\ &+ \iint \mathrm{d}\vec{r}\,''\,\mathrm{d}\vec{r}\,'''\;\boldsymbol{\chi}(\vec{r},\vec{r}\,'',\omega;\boldsymbol{R})\left[\frac{e^2}{4\pi\epsilon_0|\vec{r}\,''-\vec{r}\,'''|}+\hat{f}_{\mathrm{xc}}(\vec{r}\,'',\vec{r}\,''',\omega;\boldsymbol{R})\right]\boldsymbol{\chi}_{\mathrm{eff}}(\vec{r}\,''',\vec{r}\,',\omega;\boldsymbol{R})\end{aligned} \tag{2.51}$$

which connects the interacting with the non-interacting response function and could be solved self-consistently. The poles of $\boldsymbol{\chi}(\vec{r},\vec{r}\,',\omega;\boldsymbol{R})$ correspond to excitation energies of electronically excited states. To circumvent the numerically very demanding and — with respect to the number of unoccupied orbitals — slowly converging procedure, the problem can be recast into a non-Hermitian eigenvalue problem. In the context of DFT, this is also known as Casida equation,[178]

$$\begin{pmatrix}\boldsymbol{A} & \boldsymbol{B}\\ \boldsymbol{B}^{\star} & \boldsymbol{A}^{\star}\end{pmatrix}\begin{pmatrix}\boldsymbol{X}\\ \boldsymbol{Y}\end{pmatrix} = \omega\begin{pmatrix}-\mathbf{1} & \mathbf{0}\\ \mathbf{0} & \mathbf{1}\end{pmatrix}\begin{pmatrix}\boldsymbol{X}\\ \boldsymbol{Y}\end{pmatrix}, \tag{2.52}$$

where

$$\begin{aligned}
\boldsymbol{A}_{ar,bs}(\omega;\boldsymbol{R}) &= \omega_{ar}^{\mathrm{KS}}(\boldsymbol{R})\,\delta_{ab}\delta_{rs} + K_{ar,bs}(\omega;\boldsymbol{R}),\\
\boldsymbol{B}_{ar,bs}(\omega;\boldsymbol{R}) &= K_{ar,bs}(\omega;\boldsymbol{R}),\\
K_{ar,bs}(\omega;\boldsymbol{R}) &= \iint \mathrm{d}\vec{r}\,\mathrm{d}\vec{r}\,'\ \rho_{ra}^{\mathrm{KS}}(\vec{r};\boldsymbol{R})\ \left[\frac{e^2}{4\pi\epsilon_0\left|\vec{r}-\vec{r}\,'\right|} + \hat{f}_{\mathrm{xc}}(\vec{r},\vec{r}\,',\omega;\boldsymbol{R})\right]\rho_{bs}^{\mathrm{KS}}(\vec{r}\,';\boldsymbol{R}).
\end{aligned} \tag{2.53}$$

By inserting Eq. (2.50), the linear density response, see Eq. (2.46), has been reformulated to

$$\begin{aligned}
\rho_{\mathrm{el},1}(\vec{r},\omega;\boldsymbol{R}) = \sum_{ar}\Bigg[\ & \rho_{ra}^{\mathrm{KS}}(\vec{r};\boldsymbol{R})\left(\frac{\int \mathrm{d}\vec{r}\,'\,\rho_{ar}^{\mathrm{KS}}(\vec{r}\,';\boldsymbol{R})\,\hat{v}_{\mathrm{eff},1}(\vec{r}\,',\omega;\boldsymbol{R})}{\omega-\omega_{ar}^{\mathrm{KS}}+\imath\eta}\right)\\
&+\rho_{ar}^{\mathrm{KS}}(\vec{r};\boldsymbol{R})\left(-\frac{\int \mathrm{d}\vec{r}\,'\,\rho_{ra}^{\mathrm{KS}}(\vec{r}\,';\boldsymbol{R})\,\hat{v}_{\mathrm{eff},1}(\vec{r}\,',\omega;\boldsymbol{R})}{\omega+\omega_{ar}^{\mathrm{KS}}+\imath\eta}\right)\Bigg]\\
= \sum_{ar}\Big[\ & \rho_{ra}^{\mathrm{KS}}(\vec{r};\boldsymbol{R})\ \boldsymbol{X}_{ar}(\omega;\boldsymbol{R}) + \rho_{ar}^{\mathrm{KS}}(\vec{r};\boldsymbol{R})\ \boldsymbol{Y}_{ar}(\omega;\boldsymbol{R})\Big].
\end{aligned} \tag{2.54}$$

This relation allows the computation of additional excited state observables beyond simple excitation energies such as oscillator strengths. As a side remark, neglecting the exchange-correlation kernel in Eq. (2.53) corresponds the so-called random phase approximation, while neglecting the $\boldsymbol{B}$ matrix in Eq. (2.52) yields the so-called Tamm-Dancoff approximation,[179] which is equivalent to the CI singles formalism in the Hartree-Fock theory.

2.3 Open Quantum Systems [180,181]

A main focus of this thesis represents the study of the dynamics of quantum systems which are in contact with their environment. In order to describe these open systems, it is instructive to introduce the Liouville-von Neumann (LvN) equation

$$\begin{aligned}\frac{\partial}{\partial t}\hat{\Theta}(t) &= -\frac{\imath}{\hbar}\left[\hat{H}_{\mathrm{tot}}(t), \hat{\Theta}(t)\right] \\ &= \mathcal{L}(t)\hat{\Theta}(t)\end{aligned} \tag{2.55}$$

For the sake of generality, the coordinate dependence of all operators will be dropped henceforth, and the total Hamiltonian will be considered as a sum of a time-independent unperturbed part and a time-dependent perturbation, i.e., $\hat{H}_{\mathrm{tot}}(t) = \hat{H}_0 + \hat{H}_{\mathrm{int}}(t)$. The second line of Eq. (2.55) introduces the Liouville super-operator or Liouvillian $\mathcal{L}(t)$ in analogy to the classical Liouville equation.

For a closed system, the LvN equation is a straightforward reformulation of the time-dependent Schrödinger equation Eq. (2.1) describing the time evolution of the so-called density matrix operator. For the special case of a pure state, it can be written as

$$\hat{\Theta}(t) = \left|\Phi_{\mathrm{tot}}(t)\right\rangle\left\langle\Phi_{\mathrm{tot}}(t)\right|. \tag{2.56}$$

For a general mixed state while considering a time-independent basis, the density matrix operator is given by

$$\hat{\Theta}(t) = \sum_{nm} P_{nm}(t)\left|\Phi^{(n)}_{\mathrm{tot}}\right\rangle\left\langle\Phi^{(m)}_{\mathrm{tot}}\right|, \tag{2.57}$$

where the diagonal terms of the coefficient matrix $P_{nn}(t)$ correspond to populations, and the off-diagonal terms refer to coherences between states. Occasionally, the coefficient matrix is diagonalized to yield a statistical mixture of pure states with the eigenvalues as their statistical weights. Note that the expectation value of an arbitrary operator $\hat{A}$ with the density matrix operator may be calculated through the trace

$$\langle\hat{A}\rangle = \mathrm{Tr}\left\{\hat{A}\,\hat{\Theta}(t)\right\}. \tag{2.58}$$

When only the time-independent part of the Hamiltonian is regarded, the time evolution of the wave function of a closed system is fully governed by a unitary time propagation operator

$$\hat{U}_0(t, t_0) = e^{-\imath\hat{H}_0\cdot(t-t_0)/\hbar}. \tag{2.59}$$

This propagator can be used to transfer the LvN equation from the Schrödinger picture, cf. Eq. (2.55),

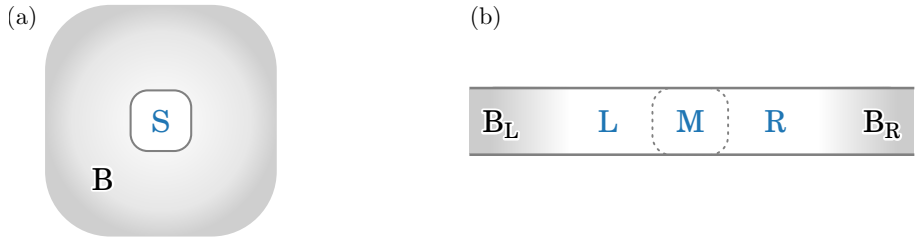

Figure 2.1: Conceptual sketch of the two scenarios of open quantum systems discussed within these sections: (a) An open system "S" weakly coupled to a macroscopic bath "B" which is in its thermal equilibrium. Here, only energy transfer is allowed. (b) An open electronic quantum system "S" consisting of three subsystems: the extended molecule "M", the left lead "L", the right lead "R". The latter two are each coupled to an electronic reservoir, "$\mathrm{B_L}$" and "$\mathrm{B_R}$", respectively. Each reservoir has a specific temperature and chemical potential. In this model, also particle transfer is allowed.

to the interaction picture

$$\frac{\partial}{\partial t}\hat{\Theta}_{\mathrm{I}}(t) = -\frac{\imath}{\hbar}\left[\hat{H}_{\mathrm{int,I}}(t), \hat{\Theta}_{\mathrm{I}}(t)\right], \tag{2.60}$$

where the subscript "I" signifies that an operator has been transformed to the interaction picture, i.e., $\hat{A}_{\mathrm{I}}(t) = \hat{U}_0^{\dagger}(t,t_0)\hat{A}\,\hat{U}_0(t,t_0)$. In integral form, the time evolution of the density matrix operator can be written as

$$\hat{\Theta}_{\mathrm{I}}(t) = \hat{\Theta}_{\mathrm{I}}(t_0) - \frac{\imath}{\hbar}\int_{t_0}^{t} \mathrm{d}t' \left[\hat{H}_{\mathrm{int,I}}(t'), \hat{\Theta}_{\mathrm{I}}(t')\right]. \tag{2.61}$$

2.3.1 The Liouville-von Neumann Equation in Lindblad Form [180,181]

Consider a finite open system "S" which is weakly coupled to a macroscopic bath "B" in its thermal equilibrium as depicted in Fig. 2.1a. It is assumed that the total system is closed, and that the interactions between both subsystems $\hat{H}_{\mathrm{int}}$ are time-independent and switched on at $t = t_0$, i.e., the initial density matrix operator for both subsystems is considered to be given by a tensor product

$$\hat{\Theta}(t_0) = \hat{\Theta}_{\mathrm{S}}(t_0) \otimes \hat{\Theta}_{\mathrm{B}}(t_0). \tag{2.62}$$

The Hamiltonian describing this scenario takes the form

$$\hat{H}_{\mathrm{tot}}(t) = \hat{H}_{\mathrm{S}} \otimes \hat{\mathbb{1}}_{\mathrm{B}} + \hat{\mathbb{1}}_{\mathrm{S}} \otimes \hat{H}_{\mathrm{B}} + \hat{H}_{\mathrm{int}} \cdot \vartheta(t - t_0) \tag{2.63}$$

with $\hat{H}_{\mathrm{S}}$ acting only on the Hilbert space of the system and $\hat{H}_{\mathrm{B}}$ acting only on the Hilbert space of the bath. The system-bath interaction Hamiltonian $\hat{H}_{\mathrm{int}}$ acts on the combined, total Hilbert space. As a side remark, the procedure described within this section can be easily extended to time-dependent situations, where the interactions with external stimuli are usually incorporated into $\hat{H}_{\mathrm{S}}$.

Inserting the integral form Eq. (2.61) into Eq. (2.60) and performing a partial trace over the bath

degrees of freedom results in the equation of motion for the reduced system

$$\frac{\partial}{\partial t}\hat{\Theta}_{\mathrm{S,I}}(t) = -\frac{1}{\hbar^2}\int_0^t \mathrm{d}t' \ \mathrm{Tr}_{\mathrm{B}}\left\{\left[\hat{H}_{\mathrm{int,I}}(t), \left[\hat{H}_{\mathrm{int,I}}(t'), \hat{\Theta}_{\mathrm{I}}(t')\right]\right]\right\}, \tag{2.64}$$

where the initial time t_0 and the term $\mathrm{Tr}_{\mathrm{B}}\left\{\left[\hat{H}_{\mathrm{int,I}}(t), \hat{\Theta}(0)\right]\right\}$ are taken to be zero. Since the system is supposed to be weakly coupled to a macroscopic bath, the latter is only negligibly affected by the interaction with the system. Consequently, it can be safely assumed that the bath is stationary and that, at all times, the total system can be approximately described by a tensor product

$$\hat{\Theta}_{\mathrm{I}}(t) \approx \hat{\Theta}_{\mathrm{S,I}}(t) \otimes \hat{\Theta}_{\mathrm{B,I}}. \tag{2.65}$$

This weak-coupling approximation is known as the Born approximation. If we further employ the Markov approximation, i.e., the time evolution at time t only depends on the density matrix operator at that time, Eq. (2.64) simplifies to

$$\frac{\partial}{\partial t}\hat{\Theta}_{\mathrm{S,I}}(t) = -\frac{1}{\hbar^2}\int_0^t \mathrm{d}t' \ \mathrm{Tr}_{\mathrm{B}}\left\{\left[\hat{H}_{\mathrm{int,I}}(t), \left[\hat{H}_{\mathrm{int,I}}(t'), \hat{\Theta}_{\mathrm{S,I}}(t) \otimes \hat{\Theta}_{\mathrm{B,I}}\right]\right]\right\}. \tag{2.66}$$

To resolve the issue that this equation still depends on the choice of the initial preparation at time $t = 0$, the variable t' can be substituted with $t - t'$, and the upper limit of the integration can be extended to infinity. This results in the following Markovian quantum master equation

$$\frac{\partial}{\partial t}\hat{\Theta}_{\mathrm{S,I}}(t) = -\frac{1}{\hbar^2}\int_0^\infty \mathrm{d}t' \ \mathrm{Tr}_{\mathrm{B}}\left\{\left[\hat{H}_{\mathrm{int,I}}(t), \left[\hat{H}_{\mathrm{int,I}}(t-t'), \hat{\Theta}_{\mathrm{S,I}}(t) \otimes \hat{\Theta}_{\mathrm{B,I}}\right]\right]\right\}. \tag{2.67}$$

This reformulation is justified, when the time scale of the system relaxation τ_{relax} is significantly larger than the time scale of the bath correlations τ_{B}, i.e., $\tau_{\mathrm{relax}} \gg \tau_{\mathrm{B}}$. All dynamics taking place on shorter time scales are not resolved. The time axis is said to be coarse-grained.

The approximations performed above are often referred to as Born-Markov approximation. Since the resulting master equation Eq. (2.67), which is usually referred to as Redfield equation[182,183], does not guarantee that the probabilistic interpretation of the density operator is maintained during the quantum dynamics,[184,185] a further approximation, the so-called secular approximation, can be used to enforce this feature. This treatment, which will be described in the following, is supposed to eliminate rapidly oscillating terms within the dynamics.

According to the spectral decomposition theorem, the interaction Hamiltonian can be expanded in

terms of tensor products of system $\hat{A}_\alpha$ and bath operators $\hat{B}_\alpha$ (here in Schrödinger picture)

$$\hat{H}_{\text{int}} = \sum_\alpha \hat{A}_\alpha \otimes \hat{B}_\alpha \tag{2.68}$$

with $\hat{A}_\alpha = \hat{A}_\alpha^\dagger$ and $\hat{B}_\alpha = \hat{B}_\alpha^\dagger$. The eigenvalues ε of the system Hamiltonian $\hat{H}_{\text{S}}$ and the projections onto the corresponding eigenvectors $\hat{P}(\varepsilon)$ can be now used to project $\hat{A}_\alpha$ onto the system eigenspace with a fixed frequency $\omega = (\varepsilon' - \varepsilon)/\hbar$

$$\hat{A}_\alpha(\omega) = \sum_{\omega=(\varepsilon'-\varepsilon)/\hbar} \hat{P}(\varepsilon)\hat{A}_\alpha\hat{P}(\varepsilon'). \tag{2.69}$$

Using the commutator relation $\left[\hat{H}_{\text{S}}, \hat{A}_\alpha(\omega)\right] = -\omega\hat{A}_\alpha(\omega)$, this operator can be straightforwardly transformed to the interaction picture

$$e^{\imath\hat{H}_{\text{S}}t/\hbar}\hat{A}_\alpha(\omega)e^{-\imath\hat{H}_{\text{S}}t/\hbar} = e^{-\imath\omega t}\hat{A}_\alpha(\omega). \tag{2.70}$$

As the eigenvectors of $\hat{H}_{\text{S}}$ form a complete set, the summation over all frequencies recovers $\hat{A}_\alpha$, and consequently, Eq. (2.68) can be reformulated in the interaction picture as

$$\begin{aligned}\hat{H}_{\text{int,I}}(t) &= \sum_{\alpha,\omega} e^{-\imath\omega t}\hat{A}_\alpha(\omega) \otimes \hat{B}_\alpha(t) \\ &= \sum_{\alpha,\omega} e^{+\imath\omega t}\hat{A}_\alpha^\dagger(\omega) \otimes \hat{B}_\alpha^\dagger(t).\end{aligned} \tag{2.71}$$

Inserting Eq. (2.71) into the Markovian master equation Eq. (2.67), yields

$$\frac{\partial}{\partial t}\hat{\Theta}_{\text{S,I}}(t) = \sum_{\omega,\omega'}\sum_{\alpha,\beta} e^{\imath(\omega'-\omega)t}\,\Gamma_{\alpha,\beta}(\omega)\left(\hat{A}_\beta(\omega)\hat{\Theta}_{\text{S,I}}(t)\hat{A}_\alpha^\dagger(\omega') - \hat{A}_\alpha^\dagger(\omega')\hat{A}_\beta(\omega)\hat{\Theta}_{\text{S,I}}(t)\right) + \text{h.c.} \tag{2.72}$$

where "h.c." stands for the Hermitian conjugate expression, and the one-sided Fourier transform of the bath correlation function is defined as

$$\begin{aligned}\Gamma_{\alpha,\beta}(\omega) &= \frac{1}{\hbar^2}\int_0^\infty \mathrm{d}t'\; e^{+\imath\omega t'}\left\langle\hat{B}_\alpha^\dagger(t)\hat{B}_\beta(t-t')\right\rangle \\ &= \frac{1}{\hbar^2}\int_0^\infty \mathrm{d}t'\; e^{+\imath\omega t'}\left\langle\hat{B}_\alpha^\dagger(t')\hat{B}_\beta(0)\right\rangle\end{aligned} \tag{2.73}$$

with the bath correlation function $\left\langle\hat{B}_\alpha^\dagger(t)\hat{B}_\beta(t-t')\right\rangle = \text{Tr}_{\text{B}}\left\{\hat{B}_\alpha^\dagger(t)\hat{B}_\beta(t-t')\hat{\Theta}_{\text{B,I}}\right\}$. Here, the second line follows from the stationarity of the bath. This shows that the bath correlation function is homo-

geneous, and that therefore, $\Gamma_{\alpha,\beta}(\omega)$ is time-independent. Commonly, $\Gamma_{\alpha,\beta}(\omega)$ is split into its real and imaginary part

$$\Gamma_{\alpha,\beta}(\omega) = \frac{1}{2}\gamma_{\alpha,\beta}(\omega) + \imath S_{\alpha,\beta}(\omega). \tag{2.74}$$

The time scale of the system relaxation τ_{relax} is considered to be large compared to the time scale of the system dynamics which is typically $\tau_{\text{S}} \sim |\omega' - \omega|^{-1}$, i.e., $\tau_{\text{relax}} \gg \tau_{\text{S}}$. Consequently, all terms with $\omega' \neq \omega$ can be neglected within the secular approximation to remove the rapidly oscillating contributions. This simplifies Eq. (2.72) to

$$\frac{\partial}{\partial t}\hat{\Theta}_{\text{S,I}}(t) = -\frac{\imath}{\hbar}\left[\hat{H}_{\text{LS}}, \hat{\Theta}_{\text{S,I}}(t)\right] + \mathcal{L}_{\text{D}}\hat{\Theta}_{\text{S,I}}(t), \tag{2.75}$$

where the Lamb shift Hamiltonian,

$$\hat{H}_{\text{LS}} = \sum_{\omega}\sum_{\alpha,\beta} S_{\alpha,\beta}(\omega)\hat{A}^{\dagger}_{\alpha}(\omega)\hat{A}_{\beta}(\omega), \tag{2.76}$$

renormalizes the unperturbed energy levels, and the dissipative Liouvillian or dissipator is defined as

$$\mathcal{L}_{\text{D}}\hat{\Theta}_{\text{S,I}}(t) = \frac{1}{2}\sum_{\omega}\sum_{\alpha,\beta}\gamma_{\alpha,\beta}(\omega)\left\{\left[\hat{A}_{\beta}(\omega), \hat{\Theta}_{\text{S,I}}(t)\hat{A}^{\dagger}_{\alpha}(\omega)\right] + \left[\hat{A}_{\beta}(\omega)\hat{\Theta}_{\text{S,I}}(t), \hat{A}^{\dagger}_{\alpha}(\omega)\right]\right\}. \tag{2.77}$$

Notice that Eq. (2.75) can be transformed to the Schrödinger picture by simply adding the free system Hamiltonian $\hat{H}_{\text{S}}$ to the Lamb shift Hamiltonian $\hat{H}_{\text{LS}}$. A final diagonalizing of the matrices $\gamma_{\alpha,\beta}(\omega)$ and the neglect of the Lamb shift Hamiltonian $\hat{H}_{\text{LS}}$ brings Eq. (2.75) to the Liouville-von Neumann equation in Lindblad form.

2.3.2 The Driven Liouville-von Neumann Equation [143]

While the Liouville-von Neumann equation in Lindblad form describes bath induced relaxation dynamics of open quantum systems towards their equilibrium, the driven Liouville-von Neumann (DLvN) equation is capable of describing electronic transport processes, where open systems are driven towards a non-equilibrium situation by their environment. While in the former, only energy is transferred, the latter methodology also involves particle transport.

More specifically, within the DLvN approach, electronic transport through a nanojunction can be described using a finite model system. As sketched in Fig. 2.1b, this open electronic system "S" consists of three subsystems: the extended molecule "M", the left lead "L", and the right lead "R". The latter two are each coupled to an electronic reservoir, "$\mathrm{B_L}$" and "$\mathrm{B_R}$", respectively. These implicit reservoirs mimic the presence of semi-infinite leads, and their specific electronic temperatures and chemical potentials drive the electron dynamics within the system. In the local basis of the three subsystems, the density matrix operator is given by

$$\hat{\Theta}(t) = \begin{pmatrix} \hat{\Theta}_{\mathrm{L}} & \hat{\Theta}_{\mathrm{LM}} & \hat{\Theta}_{\mathrm{LR}} \\ \hat{\Theta}_{\mathrm{ML}} & \hat{\Theta}_{\mathrm{M}} & \hat{\Theta}_{\mathrm{MR}} \\ \hat{\Theta}_{\mathrm{RL}} & \hat{\Theta}_{\mathrm{RM}} & \hat{\Theta}_{\mathrm{R}} \end{pmatrix} . \tag{2.78}$$

When neglecting the influence of the infinite reservoirs, the Hamiltonian of the finite system in matrix representation has the following block form

$$\hat{H}_{\mathrm{S}} = \begin{pmatrix} \hat{H}_{\mathrm{L}} & \hat{V}_{\mathrm{LM}} & 0 \\ \hat{V}_{\mathrm{LM}}^{\dagger} & \hat{H}_{\mathrm{M}} & \hat{V}_{\mathrm{RM}}^{\dagger} \\ 0 & \hat{V}_{\mathrm{RM}} & \hat{H}_{\mathrm{R}} \end{pmatrix} \tag{2.79}$$

where the left lead $\hat{H}_{\mathrm{L}}$, the extended molecule $\hat{H}_{\mathrm{M}}$, and the right lead Hamiltonian $\hat{H}_{\mathrm{R}}$ are diagonal matrices containing the respective energy eigenvalues $\{\varepsilon_a^{\mathrm{L/M/R}}\}$, and $\hat{V}_{\mathrm{LM}}$ and $\hat{V}_{\mathrm{RM}}$ describe the couplings from the left lead and the right lead to the extended molecule, respectively. The interlead couplings $\hat{V}_{\mathrm{LR}}$ are not strictly zero but negligibly small, provided the size of the extended molecule is chosen large enough.

There are two competing effects, which have to be taken into account to mimic semi-infinite leads: electron adsorption at the lead edges transferring electrons from the finite leads to the electron reservoirs and electron injection back from the electron reservoirs into the finite leads. While the former effect dephases the electrons approaching the edges of the leads and prevents backscattering, the latter accounts for the electronic temperatures and chemical potentials of the leads.

The electron adsorption is realized by supplementing the Hamiltonian Eq. (2.79) with a complex absorbing potential leading to a complex Hamiltonian with the following real and imaginary part

$$\begin{aligned}\hat{H}_\mathrm{S} &= \hat{H}_\mathrm{S}^\mathrm{Re} - \imath \hat{H}_\mathrm{S}^\mathrm{Im} \\ &= \begin{pmatrix} \hat{H}_\mathrm{L} & \hat{V}_\mathrm{LM} & 0 \\ \hat{V}_\mathrm{LM}^\dagger & \hat{H}_\mathrm{M} & \hat{V}_\mathrm{RM}^\dagger \\ 0 & \hat{V}_\mathrm{RM} & \hat{H}_\mathrm{R} \end{pmatrix} - \imath \begin{pmatrix} \hat{\Gamma}_\mathrm{L} & 0 & 0 \\ 0 & 0 & 0 \\ 0 & 0 & \hat{\Gamma}_\mathrm{R} \end{pmatrix},\end{aligned} \tag{2.80}$$

where $\hat{\Gamma}_\mathrm{L/R}$ is a diagonal matrix containing the electron adsorption or damping rate for each lead eigenstate. The Liouville-von Neumann equation for this complex valued system Hamiltonian reads

$$\frac{\partial}{\partial t}\hat{\Theta}(t) = -\frac{\imath}{\hbar}\left[\hat{H}_\mathrm{S}^\mathrm{Re}, \hat{\Theta}(t)\right] - \frac{1}{\hbar}\left[\hat{H}_\mathrm{S}^\mathrm{Im}, \hat{\Theta}(t)\right]_+ \tag{2.81}$$

with the anticommutator $[\,]_+$. Here, the first term governs the coherent time evolution of the closed finite system, cf. Eq. (2.55), and the second term captures the electron adsorption.

In order to maintain the electron balance in the system, incoherent electrons have to be injected back into the leads. This is achieved using the same expression as for the electron adsorption with the same rate constant but with opposite sign. Since the semi-infinite leads are assumed to be always in their thermal equilibrium, the time-dependent density matrix operator $\hat{\Theta}_\mathrm{L/R}(t)$ is further replaced by $\hat{\Theta}^0_\mathrm{L/R}(t)$, which is a diagonal matrix containing the equilibrium Fermi-Dirac statistics of the respective lead

$$f_\mathrm{L/R}\left(\varepsilon_a^\mathrm{L/R}, \mu_\mathrm{L/R}\right) = \frac{1}{\exp\left[\left(\varepsilon_a^\mathrm{L/R} - \mu_\mathrm{L/R}\right)\Big/ k_\mathrm{B} T_\mathrm{L/R}\right] + 1} \tag{2.82}$$

with the Boltzmann constant k_B, the lead eigenstate energies $\varepsilon_a^\mathrm{L/R}$, the electronic temperature $T_\mathrm{L/R}$, and the chemical potential $\mu_\mathrm{L/R}$.

The final driven Liouville-von Neumann equation takes the form

$$\begin{aligned}\frac{\partial}{\partial t}\hat{\Theta}(t) = &-\frac{\imath}{\hbar}\left[\hat{H}_\mathrm{S}^\mathrm{Re}, \hat{\Theta}(t)\right] \\ &- \frac{1}{2\hbar}\begin{pmatrix} \left[\hat{\Gamma}_\mathrm{L}, \left(\hat{\Theta}_\mathrm{L}(t) - \hat{\Theta}^0_\mathrm{L}\right)\right]_+ & \hat{\Gamma}_\mathrm{L}\hat{\Theta}_\mathrm{LM}(t) & \hat{\Gamma}_\mathrm{L}\hat{\Theta}_\mathrm{LR}(t) + \hat{\Theta}_\mathrm{LR}(t)\hat{\Gamma}_\mathrm{R} \\ \hat{\Theta}_\mathrm{ML}(t)\hat{\Gamma}_\mathrm{L} & 0 & \hat{\Theta}_\mathrm{MR}(t)\hat{\Gamma}_\mathrm{R} \\ \hat{\Gamma}_\mathrm{R}\hat{\Theta}_\mathrm{RL}(t) + \hat{\Theta}_\mathrm{RL}(t)\hat{\Gamma}_\mathrm{L} & \hat{\Gamma}_\mathrm{R}\hat{\Theta}_\mathrm{RM}(t) & \left[\hat{\Gamma}_\mathrm{R}, \left(\hat{\Theta}_\mathrm{R}(t) - \hat{\Theta}^0_\mathrm{R}\right)\right]_+ \end{pmatrix}.\end{aligned} \tag{2.83}$$

In the original formulation of the DLvN approach,[143,145–147] the wide-band approximation is invoked and all rates are chosen to be the same $\hat{\Gamma}_\mathrm{L} \stackrel{!}{=} \hat{\Gamma}_\mathrm{R} \stackrel{!}{=} 2\gamma\,\hat{\mathbb{1}}_\mathrm{L/R}$. This rate constant, which is the only free parameter entering the model. It is usually tuned such that the steady-state current matches non-

equilibrium Green's function (NEGF) reference calculations. This vast simplification of Eq. (2.83) is only justified for evenly distributed lead states. To circumvent this drawback, a parameter-free version of the DLvN approach has been proposed in a very recent study.[148] Here, state-specific rates are obtained directly from the self-energy obtained within a NEGF reference calculations. Interestingly, it can be shown that the DLvN approach for electron transport processes is formally an approximation to the NEGF formalism.[144]

A central quantity for the analysis of electronic transport processes is the electric current $I(t)$. In order to access this quantity, consider the time-evolution of the extended molecule block in Eq. (2.83)

$$\frac{\partial}{\partial t}\hat{\Theta}_{\mathrm{M}}(t) = -\frac{\imath}{\hbar}\left[\hat{H}_{\mathrm{M}},\hat{\Theta}(t)\right] - \frac{\imath}{\hbar}(\hat{V}_{\mathrm{ML}}\hat{\Theta}_{\mathrm{LM}}(t) - \hat{\Theta}_{\mathrm{ML}}(t)\hat{V}_{\mathrm{LM}}) - \frac{\imath}{\hbar}(\hat{V}_{\mathrm{MR}}\hat{\Theta}_{\mathrm{RM}}(t) - \hat{\Theta}_{\mathrm{MR}}(t)\hat{V}_{\mathrm{RM}}). \tag{2.84}$$

Taking the trace of this expression yields the temporal change of the number of electrons in the extended molecule region.

$$\begin{aligned}\dot{N}_{\mathrm{M}} &= \mathrm{Tr}\left\{\frac{\partial}{\partial t}\hat{\Theta}_{\mathrm{M}}(t)\right\} \\ &= \mathrm{Tr}\left\{-\frac{\imath}{\hbar}\left[\hat{H}_{\mathrm{M}},\hat{\Theta}_{\mathrm{M}}(t)\right]\right\} + \frac{2}{\hbar}\sum_{a}^{N_{\mathrm{M}}}\sum_{b}^{N_{\mathrm{L}}}\boldsymbol{V}_{\mathrm{LM}}^{(b,a)}\,\mathrm{Im}\left\{\boldsymbol{\Theta}_{\mathrm{LM}}^{(b,a)}(t)\right\} - \frac{2}{\hbar}\sum_{a}^{N_{\mathrm{M}}}\sum_{b}^{N_{\mathrm{R}}}\boldsymbol{V}_{\mathrm{MR}}^{(a,b)}\,\mathrm{Im}\left\{\boldsymbol{\Theta}_{\mathrm{MR}}^{(a,b)}(t)\right\},\end{aligned} \tag{2.85}$$

where the boldface characters stand for the eigenstate representation of the respective operator. Here, N_{L}, N_{M}, and N_{R} stand for the total number of left lead, extended molecule, and right lead eigenstates. The first term of Eq. (2.85) does not vary the number of electrons within the extended molecule region and vanishes. The second term corresponds to the net probability influx from the left lead, while the last refers to the negative net probability outflux to the right lead. Averaging both, the in- and the outflux, and multiplying this expression by the elementary charge yields the total electric current passing the junction

$$I(t) = \frac{e}{\hbar}\sum_{a}^{N_{\mathrm{M}}}\left[\sum_{b}^{N_{\mathrm{L}}}\boldsymbol{V}_{\mathrm{LM}}^{(b,a)}\,\mathrm{Im}\left\{\boldsymbol{\Theta}_{\mathrm{LM}}^{(b,a)}(t)\right\} + \sum_{b}^{N_{\mathrm{R}}}\boldsymbol{V}_{\mathrm{MR}}^{(a,b)}\,\mathrm{Im}\left\{\boldsymbol{\Theta}_{\mathrm{MR}}^{(a,b)}(t)\right\}\right]. \tag{2.86}$$

In a steady-state, both terms are identical, i.e., the number of electrons flowing from the left lead to the extended molecule region is identical to the number of electrons flowing from the extended molecule region to the right lead.

2.3.3 The Non-Equilibrium Green's Function Formalism [143,186,187]

The DLvN approach represents a very straightforward and transparent method to describe explicitly time-dependent electron transport processes. However, the standard method to characterize steady-state currents for electronic transport processes is the above mentioned non-equilibrium Green's function (NEGF) formalism which will be described in the subsequent section, closely following Ref. [186].

The starting point for this approach is the complete, closed system, the Hamiltonian $\hat{H}_\mathrm{S}$ of which is equivalent to the Hamiltonian of the DLvN approach, cf. Eq. (2.79). The Green's function $\hat{G}$ of the system is defined as

$$(E - \hat{H}_\mathrm{S})\,\hat{G} = \hat{\mathbb{1}}$$
$$\begin{pmatrix} E-\hat{H}_\mathrm{L} & -\hat{V}_\mathrm{LM} & 0 \\ -\hat{V}_\mathrm{LM}^\dagger & E-\hat{H}_\mathrm{M} & -\hat{V}_\mathrm{RM}^\dagger \\ 0 & -\hat{V}_\mathrm{RM} & E-\hat{H}_\mathrm{R} \end{pmatrix} \begin{pmatrix} \hat{G}_\mathrm{L} & \hat{G}_\mathrm{LM} & \hat{G}_\mathrm{LR} \\ \hat{G}_\mathrm{ML} & \hat{G}_\mathrm{M} & \hat{G}_\mathrm{MR} \\ \hat{G}_\mathrm{RL} & \hat{G}_\mathrm{RM} & \hat{G}_\mathrm{R} \end{pmatrix} = \begin{pmatrix} \hat{\mathbb{1}}_\mathrm{L} & 0 & 0 \\ 0 & \hat{\mathbb{1}}_\mathrm{M} & 0 \\ 0 & 0 & \hat{\mathbb{1}}_\mathrm{R} \end{pmatrix}. \tag{2.87}$$

Accordingly, the Green's function for the extended molecule, which in this context is often referred to as scattering region or device, can be written as

$$\hat{G}_\mathrm{M} = (E - \hat{H}_\mathrm{M} - \hat{\Sigma}_\mathrm{L} - \hat{\Sigma}_\mathrm{R})^{-1}, \tag{2.88}$$

where the self-energy of the left and right lead describes the influence of the respective lead on the device and is given by $\hat{\Sigma}_\mathrm{L/R} = \hat{V}_\mathrm{LM/RM}^\dagger \hat{g}_\mathrm{L/R} \hat{V}_\mathrm{LM/RM}$ with the Green's function of the respective isolated lead $\hat{g}_\mathrm{L/R} = (E - \hat{H}_\mathrm{L/R})^{-1}$. The latter quantity can be straightforwardly calculated using iterative methods.[187–193] Eq. (2.88) illustrates that the Green's function formalism allows to circumvent the treatment of the full system by dividing the problem into smaller subproblems.

Consider a non-equilibrium situation, where both leads have different chemical potentials. The electrons which flow from the left lead into the device correspond, from the viewpoint of the isolated lead, to a wave function which is totally reflected at lead edge $|\psi_{\mathrm{L},n}\rangle$ with n being a quantum number. The resulting wave functions for the compound system responding to this incoming wave can be formulated as

$$\begin{aligned} |\psi_\mathrm{M}\rangle &= \hat{G}_\mathrm{M} \hat{V}_\mathrm{LM}^\dagger |\psi_{\mathrm{L},n}\rangle \\ |\psi_\mathrm{R}\rangle &= \hat{g}_\mathrm{R} \hat{V}_\mathrm{RM} \hat{G}_\mathrm{M} \hat{V}_\mathrm{LM}^\dagger |\psi_{\mathrm{L},n}\rangle \\ |\psi_\mathrm{L}\rangle &= (1 + \hat{g}_\mathrm{L} \hat{V}_\mathrm{LM} \hat{G}_\mathrm{M} \hat{V}_\mathrm{LM}^\dagger) |\psi_{\mathrm{L},n}\rangle. \end{aligned} \tag{2.89}$$

Assuming a steady-state condition and following the approach of Eqs. (2.84) and (2.85), the electric

current from the extended molecule to the right lead transported by $\left|\psi_{\mathrm{L},n}\right\rangle$ takes the form

$$\begin{aligned} I_{\mathrm{R}}^{(\mathrm{L},n)} &= -\frac{\imath e}{\hbar}\left(\left\langle\psi_{\mathrm{R}}\middle|\hat{V}_{\mathrm{RM}}\middle|\psi_{\mathrm{M}}\right\rangle - \left\langle\psi_{\mathrm{M}}\middle|\hat{V}_{\mathrm{MR}}\middle|\psi_{\mathrm{R}}\right\rangle\right) \\ &= -\frac{\imath e}{\hbar}\left\langle\psi_{\mathrm{L},n}\middle|\hat{V}_{\mathrm{LM}}\hat{G}_{\mathrm{M}}^{\dagger}\hat{V}_{\mathrm{RM}}^{\dagger}(\hat{g}_{\mathrm{R}}-\hat{g}_{\mathrm{R}}^{\dagger})\hat{V}_{\mathrm{RM}}\hat{G}_{\mathrm{M}}\hat{V}_{\mathrm{LM}}^{\dagger}\middle|\psi_{\mathrm{L},n}\right\rangle \\ &= \frac{e}{\hbar}\left\langle\psi_{\mathrm{L},n}\middle|\hat{V}_{\mathrm{LM}}\hat{G}_{\mathrm{M}}^{\dagger}\hat{\Gamma}_{\mathrm{R}}\hat{G}_{\mathrm{M}}\hat{V}_{\mathrm{LM}}^{\dagger}\middle|\psi_{\mathrm{L},n}\right\rangle \end{aligned} \tag{2.90}$$

with the broadening function $\hat{\Gamma}_{\mathrm{L/R}} = \imath\left(\hat{\Sigma}_{\mathrm{L/R}} - \hat{\Sigma}_{\mathrm{L/R}}^{\dagger}\right)$. A thermal population of all possible incoming waves yields

$$\begin{aligned} I_{\mathrm{R}} &= \frac{e}{\hbar}\int_{-\infty}^{\infty}\mathrm{d}E\ f_{\mathrm{L}}(E,\mu_{\mathrm{L}})\sum_{n}\delta(E-\varepsilon_n)\left\langle\psi_{\mathrm{L},n}\middle|\hat{V}_{\mathrm{LM}}\hat{G}_{\mathrm{M}}^{\dagger}\hat{\Gamma}_{\mathrm{R}}\hat{G}_{\mathrm{M}}\hat{V}_{\mathrm{LM}}^{\dagger}\middle|\psi_{\mathrm{L},n}\right\rangle \\ &= \frac{e}{\hbar}\int_{-\infty}^{\infty}\mathrm{d}E\ f_{\mathrm{L}}(E,\mu_{\mathrm{L}})\sum_{m,n}\delta(E-\varepsilon_n)\left\langle\psi_{\mathrm{L},n}\middle|\hat{V}_{\mathrm{LM}}\middle|m\right\rangle\left\langle m\middle|\hat{G}_{\mathrm{M}}^{\dagger}\hat{\Gamma}_{\mathrm{R}}\hat{G}_{\mathrm{M}}\hat{V}_{\mathrm{LM}}^{\dagger}\middle|\psi_{\mathrm{L},n}\right\rangle \\ &= \frac{e}{\hbar}\int_{-\infty}^{\infty}\mathrm{d}E\ f_{\mathrm{L}}(E,\mu_{\mathrm{L}})\sum_{m}\left\langle m\middle|\hat{G}_{\mathrm{M}}^{\dagger}\hat{\Gamma}_{\mathrm{R}}\hat{G}_{\mathrm{M}}\hat{V}_{\mathrm{LM}}^{\dagger}\left(\sum_{n}\delta(E-\varepsilon_n)\middle|\psi_{\mathrm{L},n}\right\rangle\left\langle\psi_{\mathrm{L},n}\middle|\right)\hat{V}_{\mathrm{LM}}\middle|m\right\rangle \\ &= \frac{e}{2\pi\hbar}\int_{-\infty}^{\infty}\mathrm{d}E\ f_{\mathrm{L}}(E,\mu_{\mathrm{L}})\mathrm{Tr}\left\{\hat{G}_{\mathrm{M}}^{\dagger}\hat{\Gamma}_{\mathrm{R}}\hat{G}_{\mathrm{M}}\hat{\Gamma}_{\mathrm{L}}\right\}. \end{aligned} \tag{2.91}$$

Here, the definition spectral function of the isolated left lead $\hat{a}_{\mathrm{L}} = 2\pi\sum_n \delta(E-\varepsilon_n)\left|\psi_{\mathrm{L},n}\right\rangle\left\langle\psi_{\mathrm{L},n}\right|$ is used to introduce the broadening function of the left lead $\hat{\Gamma}_{\mathrm{L}} = \hat{V}_{\mathrm{LM}}^{\dagger}\hat{a}_{\mathrm{L}}\hat{V}_{\mathrm{LM}}$ into Eq. (2.91). A final subtraction of the respective contributions for incoming waves from the right lead I_{L} results in the famous Landau-Büttiker formalism for the electric current

$$I = I_{\mathrm{R}} - I_{\mathrm{L}} = \frac{e}{h}\int_{-\infty}^{\infty}\mathrm{d}E\ \left[f_{\mathrm{L}}(E,\mu_{\mathrm{L}}) - f_{\mathrm{R}}(E,\mu_{\mathrm{R}})\right]T(E) \tag{2.92}$$

with the transmission $T(E) = \mathrm{Tr}\left\{\hat{G}_{\mathrm{M}}^{\dagger}\hat{\Gamma}_{\mathrm{R}}\hat{G}_{\mathrm{M}}\hat{\Gamma}_{\mathrm{L}}\right\}$.

2.4 The Electronic Continuity Equation

The last theory section is devoted to the introduction of the electronic continuity equation, which describes the connection between the electron density $\rho_{\mathrm{el}}(\vec{r},t)$ and the electronic flux density $\vec{j}_{\mathrm{el}}(\vec{r},t)$. This fundamental relation allows for the intuitive interpretation of the electron density as a conserved probability fluid.

Consider the coherent dynamics of a molecular system evolving freely from an initial state. In position representation, the Liouville-von Neumann equation describing this scenario is given by

$$\begin{aligned}\Big\langle \boldsymbol{r},\boldsymbol{R}\Big|\frac{\partial}{\partial t}\hat{\Theta}(t)\Big|\boldsymbol{r},\boldsymbol{R}\Big\rangle &= -\frac{\imath}{\hbar}\Big\langle \boldsymbol{r},\boldsymbol{R}\Big|\Big[\hat{H}_{\mathrm{mol}}(\boldsymbol{r},\boldsymbol{R}),\hat{\Theta}(t)\Big]\Big|\boldsymbol{r},\boldsymbol{R}\Big\rangle \\ &= -\frac{\imath}{\hbar}\Big(\Big\langle \boldsymbol{r},\boldsymbol{R}\Big|\hat{T}_{\mathrm{nuc}}(\boldsymbol{R})\hat{\Theta}(t)\Big|\boldsymbol{r},\boldsymbol{R}\Big\rangle - \Big\langle \boldsymbol{r},\boldsymbol{R}\Big|\hat{\Theta}(t)\hat{T}_{\mathrm{nuc}}(\boldsymbol{R})\Big|\boldsymbol{r},\boldsymbol{R}\Big\rangle \\ &\quad + \Big\langle \boldsymbol{r},\boldsymbol{R}\Big|\hat{T}_{\mathrm{el}}(\boldsymbol{r})\hat{\Theta}(t)\Big|\boldsymbol{r},\boldsymbol{R}\Big\rangle - \Big\langle \boldsymbol{r},\boldsymbol{R}\Big|\hat{\Theta}(t)\hat{T}_{\mathrm{el}}(\boldsymbol{r})\Big|\boldsymbol{r},\boldsymbol{R}\Big\rangle \\ &\quad + \Big\langle \boldsymbol{r},\boldsymbol{R}\Big|\hat{V}_{\mathrm{coul}}(\boldsymbol{r},\boldsymbol{R})\hat{\Theta}(t)\Big|\boldsymbol{r},\boldsymbol{R}\Big\rangle - \Big\langle \boldsymbol{r},\boldsymbol{R}\Big|\hat{\Theta}(t)\hat{V}_{\mathrm{coul}}(\boldsymbol{r},\boldsymbol{R})\Big|\boldsymbol{r},\boldsymbol{R}\Big\rangle\Big),\end{aligned} \tag{2.93}$$

where the last line vanishes, since the Coulomb operator is a multiplicative operator in position representation. Applying the basic operator definitions introduced in Eqs. (2.2) and (2.3) and the ansatz $\hat{\Theta}(t) = \big|\Phi_{\mathrm{tot}}(t)\big\rangle\big\langle\Phi_{\mathrm{tot}}(t)\big|$, for a pure state, the quantum mechanical total continuity equation is defined as

$$\begin{aligned}&\frac{\partial}{\partial t}\Big|\Phi_{\mathrm{tot}}(\boldsymbol{r},\boldsymbol{R},t)\Big|^2 \\ &\quad= -\sum_A^M \vec{\nabla}_{\vec{R}_A}\cdot\left[-\frac{\imath\hbar}{2M_A}\Big(\Phi^\dagger_{\mathrm{tot}}(\boldsymbol{r},\boldsymbol{R},t)\vec{\nabla}_{\vec{R}_A}\Phi_{\mathrm{tot}}(\boldsymbol{r},\boldsymbol{R},t) - \Phi_{\mathrm{tot}}(\boldsymbol{r},\boldsymbol{R},t)\vec{\nabla}_{\vec{R}_A}\Phi^\dagger_{\mathrm{tot}}(\boldsymbol{r},\boldsymbol{R},t)\Big)\right] \\ &\quad\quad -\sum_k^N \vec{\nabla}_{\vec{r}_k}\cdot\left[-\frac{\imath\hbar}{2m_e}\Big(\Phi^\dagger_{\mathrm{tot}}(\boldsymbol{r},\boldsymbol{R},t)\vec{\nabla}_{\vec{r}_k}\Phi_{\mathrm{tot}}(\boldsymbol{r},\boldsymbol{R},t) - \Phi_{\mathrm{tot}}(\boldsymbol{r},\boldsymbol{R},t)\vec{\nabla}_{\vec{r}_k}\Phi^\dagger_{\mathrm{tot}}(\boldsymbol{r},\boldsymbol{R},t)\Big)\right].\end{aligned} \tag{2.94}$$

Note that the spin-free representation is used throughout the whole section. Integrating over all nuclear degrees of freedom and all but one electronic coordinate and utilizing the divergence theorem results in the electronic continuity equation

$$\frac{\partial}{\partial t}\rho_{\mathrm{el}}(\vec{r},t) = -\vec{\nabla}_{\vec{r}}\cdot\vec{j}_{\mathrm{el}}(\vec{r},t) \tag{2.95}$$

which describes the probability conservation maintained by the electron density $\rho_{\mathrm{el}}(\vec{r},t)$ and the electronic flux density $\vec{j}_{\mathrm{el}}(\vec{r},t)$. Incidentally, multiplying Eq. (2.95) by the elementary charge yields the continuity equation for charge conservation connecting the temporal variation of the electronic charge density, $e\cdot\rho_{\mathrm{el}}(\vec{r},t)$, with the spatial variation of the electronic current density, $e\cdot\vec{j}_{\mathrm{el}}(\vec{r},t)$. Among other things, this relation is used to obtain the current $I(t)$ within the framework of the DLvN and

the NEGF formalism.

Let the system's wave function be defined by a Born-Huang expansion, cf. Eq. (2.6), where the electronic part has been solved within the clamped nuclei approximation. The corresponding density matrix operator is given by

$$\hat{\Theta}(t) = \sum_{\lambda,\nu} \left|\Psi^{(\lambda)}\right\rangle \left|\chi^{(\lambda)}(t)\right\rangle \left\langle\chi^{(\nu)}(t)\right| \left\langle\Psi^{(\nu)}\right|, \tag{2.96}$$

and thus, the time-derivative of the electron density, which we will refer to as electron flow, takes the form

$$\frac{\partial}{\partial t}\rho_{\mathrm{el}}(\vec{r},t) = \sum_{\lambda,\nu} \int \mathrm{d}\boldsymbol{R}\; \rho_{\mathrm{el}}^{(\lambda,\nu)}(\vec{r};\boldsymbol{R})\; \frac{\partial}{\partial t}\rho_{\mathrm{nuc}}^{(\lambda,\nu)}(\boldsymbol{R},t) \tag{2.97}$$

with the time-dependent nuclear and the time-independent electronic transition density between the electronic states λ and ν

$$\rho_{\mathrm{nuc}}^{(\lambda,\nu)}(\boldsymbol{R},t) = \left(\chi^{(\nu)}(\boldsymbol{R},t)\right)^{\dagger} \chi^{(\lambda)}(\boldsymbol{R},t) \tag{2.98}$$

$$\rho_{\mathrm{el}}^{(\lambda,\nu)}(\vec{r};\boldsymbol{R}) = \int\cdots\int \mathrm{d}\vec{r}_2 \cdots \mathrm{d}\vec{r}_N\; \Psi^{(\nu)}(\boldsymbol{r},\boldsymbol{R})\Psi^{(\lambda)}(\boldsymbol{r},\boldsymbol{R}). \tag{2.99}$$

For clarity, the normalization constant of the electronic transition density is assumed to be incorporated into the electronic wave function, cf. Eq. (2.22).

The right-hand side of Eq. (2.95) describes the spatial variation of the electronic flux density. This fundamental quantity intuitively describes the spatially resolved instantaneous flow of electrons and has the general form

$$\vec{j}_{\mathrm{el}}(\vec{r},t) = \sum_{\lambda,\nu} \int \mathrm{d}\boldsymbol{R}\; \rho_{\mathrm{nuc}}^{(\lambda,\nu)}(\boldsymbol{R},t)\; \vec{j}_{\mathrm{el}}^{(\lambda,\nu)}(\vec{r};\boldsymbol{R}). \tag{2.100}$$

Here, the time-independent electronic transition flux density from state λ and state ν reads

$$\vec{j}_{\mathrm{el}}^{(\lambda,\nu)}(\vec{r};\boldsymbol{R}) = -\frac{i\hbar}{2m_e} \int\cdots\int \mathrm{d}\vec{r}_2 \cdots \mathrm{d}\vec{r}_N\; \left(\Psi^{(\nu)}(\boldsymbol{r},\boldsymbol{R})\vec{\nabla}_{\vec{r}}\,\Psi^{(\lambda)}(\boldsymbol{r},\boldsymbol{R}) - \Psi^{(\lambda)}(\boldsymbol{r},\boldsymbol{R})\vec{\nabla}_{\vec{r}}\,\Psi^{(\nu)}(\boldsymbol{r},\boldsymbol{R})\right). \tag{2.101}$$

As a direct consequence of the clamped nuclei approximation, the adiabatic electronic flux density, i.e., the diagonal terms of Eq. (2.101), vanishes, since the electronic states are real-valued. This unphysical phenomenon is a long-known issue,[152] and so far, only a few approaches have been proposed to circumvent this drawback.[18,70–78, B3] One of which, the Born-Oppenheimer broken-symmetry ansatz, has been developed within this dissertation and is published in **Paper B3**. This paper also features a more detailed view on this problem.

Interestingly, the electronic current density is the integrand of the electronic dipole moment in

velocity gauge. For the time-independent transition electronic current density between two electronic states, it is defined as

$$\mu_{\mathrm{el,v}}^{(\lambda,\nu)}(\boldsymbol{R}) = -e \int \mathrm{d}\vec{r}\; \vec{j}_{\mathrm{el}}^{(\lambda,\nu)}(\vec{r};\boldsymbol{R}). \tag{2.102}$$

The corresponding quantity in length gauge is given in terms of the charge density by

$$\mu_{\mathrm{el,r}}^{(\lambda,\nu)}(\boldsymbol{R}) = -e \int \mathrm{d}\vec{r}\; \vec{r} \cdot \rho_{\mathrm{el}}^{(\lambda,\nu)}(\vec{r};\boldsymbol{R}), \tag{2.103}$$

The dipole moments in both gauges are related via[194]

$$\left(\mu_{\mathrm{el,v}}^{(\lambda,\nu)}(\boldsymbol{R})\right)_{\mathrm{r}} = \frac{\imath\hbar}{\left(E_{\mathrm{el}}^{(\nu)}(\boldsymbol{R}) - E_{\mathrm{el}}^{(\lambda)}(\boldsymbol{R})\right)} \mu_{v,\mathrm{el}}^{(\lambda,\nu)}(\boldsymbol{R}) \tag{2.104}$$

Eq. (2.104) represents a valuable tool to estimate the convergence of high-level quantum chemistry calculations.[D1,B1]

Chapter 3

Publications

The following chapter contains the scientific papers published in the context of this thesis. These publications are ordered thematically, belonging to three main topics: **A** the investigation of charge migration processes in superposition states of benzene, **B** method development for the computation of the electronic flux density, and **C** the analysis of field-driven electron dynamics in nanojunctions. For each publication, the contributions by the individual authors are outlined.

Paper A1

"Multidirectional Angular Electronic Flux during Adiabatic Attosecond Charge Migration in Excited Benzene"

G. Hermann, C. Liu, J. Manz, B. Paulus, J. F. Pérez-Torres, V. Pohl, and J. C. Tremblay

J. Phys. Chem. A **120**, 5360–5369 (2016)

DOI: 10.1021/acs.jpca.6b01948

URL: http://dx.doi.org/10.1021/acs.jpca.6b01948

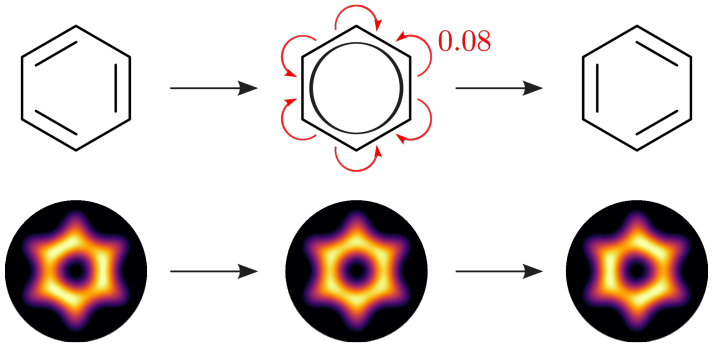

Figure 3.1: Graphical Abstract. Reprint with permission from Hermann et al.[A1] (©2016 American Chemical Society)

Author contributions

The conception of this work and the methodology were conceived by Jörn Manz and Jhon Fredy Pérez-Torres. Jhon Fredy Pérez-Torres did preliminary CI calculations and ChunMei Liu prepared preliminary results for the novel methodology. Preliminary figures to visualize those results were prepared by ChunMei Liu and Jhon Fredy Pérez-Torres. I performed the CASSCF calculations, which are presented in the final version of the paper, with input from Beate Paulus and Jean Christophe Tremblay. Gunter Hermann and I, in equal parts, did the final implementation of the methodology and prepared the final results. The final data visualization was done by Gunter Hermann and myself with input from all other coauthors. All coauthors discussed the final results. The manuscript was predominantly written by Jörn Manz. All coauthors contributed to the final version of this manuscript.

Paper A2

"Attosecond Angular Flux of Partial Charges on the Carbon Atoms of Benzene in Non-Aromatic Excited State"

G. Hermann, C. Liu, J. Manz, B. Paulus, V. Pohl, and J. C. Tremblay

Chem. Phys. Lett. **683**, 553–558 (2017)

DOI: 10.1016/j.cplett.2017.01.030

URL: http://dx.doi.org/10.1016/j.cplett.2017.01.030

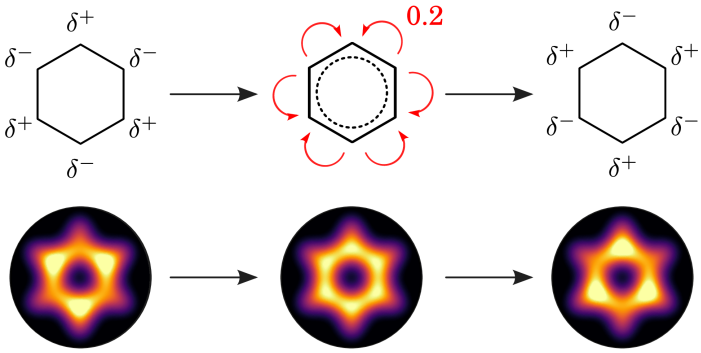

Figure 3.2: Graphical Abstract. Reprint with permission from Hermann et al.[A2] (©2017 Elsevier B.V. All rights reserved.)

Author contributions

The idea behind this work was conceived by Jörn Manz. I performed the CASSCF calculations with input from Beate Paulus and Jean Christophe Tremblay. ChunMei Liu applied the methodology of **Paper A1** and prepared results for the comparison to the new improved methodology. Gunter Hermann and I together with Jean Christophe Tremblay developed DETCI@ORBKIT.[B1] Based on this program Gunter Hermann and I, in equal parts, implemented the new improved methodology, and prepared the final results. We additionally did the final data visualization with input from all other coauthors. The first version of the manuscript was written by Jörn Manz. All coauthors contributed to the final version of this manuscript.

Paper A3

"Quantum Control of Electronic Fluxes during Adiabatic Attosecond Charge Migration in Degenerate Superposition States of Benzene"

D. Jia, J. Manz, B. Paulus, V. Pohl, J. C. Tremblay, and Y. Yang

Chem. Phys. **482**, 146–159 (2017)

DOI: 10.1016/j.chemphys.2016.09.021

URL: http://dx.doi.org/10.1016/j.chemphys.2016.09.021

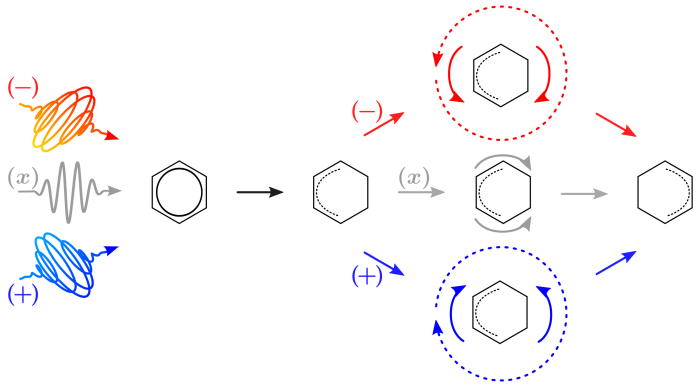

Figure 3.3: Graphical Abstract. Reprint with permission from Jia et al.[A3] (©2016 Elsevier B.V. All rights reserved.)

Author contributions

The idea behind this work was conceived by Jörn Manz. I performed the CASSCF calculations with input from Beate Paulus and Jean Christophe Tremblay. The optimization of the laser pulse for the state-selective excitation of different degenerate superposition states of benzene was done by Dongming Jia and Yonggang Yang. I used DETCI@ORBKIT[B1] and applied the methodology of **Paper A1** and **Paper A2** to prepare the remaining results. The graphical representation of those results was also done by myself. The mechanistic interpretation was done by Jean Christophe Tremblay and myself with very helpful input from Gunter Hermann and Jörn Manz. The first version of the manuscript was written by Jörn Manz. All coauthors contributed to the final version of this manuscript.

Paper B1

"An Open-Source Framework for Analyzing N-Electron Dynamics. I. Multideterminantal Wave Functions"

V. Pohl, G. Hermann, and J. C. Tremblay

J. Comput. Chem. **38**, 1515–1527 (2017)

DOI: 10.1002/jcc.24792

URL: http://dx.doi.org/10.1002/jcc.24792

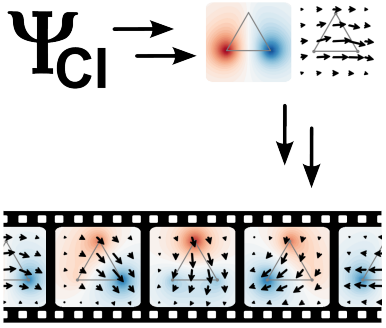

Figure 3.4: Graphical Abstract. Reprint with permission from Pohl et al.[B1] (©2017 Wiley Periodicals, Inc.)

Author contributions

Based on ORBKIT (cf. **Paper D2**), a rudimentary precursor version of the program detCI@ORBKIT was developed by Gunter Hermann and myself, in equal parts, during the preparation of **Paper D1** under the supervision of Jhon Fredy Pérez Torres. The final version was programed by Gunter Hermann and myself, in equal parts, after the preparation of **Paper A1** to enable the new methodology presented in **Paper A2** and **Paper A3**. The derivation of the algorithms was also done by us together with Jean Christophe Tremblay. I performed the Full CI and the CASSCF calculations and programmed the interfaces to the respective quantum chemical programs (PSI4[195] and MOLPRO[196]) with detCI@ORBKIT. Gunter Hermann and I processed the quantum chemical data and prepared the figures for visualizing the results. The manuscript was written by Gunter Hermann with considerable input from Jean Christophe Tremblay and myself.

Paper B2

"An Open-Source Framework for Analyzing N-Electron Dynamics. II. Hybrid Density Functional Theory/Configuration Interaction Methodology"

G. Hermann, V. Pohl, and J. C. Tremblay

J. Comput. Chem. **38**, 2378–2387 (2017)

DOI: 10.1002/jcc.24896

URL: http://dx.doi.org/10.1002/jcc.24896

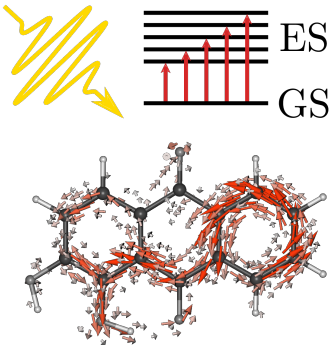

Figure 3.5: Graphical Abstract. Reprint with permission from Hermann et al.[B2] (©2017 Wiley Periodicals, Inc.)

Author contributions

The initial idea for the hybrid DFT/CI methodology was conceived by Jean Christophe Tremblay. Gunter Hermann and I implemented this approach into the framework of the program DETCI@ORBKIT. Gunter Hermann performed the TD-DFT calculations and interfaced the respective quantum chemical programs, i.e., TURBOMOLE[197] and GAMESS (US),[198] to DETCI@ORBKIT. Gunter Hermann and I processed the quantum chemical data and prepared the figures for visualizing the results. The manuscript was written by Jean Christophe Tremblay and Gunter Hermann with input from myself.

Paper B3

"Adiabatic Electronic Flux Density: A Born-Oppenheimer Broken-Symmetry Ansatz"

V. Pohl and J. C. Tremblay

Phys. Rev. A **93**, 012504 (2016)

DOI: 10.1103/PhysRevA.93.012504

URL: http://dx.doi.org/10.1103/PhysRevA.93.012504

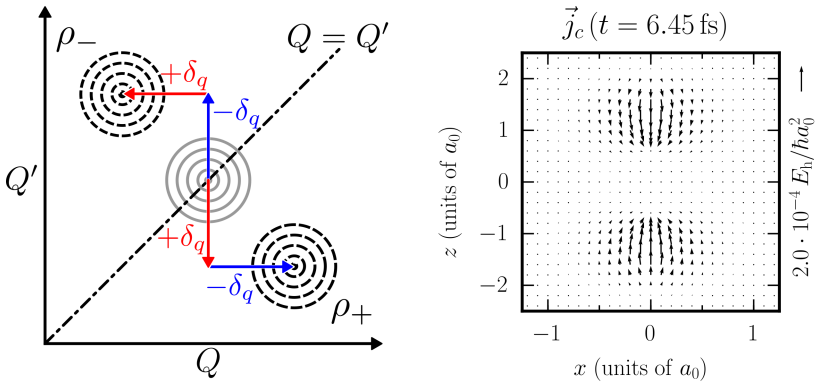

Figure 3.6: Graphical Abstract. Produced exclusively for this dissertation using figures from Paper B3.

Author contributions

The general concept behind the Born-Oppenheimer broken symmetry ansatz was conceived by Jean Christophe Tremblay. Jean Christophe Tremblay and I together did the subsequent derivation of this ansatz. I did the implementation of this ansatz, performed the numerical simulations, and prepared the figures for visualizing the results. Jean Christophe Tremblay and I wrote the manuscript in equal parts.

Paper C1

"Field-Induced Conformational Change in a Single-Molecule-Graphene–Nanoribbon Junction: Effect of Vibrational Energy Redistribution"

V. Pohl and J. C. Tremblay

J. Phys. Chem. C **120**, 28808–28819 (2016)

DOI: 10.1021/acs.jpcc.6b09682

URL: http://dx.doi.org/10.1021/acs.jpcc.6b09682

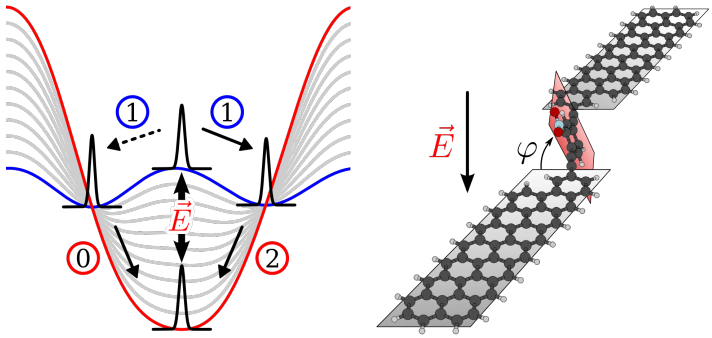

Figure 3.7: Graphical Abstract. Reprint with permission from Pohl et al.[C1] (©2016 American Chemical Society)

Author contributions

The project was initially conceived by Jean Christophe Tremblay and myself. Jean Christophe Tremblay derived the model for dissipation with considerable input from myself. I performed all numerical simulations and worked out the implementation. The manuscript was written by myself with significant input from Jean Christophe Tremblay.

Paper C2

"Electronic Flux Density Maps Reveal Unique Current Patterns in a Single-Molecule-Graphene–Nanoribbon Junction"

V. Pohl, L. E. Marsoner Steinkasserer, and J. C. Tremblay

arXiv preprint arXiv:1707.07635 (2017)

URL: https://arxiv.org/abs/1707.07635 (2017)

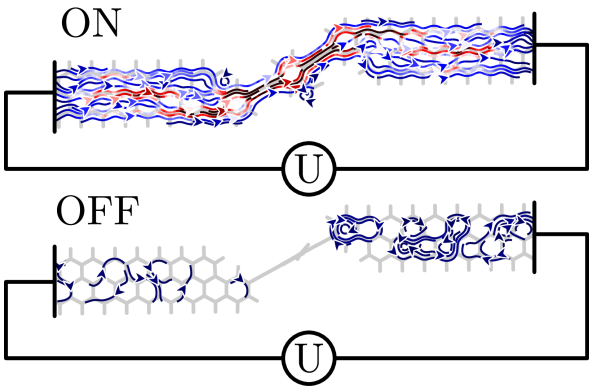

Figure 3.8: Graphical Abstract. Reprint with permission from Pohl et al.[C2]

Author contributions

The project was initially conceived by myself. Jean Christophe Tremblay proposed the novel localization scheme and the tight-binding scheme, and I proposed the route to compute electronic flux density. The derivation of the theoretical framework was done by Jean Christophe Tremblay and myself in equal parts. I implemented the localization scheme and the driven Liouville-von Neumann formalism and performed the dynamical simulations. Lukas Eugen Marsoner Steinkasserer and I, in equal parts, implemented the current-voltage characteristics into ASE.[199,200] Together we performed the NEGF reference calculations. All coauthors discussed and interpreted the results. The manuscript was written by myself with input from Jean Christophe Tremblay and Lukas Eugen Marsoner Steinkasserer.

Chapter 4

Summary

The primary goal of this dissertation was to gain deeper insight into the mechanistic details of electronic motion during various processes. For this reason, a main focus was the development of versatile methods for the analysis and visualization of N-electron dynamics with an emphasis on the components of the electronic continuity equation. This methodological framework was then used, among others, for quantitative investigations of attosecond charge migration processes in different electronic superposition states of the benzene molecule, and for the mechanistic study of the dynamics of electron transport through a single-molecule-graphene-nanoribbon junction driven by chemical potentials.

Ulusoy and Nest[13] have demonstrated that the aromaticity of oriented benzene can be controlled by well-designed laser pulses. They applied optimal control theory to selectively populate two non-aromatic electronic superposition states of benzene: one superposition state with equal populations in the electronic ground $S_0(1^1A_{1g})$ and the first excited state $S_1(1^1B_{2u})$ and another with equal populations in the electronic ground and the second excited state $S_2(1^1B_{1u})$. The respective bond orders and Mulliken charges were used as a measure for the aromaticity, and they revealed that the electron density of these superposition states is partially localized on alternating bonds for the $S_0 + S_1$, or on alternating atoms for the $S_0 + S_2$ case. While the former resembles the typically sketched non-aromatic Kekulé structures (see Fig. 4.1a), the latter corresponds to a situation, where the carbon atoms show alternating partial charges (see Fig. 4.1b). Both localizations result in periodic charge migration between the two possible localization patterns as shown in Figs. 4.1a and 4.1b.

In **Paper A1** and **Paper A2**, we investigated the mechanisms of both charge migration processes. Here, we adapted a methodology originally developed for the study of concerted electronic and nuclear fluxes during coherent tunneling,[18] and reformulated this ansatz for charge migration processes.[A1] This new methodology allows to compute the one-dimensional electronic probability flux from the

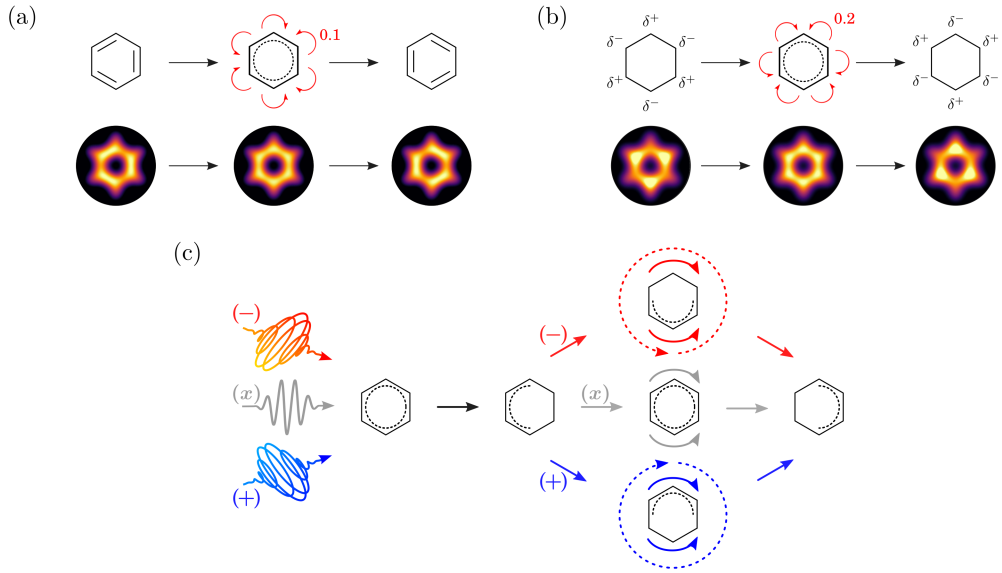

Figure 4.1: Mechanistic studies of the attosecond charge migration in different superposition states of the benzene molecule. (a,b) The time evolution of the electron density (lower row) and the associated Lewis structures of (a) the $S_0(1^1A_{1g}) + S_1(1^1B_{2u})$ and (b) the $S_0(1^1A_{1g}) + S_2(1^1B_{1u})$ superposition state of the benzene molecule. The red arrows highlight the charge migration mechanisms. Each arrow corresponds to the motion of (a) 0.1 and (b) 0.2 electrons. (c) Demonstration of the control of the charge migration mechanism. By varying the polarization of the laser pulses, different superposition stats of the 1^1A_{1g} electronic ground state and the degenerate 1^1E_{1u} excited state are populated. While the initial and final electron distribution is identical, the charge migration mechanisms are qualitatively different. The Lewis structures correspond to representative snapshots of the time evolution of the electron density of the respective charge migration processes. From left to right: before the preparation, at $t = 0$, $t = \bar{\tau}/4$, and $t = \bar{\tau}/2$, where $\bar{\tau} = 504\,\text{as}$ is the period. The arrows highlight the charge migration mechanisms. These depictions are adapted from Papers A1–A3.

electronic probability density by exploiting symmetry conditions and the electronic continuity equation. The electronic flux is an insightful quantity allowing one to make quantitative mechanistic statements for charge migration. This is illustrated in the first applications of this methodology.[A1,A2] Based on state-averaged CASSCF(6,6) calculations for the wave functions and additional MRCI singles and doubles calculations for the excitation energies, we determined the angular electronic fluxes for the $S_0 + S_1$ and the $S_0 + S_2$ superposition state. While the calculations in **Paper A1** were restricted to using the dominant Slater determinant, the development of our new program DETCI@ORBKIT[B1,B2] allowed us to consider the full wave functions in follow-up **Paper A2**. Here, we found that, although the charge migration mechanisms stayed unchanged, the renormalization slightly changed the magnitude of the flux.

As graphically summarized in Figs. 4.1a and 4.1b, the two scenarios S_0+S_1 and S_0+S_2 exhibit some interesting characteristics: The localization patterns vary periodically with a period in the attosecond time regime, i.e., $\bar{\tau} = 830\,\text{as}$ and $\bar{\tau} = 590\,\text{as}$. The dynamics is mediated by a flux following a pincer-type motion with the sources and the sinks for fluxes at the bond centers for $S_0 + S_1$ and at the atoms for S_0+S_2. This confirms the working hypothesis of Ulusoy and Nest for the S_0+S_1 superposition state.[13]

Furthermore, we found that the maximum number of electrons flowing during the charge migration process is $N_f = 6 \times 0.12 = 0.72$ and $N_f = 6 \times 0.2 = 1.2$, respectively. Remarkably, these numbers are significantly smaller than the six electrons implied by the simple traditional model of oscillating the Lewis structures. This discovery is mainly caused by the delocalization of the electrons which enables the formation of a new bond while requiring only a small reorganization of the electrons. Broadly speaking, our methodology may be seen as a frist-principles numerical pendant to the traditional Lewis structure based model.

In **Paper A3**, we demonstrated quantum control of attosecond charge migration. We designed resonant linearly and circularly polarized $\pi/2$-laser pulses to selectively populate four different degenerate superposition states with equal population in the electronic ground and one of four degenerate excited states. These excited states include complex-valued linear combinations of the two components of the 1^1E_{1u} state. The dipole-allowed transitions induce charge migration with a period of $\bar{\tau} = 504\,\text{as}$ which we subsequently investigated with our methodology. Analysis of the angular electronic fluxes revealed that similar initial conditions, i.e., a partial localization of the density on one side of the molecule, created from different pulses yielded widely different mechanisms for the charge migration process. For the laser excitations with linearly polarized light, there were fixed sources and sinks on opposite sides of the ring and the fluxes followed a pincer-type motion. For the laser excitations with circularly polarized light, the sources and sinks rotated as a function of time and the flux mechanism was more involved. Although from the perspective of the electron density, the localization rotates clockwise or anti-clockwise, the flux still follows the pincer-type mechanism which itself undergoes an overall rotation. In conclusion, while three of the four degenerate superposition states show exactly the same initial and final electron distribution, the attosecond charge migration proceeds via an entirely different mechanism. This is illustrated in Fig. 4.1c.

Although the procedure presented in **Papers A1–A3** is very powerful and allows for quantitative statements deduced from the electron density, sophisticated symmetry arguments were required to unravel the exact mechanisms of the charge migration processes, and more importantly, the approach is not applicable to every system. However, this procedure can be circumvented by regarding a complementary quantity: the electronic flux density (not to be confused with the electronic flux). Being related to the electron density via the continuity equation, the electronic flux density is a vector field describing the instantaneous flow of electrons. It gives an intuitive picture of the electronic motion and allows for mechanistic insights at a single glance. This promising perspective motivated us to develop a program that is capable of computing this quantity and further, to benchmark the applicability of the flux density for the analysis of charge migration processes. In **Paper B1**, we presented

detCI@ORBKIT, our new general open-source framework to analyze and visualize N-electron dynamics. This new program extends our recently published post-processing Python library ORBKIT[D2] to determinant-based configuration interaction wave functions. While requiring only the output of standard quantum chemistry programs, detCI@ORBKIT is capable of computing various one-electron properties, such as the electron density, the electronic flux density, other derived observables, and their analytical integrals, allowing for a balanced study of charge migration processes. The modular structure of detCI@ORBKIT allows to straightforwardly implement other (non-standard) quantities. This opportunity was used in **Paper A2** and **Paper A3** to improve the methodology of **Paper A1** to consider the full wave functions, which significantly enhanced the quality of the results. In the second part of **Paper B1**, we applied detCI@ORBKIT to a few benchmark systems: the trihydrogen cation and the lithium hydride molecule. We initiated a charge migration process by preparing superposition states. Our proposed analysis toolset combined with different visualization techniques provided deep insight into mechanistic details. Here, especially the electronic flux density has proven as valuable tool allowing for an intuitive interpretation of the charge migration mechanism. The last part of **Paper B1** focused on the convergence of the electronic flux density. By comparing the electron flow, i.e., the time derivative of the electron density, with the divergence of the electronic flux density, the basis set convergence was benchmarked for full CI calculations of the trihydrogen cation. The convergence with respect to the electronic structure theory method was then tested with CI singles, RAS-CI, CASSCF, and full CI calculations for the lithium hydride molecule. While the qualitative features of the electronic flux density turned out to be very robust with respect to the method and the atomic basis set, except for the minimal basis set, the quantitative convergence appeared to be quite slow. Thus, for quantitative statements concerning the flux of electrons, the focus of the analysis should be laid on the electron density and derived quantities, as done in **Papers A1**–**A3**. For mechanistic studies, the electronic flux density is preferable.

With increasing system size, the computational effort of the high-level wave function-based quantum chemical treatment required for the mechanistic study of charge migration processes quickly becomes prohibitively large. For this purpose, we presented a hybrid density functional theory/configuration interaction methodology in **Paper B2**. In this novel procedure, which complements the functionalities of detCI@ORBKIT, we proposed to use LR-TDDFT calculations to generate a basis of pseudo-CI vectors and energies to describe the N-electron dynamics. While retaining the simple picture of a CI singles wave function, the energetic description of the system can be significantly improved at about the cost of a CI singles calculation. In **Paper B2**, the applicability of this approach was demonstrated for the lithium hydride molecule. Here, we benchmarked results on the B2-PLYP level of theory against CI

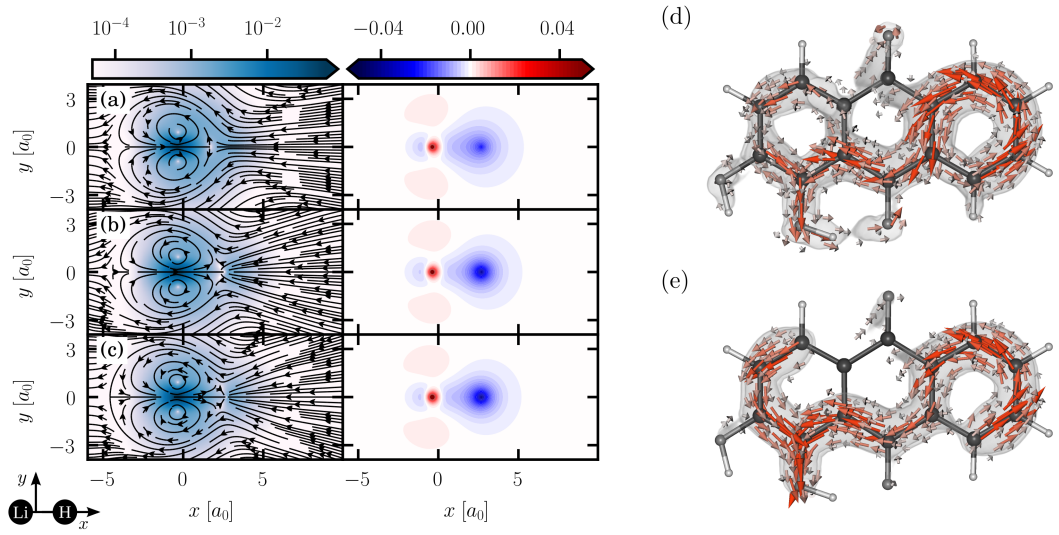

Figure 4.2: (a-c) Representative snapshot of the electronic flux density (left panels, in units of $E_\mathrm{h}/\hbar a_0^2$) and the difference density (right panels, in units of $1/a_0^3$) for the charge migration in the lithium hydride molecule applying different quantum chemical methods: (a) full CI, (b) CI singles, and (c) hybrid TDDFT/CI singles methodology on the B2-PLYP level of theory. (e,f) Representative snapshot of the electronic flux density in the alizarin molecule after a broadband laser excitation applying the hybrid TDDFT/CI singles methodology on the B3LYP level of theory. Two thresholds are applied to the pseudo-CI basis: (e) $|D_a^{r(\lambda)}| > 10^{-3}$ and (f) $|D_a^{r(\lambda)}| > 10^{-1}$. The vectors are colored according to their magnitude, and the grey isosurface corresponds to the magnitude $3 \cdot 10^{-4} E_\mathrm{h}/\hbar a_0^2$. These depictions are adapted from Paper B2.

singles and full CI reference calculations.[B1] The results are depicted in Figs. 4.2a–4.2c, and two main conclusions can be drawn: Firstly, as expected, a good choice of functional can improve the energetic description to almost the full CI reference, and secondly, the character of the pseudo-CI wave function is very similar to the CI singles reference wave function. Accordingly, as for the CI singles calculations, the respective observables agree semi-quantitatively with the full CI reference. In order to demonstrate the scalability of our approach, we simulate a broadband laser excitation in an alizarin molecule. Once again, the flux density directly gives valuable insights into the charge migration mechanism, as can be seen from the representative snapshot depicted in Fig. 4.2d. To further improve the scalability, we tested a truncation of the pseudo-CI basis (cf., Figs. 4.2d and 4.2e) and proved that except for minor features, the electronic flux density is very robust even for very stringent threshold values. This strategy extends the scope of our method for reconstructing the electronic flux density to larger, even nanoscale systems.

Clearly, the electronic flux density is a potentially very useful tool for visualizing electron dynamics. Unfortunately, for vibrational nuclear quantum dynamics in the electronic ground state, this quantity vanishes, since in the Born-Oppenheimer approximation, the electrons are always in a real-valued stationary state. In **Paper B3**, we illuminated this counterintuitive result in detail. Starting from the Liouville-von Neumann equation, we tried to derive the electronic continuity equation following two

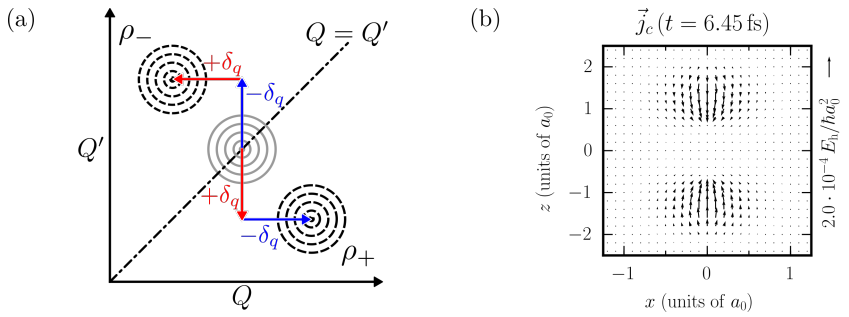

Figure 4.3: (a) Conceptual sketch of the Born-Oppenheimer broken symmetry (BOBS) ansatz. The density matrix is translated pairwise anti-symmetrically in the nuclear configuration space. (b) Representative snapshot of the electronic flux density of the hydrogen molecular ion H_2^+ vibrating in its electronic ground state $^2\Sigma_g^+$ computed with the BOBS ansatz. These depictions are adapted from Paper B3.

different routes — yielding two contradictory results. To resolve this issue and to restore the intuitive picture of electrons following the nuclei, we proposed to correlate the electronic with the nuclear motion by translating the density matrix pairwise anti-symmetrically in the nuclear configuration space, as sketched in Fig. 4.3a. Our novel Born-Oppenheimer broken symmetry (BOBS) ansatz yields a unique definition of an electronic flux density. By varying the so-called correlation length, i.e., the length of the translation, this real-valued electronic flux density can be forced to approximately fulfill the electronic continuity equation. Certainly, applying a translation operator to the density matrix in position space can be computationally very demanding. Thus, in a further step, we introduced a Taylor series expansion to second order to our BOBS ansatz, where the correlation length only acts as a linear parameter. This is computationally significantly more efficient while yielding nearly the same results as the non-linear BOBS ansatz. Additionally, the Taylor series expansion revealed very interesting connections to non-adiabatic couplings. When comparing our BOBS ansatz in the non-linear form to the time-shift flux of Okuyama and Takatsuka,[74] it becomes clear that both approaches follow the same idea. Specifically, the time-shift flux arises from a time delay, which can be interpreted as a spatial translation in the nuclear configuration space in the context of ab-initio molecular dynamics. In contrast, applying a time delay in quantum dynamics leads to a vanishing flux density. Concerning our BOBS ansatz in the linearized form, it can be shown that the formula for the electronic flux density is equivalent to the formula derived by Diestler[77] following a completely different, considerably more complex route involving excited states and perturbation theory. Consequently, all three approaches, the BOBS ansatz, the time-shift flux, and the perturbative approach by Diestler, are closely related. On the other hand, only the BOBS ansatz gives access to an approximate electronic continuity, and thus, provides an error estimate for the quality of the mechanistic predictions.

In the subsequent part of **Paper B3**, we applied our BOBS ansatz to the hydrogen molecular ion H_2^+ vibrating in its electronic ground state $^2\Sigma_g^+$, since for this particular scenario, non-Born-Oppenheimer

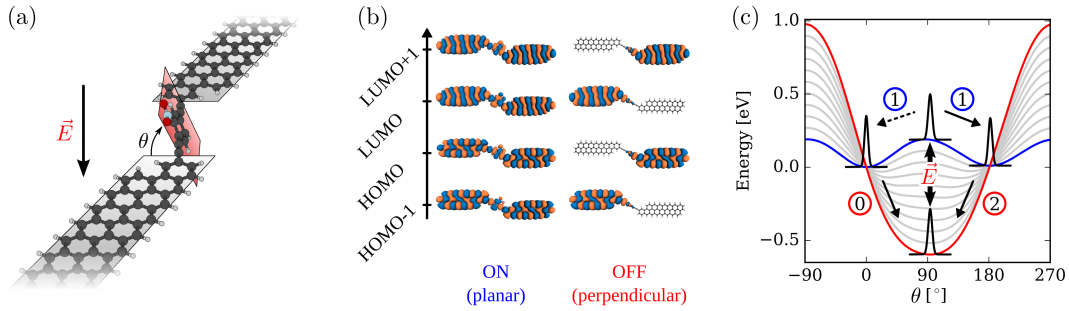

Figure 4.4: (a) Cartoon of the OPE-GNR nanojunction. The application of an external static electric field $\vec{E}$ causes a rotation of the central nitrophenyl group, and thus, switches the junction from a conductive (ON, $\Theta = 0°$) to a less conductive conformation (OFF, $\Theta = 90°$). The rotation causes a breakdown of the delocalized π-system. (b) The frontier molecular orbitals for the two logical states. (c) The potential energy curve as a function of the dihedral angle Θ with (grey and red curves) and without external electric field (blue curve) and a sketch of the proposed switching cycle. These depictions are adapted from Papers C1.

results are available as a reference.[63] The investigation showed that the numerical error minimization reliably leads to a unique minimum, and that the BOBS ansatz only negligibly alters the electron flow. Thus, the latter still agrees very well with the non-Born-Oppenheimer results. The electronic flux density (cf. Fig. 4.3b), although it is too localized and circles around the nuclei, agrees qualitatively with the non-Born-Oppenheimer results and captures the main features, i.e., the correct symmetry properties and nodal planes, at all times. In summary, the BOBS ansatz is a transparent, generally applicable formalism which yields semi-quantitative and validatable results. Moreover, the numerical procedure behind this approach is robust and simple. This lays the foundation for future detailed mechanistic investigations on a variety of chemical reactions, such as Diels-Alder reactions or pericyclic reactions.

The last part of the dissertation focused on electron dynamics through a single-molecule-graphene-nanoribbon junction driven by a potential bias. Our selected nanojunction is sketched in Fig. 4.4a and consists of nitro-substituted oligo-(phenylene ethynylene) covalently bound to graphene nanoribbon leads (OPE-GNR). It was proposed and first studied by Agapito and Cheng.[134] They applied the NEGF formalism and found two distinct conformers or logical states that differ significantly in their conductivity: one planar conducting (ON, $\Theta = 0°$) and one perpendicular less conducting conformer (OFF, $\Theta = 90°$). As visualized in Fig. 4.4b, the rotation of the central nitrophenyl group about the triple bound breaks the conjugation of the delocalized π-system and leads to a drastic decrease in the conductivity of the graphene wire. In **Paper C1**, we aimed at describing the dynamical switching of this system using dissipative quantum dynamics. First, we optimized both logical states and modeled the full reaction path between the two conducting conformers ON and ON' ($\Theta = 180°$) using a nudged elastic band calculation. These simulations and a normal mode analysis unambiguously identified the OFF conformer as transition state as can be seen from the blue curve in Fig. 4.4c. Fortunately,

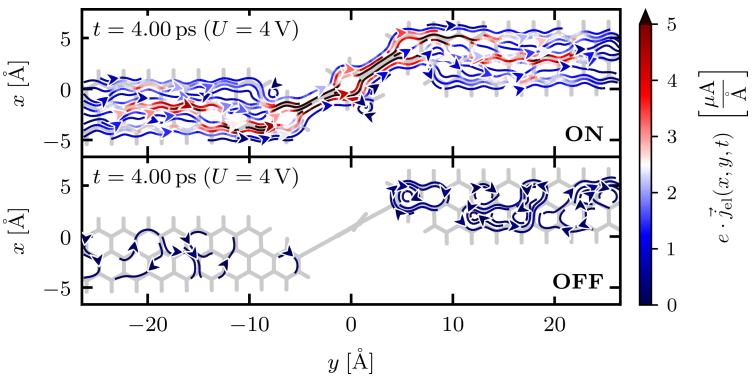

Figure 4.5: Streamline plot of the electronic current density through the OPE-GNR nanojunction (see Fig. 4.4a) at a bias voltage of $U = 4\,\mathrm{V}$ for both of its logical states: ON ($\Theta = 0°$, upper panel) and OFF ($\Theta = 90°$, lower panel). The current density is integrated over the z-coordinate and color coded according to its magnitude. All values smaller than $0.05\,\mu\mathrm{A/\AA}$ are neglected. These depictions are adapted from Papers C2.

we discovered that the dipole moment of the central nitrophenyl group can be used to access this energetically unfavored conformer by applying a static external electric field in top-gate position, in the spirit of a traditional field effect transistor. Based on these findings, we parameterized a microscopic model Hamiltonian for the quasi-one-dimensional reaction path coupled to the bath of lead phonons from first principles using DFT. In the subsequent part of **Paper C1**, the full switching cycle was simulated. As soon as the electric field is turned on (see red curve in Fig. 4.4c), the OFF conformer becomes the energetically favored structure. This initiates a nuclear dynamics that is dominated by three characteristic time regimes: a coherent, a delocalization, and a vibrational–relaxation regime. In the first regime, the oligomer unit oscillates harmonically between ON and ON', before the wave packet spreads out over a wide angular range in the delocalization regime. In the last regime, the highly rotationally excited wave packet relaxes to its equilibrium geometry — the OFF conformer. If now the field is again turned off, the system relaxes back to a conducting conformer following the same mechanism. Analysis of the individual relaxation channels showed that the energy is mainly dissipated to only a few transversal acoustic phonons of the graphene nanoribbon frame. Since the dynamics proceeds without any memory effects, the device and thus the conductivity can be reliably switched from one logical state to the other in the nanosecond time regime. To reduce this time scale, one could either decrease or increase the size of the central unit. While the former reduces the moment of inertia and allows for a faster relaxation, the latter increases the bulkyness of the central group and reduces its mobility.

In **Paper C2**, we investigated the spatially resolved electron transport through the OPE-GNR nanojunction driven by a chemical potential. The starting point for this study was the driven Liouville-von Neumann (DLvN) formalism for time-dependent electronic transport calculations. Supplemented by a novel molecular orbital localization scheme based on standard DFT calculations, we were able to

simulate the electron dynamics for both logical states under the influence of a time-dependent linear bias voltage ramp. Although both conformers have the same energy spectrum, only the ON conformer possesses conductive channels from one lead to the other. Thus, as the bias voltage increases, these channels are sequentially populated leading to steps in the current-voltage characteristic. In contrast, the OFF conformer remains non-conductive, i.e., the current-voltage characteristic hardly shows any observable increase. The results agree qualitatively with reference NEGF calculations. In order to converge our time-dependent results to this reference (The DLvN formalism is an approximation to the NEGF theory.[144]), we parameterized a tight-binding Hamiltonian from our DFT results and extended the finite contacts by additional lead units. For the subsequent detailed mechanistic study of the electron dynamics associated with this transport process, we exploited the transparency of the DLvN approach and used the directly accessible density matrix to compute the electronic flux density. In general, the electron dynamics proceeds through the π-system mainly along the bonds. While for the OFF conformer (see lower panel in Fig. 4.5), the electronic motion is undirected and no flux density passes the central unit, for the ON conformer (see upper panel in Fig. 4.5), the electrons flow directed from one side of the junction to the other. Consider now only the latter, conducting case. The electronic flux density is, as expected, largest at the bottleneck of the nanojunction, i.e., on the triple bonds connecting the leads with nitrophenyl group. Interestingly, due to a non-zero angle between the overall electron transport direction and the direction prescribed by the central unit, the electronic flux density is reflected at the edges of the GNR leads. This forces the flux density to follow a wide meandering path along the leads. Potentially, this finding could be exploited to enhance the conductance properties of this device by bringing both transport axes into coincidence.

To draw a conclusion, during my doctoral studies, I co-developed a robust and versatile set of tools to analyze and visualize electrons in motion. The application of this framework has proven to be very useful for the qualitative and quantitative understanding of a wide range of processes. Particularly noteworthy is the electronic flux density because the study of this quantity potentially opens up the opportunity to facilitate the understanding of chemical reactions or to enhance the properties of molecular electronic components.

Bibliography

[1] P. Y. Bruice, *Organic Chemistry*, 4th ed. (Pearson/Prentice Hall, Upper Saddle River, 2004) (cit. on p. 1).

[2] K. P. C. Vollhardt and N. E. Schore, *Organic Chemistry : Structure and Function*, 5th ed. (W.H. Freeman, New York, 2007) (cit. on p. 1).

[3] J. Clayden, N. Greeves, S. Warren, and P. Wothers, *Organic Chemistry*, 2nd ed. (Oxford University Press, Oxford, New York, 2012) (cit. on p. 1).

[4] M. B. Smith and J. March, *March's Advanced Organic Chemistry: Reactions, Mechanisms, and Structure*, 7th ed. (Wiley, Hoboken, 2013) (cit. on p. 1).

[5] B. Friedrich and D. Herschbach, "Alignment and Trapping of Molecules in Intense Laser Fields", Phys. Rev. Lett. **74**, 4623–4626 (1995) (cit. on p. 1).

[6] H. Stapelfeldt and T. Seideman, "Colloquium: Aligning Molecules with Strong Laser Pulses", Rev. Mod. Phys. **75**, 543–557 (2003) (cit. on p. 1).

[7] M. Leibscher, I. S. Averbukh, and H. Rabitz, "Molecular Alignment by Trains of Short Laser Pulses", Phys. Rev. Lett. **90**, 213001 (2003) (cit. on p. 1).

[8] R. d. Nalda, E. Heesel, M. Lein, N. Hay, R. Velotta, E. Springate, M. Castillejo, and J. P. Marangos, "Role of Orbital Symmetry in High-Order Harmonic Generation from Aligned Molecules", Phys. Rev. A **69**, 031804 (2004) (cit. on p. 1).

[9] S. Fleischer, I. S. Averbukh, and Y. Prior, "Selective Alignment of Molecular Spin Isomers", Phys. Rev. Lett. **99**, 093002 (2007) (cit. on p. 1).

[10] K. Oda, M. Hita, S. Minemoto, and H. Sakai, "All-Optical Molecular Orientation", Phys. Rev. Lett. **104**, 213901 (2010) (cit. on p. 1).

[11] T. Grohmann and M. Leibscher, "Nuclear Spin Selective Alignment of Ethylene and Analogues", J. Chem. Phys. **134**, 204316 (2011) (cit. on p. 1).

[12] A. Schild, D. Choudhary, V. D. Sambre, and B. Paulus, "Electron Density Dynamics in the Electronic Ground State: Motion Along the Kekulé Mode of Benzene", J. Phys. Chem. A **116**, 11355–11360 (2012) (cit. on p. 1).

[13] I. S. Ulusoy and M. Nest, "Correlated Electron Dynamics: How Aromaticity Can Be Controlled", J. Am. Chem. Soc. **133**, 20230–20236 (2011) (cit. on pp. 1–3, 147, 148).

[14] K. Ueda, "To Catch and Smash Charge on the Hop", Science **350**, 740–741 (2015) (cit. on p. 1).

[15] H.-C. Hege, J. Manz, F. Marquardt, B. Paulus, and A. Schild, "Electron Flux during Pericyclic Reactions in the Tunneling Limit: Quantum Simulation for Cyclooctatetraene", Chem. Phys. **376**, 46–55 (2010) (cit. on p. 2).

[16] D. Andrae, I. Barth, T. Bredtmann, H.-C. Hege, J. Manz, F. Marquardt, and B. Paulus, "Electronic Quantum Fluxes during Pericyclic Reactions Exemplified for the Cope Rearrangement of Semibullvalene", J. Phys. Chem. B **115**, 5476–5483 (2011) (cit. on p. 2).

[17] T. Bredtmann and J. Manz, "Electronic Bond-To-Bond Fluxes in Pericyclic Reactions: Synchronous or Asynchronous?", Angew. Chem. Int. Ed. **50**, 12652–12654 (2011) (cit. on p. 2).

[18] T. Bredtmann, D. J. Diestler, S.-D. Li, J. Manz, J. F. Pérez-Torres, W.-J. Tian, Y.-B. Wu, Y. Yang, and H.-J. Zhai, "Quantum Theory of Concerted Electronic and Nuclear Fluxes Associated with Adiabatic Intramolecular Processes", Phys. Chem. Chem. Phys. **17**, 29421–29464 (2015) (cit. on pp. 2–4, 32, 147).

[19] H. Eyring, J. Walter, and G. E. Kimball, in *Quantum Chemistry* (John Wiley & Sons, New York, 1944) Chap. 11 (cit. on p. 2).

[20] R. Weinkauf, P. Schanen, D. Yang, S. Soukara, and E. W. Schlag, "Elementary Processes in Peptides: Electron Mobility and Dissociation in Peptide Cations in the Gas Phase", J. Phys. Chem. **99**, 11255–11265 (1995) (cit. on p. 2).

[21] R. Weinkauf, P. Schanen, A. Metsala, E. W. Schlag, M. Bürgle, and H. Kessler, "Highly Efficient Charge Transfer in Peptide Cations in the Gas Phase: Threshold Effects and Mechanism", J. Phys. Chem. **100**, 18567–18585 (1996) (cit. on p. 2).

[22] R. Weinkauf, E. W. Schlag, T. J. Martinez, and R. D. Levine, "Nonstationary Electronic States and Site-Selective Reactivity", J. Phys. Chem. A **101**, 7702–7710 (1997) (cit. on p. 2).

[23] E. W. Schlag, H. L. Selzle, P. Schanen, R. Weinkauf, and R. D. Levine, "Dissociation Kinetics of Peptide Ions", J. Phys. Chem. A **110**, 8497–8500 (2006) (cit. on p. 2).

[24] F. Remacle, R. Levine, and M. Ratner, "Charge Directed Reactivity: a Simple Electronic Model, Exhibiting Site Selectivity, for the Dissociation of Ions", Chem. Phys. Lett. **285**, 25–33 (1998) (cit. on p. 2).

[25] F. Remacle and R. D. Levine, "An Electronic Time Scale in Chemistry", Proc. Natl. Acad. Sci. U. S. A. **103**, 6793–6798 (2006) (cit. on p. 2).

[26] B. Mignolet, R. D. Levine, and F. Remacle, "Charge Migration in the Bifunctional PENNA Cation Induced and Probed by Ultrafast Ionization: a Dynamical Study", J. Phys. B: At. Mol. Opt. Phys. **47**, 124011 (2014) (cit. on p. 2).

[27] L. S. Cederbaum and J. Zobeley, "Ultrafast Charge Migration by Electron Correlation", Chem. Phys. Lett. **307**, 205–210 (1999) (cit. on p. 2).

[28] J. Breidbach and L. S. Cederbaum, "Migration of Holes: Formalism, Mechanisms, and Illustrative Applications", J. Chem. Phys. **118**, 3983–3996 (2003) (cit. on p. 2).

[29] H. Hennig, J. Breidbach, and L. S. Cederbaum, "Electron Correlation as the Driving Force for Charge Transfer: Charge Migration Following Ionization in *N*-Methyl Acetamide", J. Phys. Chem. A **109**, 409–414 (2005) (cit. on p. 2).

[30] S. Lünnemann, A. I. Kuleff, and L. S. Cederbaum, "Ultrafast Charge Migration in 2-Phenylethyl-*N*,*N*-Dimethylamine", Chem. Phys. Lett. **450**, 232–235 (2008) (cit. on p. 2).

[31] A. I. Kuleff, S. Lünnemann, and L. S. Cederbaum, "Electron-Correlation-Driven Charge Migration in Oligopeptides", Chem. Phys. **414**, 100–105 (2013) (cit. on p. 2).

[32] A. I. Kuleff and L. S. Cederbaum, "Ultrafast Correlation-Driven Electron Dynamics", J. Phys. B: At., Mol. Opt. Phys. **47**, 124002 (2014) (cit. on p. 2).

[33] A. I. Kuleff, N. V. Kryzhevoi, M. Pernpointner, and L. S. Cederbaum, "Core Ionization Initiates Subfemtosecond Charge Migration in the Valence Shell of Molecules", Phys. Rev. Lett. **117**, 093002 (2016) (cit. on p. 2).

[34] G. L. Yudin, S. Chelkowski, J. Itatani, A. D. Bandrauk, and P. B. Corkum, "Attosecond Photoionization of Coherently Coupled Electronic States", Phys. Rev. A **72**, 051401 (2005) (cit. on p. 2).

[35] A. D. Bandrauk, S. Chelkowski, P. B. Corkum, J. Manz, and G. L. Yudin, "Attosecond Photoionization of a Coherent Superposition of Bound and Dissociative Molecular States: Effect of Nuclear Motion", J. Phys. B: At. Mol. Opt. Phys. **42**, 134001 (2009) (cit. on p. 2).

[36] M. N. Daud, H. Lu, S. Chelkowski, and A. D. Bandrauk, "Quantum Control of Electron-Proton Symmetry Breaking in Dissociative Ionization of H_2 by Intense Laser Pulses", Int. J. Quantum Chem. **115**, 369–380 (2014) (cit. on p. 2).

[37] M. Kanno, H. Kono, and Y. Fujimura, "Control of π-Electron Rotation in Chiral Aromatic Molecules by Nonhelical Laser Pulses", Angew. Chem. Int. Ed. **45**, 7995–7998 (2006) (cit. on p. 2).

[38] H. Mineo, S. H. Lin, and Y. Fujimura, "Coherent π-Electron Dynamics of (P)-$2,2'$-Biphenol Induced by Ultrashort Linearly Polarized UV Pulses: Angular Momentum and Ring Current", J. Chem. Phys. **138**, 074304 (2013) (cit. on p. 2).

[39] H. Mineo, S. Lin, and Y. Fujimura, "Vibrational Effects on UV/Vis Laser-Driven π-Electron Ring Currents in Aromatic Ring Molecules", Chem. Phys. **442**, 103–110 (2014) (cit. on p. 2).

[40] I. Barth and J. Manz, "Periodic Electron Circulation Induced by Circularly Polarized Laser Pulses: Quantum Model Simulations for Mg Porphyrin", Angew. Chem. Int. Ed. **45**, 2962–2965 (2006) (cit. on p. 2).

[41] M. F. Kling, P. von den Hoff, I. Znakovskaya, and R. de Vivie-Riedle, "(Sub-)femtosecond Control of Molecular Reactions via Tailoring the Electric Field of Light", Phys. Chem. Chem. Phys. **15**, 9448 (2013) (cit. on p. 2).

[42] F. Calegari, D. Ayuso, A. Trabattoni, L. Belshaw, S. D. Camillis, S. Anumula, F. Frassetto, L. Poletto, A. Palacios, P. Decleva, J. B. Greenwood, F. Martin, and M. Nisoli, "Ultrafast Electron Dynamics in Phenylalanine Initiated by Attosecond Pulses", Science **346**, 336–339 (2014) (cit. on p. 2).

[43] V. Despré, A. Marciniak, V. Loriot, M. C. E. Galbraith, A. Rouzée, M. J. J. Vrakking, F. Lépine, and A. I. Kuleff, "Attosecond Hole Migration in Benzene Molecules Surviving Nuclear Motion", J. Phys. Chem. Lett. **6**, 426–431 (2015) (cit. on p. 2).

[44] N. V. Golubev and A. I. Kuleff, "Control of Charge Migration in Molecules by Ultrashort Laser Pulses", Phys. Rev. A **91**, 051401 (2015) (cit. on p. 2).

[45] M. Hentschel, R. Kienberger, C. Spielmann, G. A. Reider, N. Milosevic, T. Brabec, P. Corkum, U. Heinzmann, M. Drescher, and F. Krausz, "Attosecond Metrology", Nature **414**, 509–513 (2001) (cit. on p. 2).

[46] R. Kienberger, M. Hentschel, M. Uibracker, C. Spielmann, M. Kitzler, A. Scrinzi, M. Wieland, T. Westerwalbesloh, U. Kleineberg, U. Heinzmann, M. Drescher, and F. Krausz, "Steering Attosecond Electron Wave Packets with Light", Science **297**, 1144–1148 (2002) (cit. on p. 2).

[47] M. Drescher, M. Hentschel, R. Kienberger, M. Uiberacker, V. Yakovlev, A. Scrinzi, T. Westerwalbesloh, U. Kleineberg, U. Heinzmann, and F. Krausz, "Time-Resolved Atomic Inner-Shell Spectroscopy", Nature **419**, 803–807 (2002) (cit. on p. 2).

[48] P. H. Bucksbaum, "Attophysics: Ultrafast Control", Nature **421**, 593–594 (2003) (cit. on p. 2).

[49] G. G. Paulus, F. Lindner, H. Walther, A. Baltuška, E. Goulielmakis, M. Lezius, and F. Krausz, "Measurement of the Phase of Few-Cycle Laser Pulses", Phys. Rev. Lett. **91**, 253004 (2003) (cit. on p. 2).

[50] J. Itatani, J. Levesque, D. Zeidler, H. Niikura, H. Pépin, J. C. Kieffer, P. B. Corkum, and D. M. Villeneuve, "Tomographic Imaging of Molecular Orbitals", Nature **432**, 867–871 (2004) (cit. on p. 2).

[51] A. Föhlisch, P. Feulner, F. Hennies, A. Fink, D. Menzel, D. Sanchez-Portal, P. M. Echenique, and W. Wurth, "Direct Observation of Electron Dynamics in the Attosecond Domain", Nature **436**, 373–376 (2005) (cit. on p. 2).

[52] M. F. Kling, C. Siedschlag, A. J. Verhoef, J. I. Khan, M. Schultze, T. Uphues, Y. Ni, M. Uiberacker, M. Drescher, F. Krausz, and M. J. J. Vrakking, "Control of Electron Localization in Molecular Dissociation", Science **312**, 246–248 (2006) (cit. on p. 2).

[53] P. B. Corkum and F. Krausz, "Attosecond Science", Nat. Phys. **3**, 381–387 (2007) (cit. on p. 2).

[54] F. Krausz and M. Ivanov, "Attosecond Physics", Rev. Mod. Phys. **81**, 163–234 (2009) (cit. on p. 2).

[55] H. J. Wörner, J. B. Bertrand, D. V. Kartashov, P. B. Corkum, and D. M. Villeneuve, "Following a Chemical Reaction Using High-Harmonic Interferometry", Nature **466**, 604–607 (2010) (cit. on p. 2).

[56] P. M. Kraus, B. Mignolet, D. Baykusheva, A. Rupenyan, L. Hórny, E. F. Penka, G. Grassi, O. I. Tolstikhin, J. Schneider, F. Jensen, L. B. Madsen, A. D. Bandrauk, F. Remacle, and H. J. Wörner, "Measurement and Laser Control of Attosecond Charge Migration in Ionized Iodoacetylene", Science **350**, 790–795 (2015) (cit. on p. 2).

[57] S. Pirhadi, J. Sunseri, and D. R. Koes, "Open Source Molecular Modeling", J. Mol. Graph. Model. **69**, 127–143 (2016) (cit. on p. 3).

[58] G. Paramonov, "Ionization and Dissociation of Simple Molecular Ions in Intense Infrared Laser Fields: Quantum Dynamical Simulations for Three-Dimensional Models of HD^+ and H_2^+", Chem. Phys. Lett. **411**, 350–356 (2005) (cit. on p. 4).

[59] H. Kono, Y. Sato, M. Kanno, K. Nakai, and T. Kato, "Theoretical Investigations of the Electronic and Nuclear Dynamics of Molecules in Intense Laser Fields: Quantum Mechanical Wave Packet Approaches", Bull. Chem. Soc. Jpn. **79**, 196–227 (2006) (cit. on p. 4).

[60] J. P. Karr and L Hilico, "High Accuracy Results for the Energy Levels of the Molecular Ions H_2^+, D_2^+ and HD^+, up to $J = 2$", J. Phys. B **39**, 2095–2105 (2006) (cit. on p. 4).

[61] T. Niederhausen, U. Thumm, and F. Martín, "Laser-Controlled Vibrational Heating and Cooling of Oriented H_2^+ Molecules", J. Phys. B **45**, 105602 (2012) (cit. on p. 4).

[62] A. Ishikawa, H. Nakashima, and H. Nakatsuji, "Accurate Solutions of the Schrödinger and Dirac Equations of HD^+, and HT^+: With and without Born-Oppenheimer Approximation and under Magnetic Field", Chem. Phys. **401**, 62–72 (2012) (cit. on p. 4).

[63] J. F. Pérez-Torres, "Electronic Flux Densities in Vibrating H_2^+ in Terms of Vibronic Eigenstates", Phys. Rev. A **87**, 062512 (2013) (cit. on pp. 4, 153).

[64] B. Chen and J. B. Anderson, "Improved Quantum Monte Carlo Calculation of the Ground-State Energy of the Hydrogen Molecule", J. Chem. Phys. **102**, 2802–2805 (1995) (cit. on p. 4).

[65] S. Bubin, F. Leonarski, M. Stanke, and L. Adamowicz, "Non-Adiabatic Corrections to the Energies of the Pure Vibrational States of", Chem. Phys. Lett. **477**, 12–16 (2009) (cit. on p. 4).

[66] K. Pachucki and J. Komasa, "Schrödinger Equation Solved for the Hydrogen Molecule with Unprecedented Accuracy", J. Chem. Phys. **144**, 164306 (2016) (cit. on p. 4).

[67] K. Jones, M. Formanek, and L. Adamowicz, "Non-Born-Oppenheimer Calculations of the Rovibrational Spectrum of H2 Excited to the Second Rotational Level", Chem. Phys. Lett. **669**, 188–191 (2017) (cit. on p. 4).

[68] E. Mátyus, J. Hutter, U. Müller-Herold, and M. Reiher, "Extracting Elements of Molecular Structure from the All-Particle Wave Function", J. Chem. Phys. **135**, 204302 (2011) (cit. on p. 4).

[69] E. Mátyus and M. Reiher, "Molecular Structure Calculations: A Unified Quantum Mechanical Description of Electrons and Nuclei Using Explicitly Correlated Gaussian Functions and the Global Vector Representation", J. Chem. Phys. **137**, 024104 (2012) (cit. on p. 4).

[70] D. J. Diestler, "Coupled-Channels Quantum Theory of Electronic Flux Density in Electronically Adiabatic Processes: Fundamentals", J. Phys. Chem. A **116**, 2728–2735 (2012) (cit. on pp. 4, 32).

[71] D. J. Diestler, A. Kenfack, J. Manz, and B. Paulus, "Coupled-Channels Quantum Theory of Electronic Flux Density in Electronically Adiabatic Processes: Application to the Hydrogen Molecule Ion", J. Phys. Chem. A **116**, 2736–2742 (2012) (cit. on pp. 4, 32).

[72] D. J. Diestler, A. Kenfack, J. Manz, B. Paulus, J. F. Pérez-Torres, and V. Pohl, "Computation of the Electronic Flux Density in the Born-Oppenheimer Approximation", J. Phys. Chem. A **117**, 8519–8527 (2013) (cit. on pp. 4, 32).

[73] D. J. Diestler, "Quasi-Classical Theory of Electronic Flux Density in Electronically Adiabatic Molecular Processes", J. Phys. Chem. A **116**, 11161–11166 (2012) (cit. on pp. 4, 32).

[74] M. Okuyama and K. Takatsuka, "Electron Flux in Molecules Induced by Nuclear Motion", Chem. Phys. Lett. **476**, 109–115 (2009) (cit. on pp. 4, 32, 152).

[75] L. A. Nafie, "Adiabatic Molecular Properties beyond the Born-Oppenheimer Approximation. Complete Adiabatic Wave Functions and Vibrationally Induced Electronic Current Density", J. Chem. Phys. **79**, 4950–4957 (1983) (cit. on pp. 4, 32).

[76] S. Patchkovskii, "Electronic Currents and Born-Oppenheimer Molecular Dynamics", J. Chem. Phys. **137**, 084109 (2012) (cit. on pp. 4, 32).

[77] D. J. Diestler, "Beyond the Born-Oppenheimer Approximation: A Treatment of Electronic Flux Density in Electronically Adiabatic Molecular Processes", J. Phys. Chem. A **117**, 4698–4708 (2013) (cit. on pp. 4, 32, 152).

[78] A. Schild, F. Agostini, and E. K. U. Gross, "Electronic Flux Density beyond the Born-Oppenheimer Approximation", J. Phys. Chem. A **120**, 3316–3325 (2016) (cit. on pp. 4, 32).

[79] M. Ratner, "A Brief History of Molecular Electronics", Nat. Nanotechnol. **8**, 378–381 (2013) (cit. on p. 4).

[80] L. Sun, Y. A. Diaz-Fernandez, T. A. Gschneidtner, F. Westerlund, S. Lara-Avila, and K. Moth-Poulsen, "Single-Molecule Electronics: from Chemical Design to Functional Devices", Chem. Soc. Rev. **43**, 7378–7411 (2014) (cit. on p. 4).

[81] D. Xiang, X. Wang, C. Jia, T. Lee, and X. Guo, "Molecular-Scale Electronics: From Concept to Function", Chem. Rev. **116**, 4318–4440 (2016) (cit. on p. 4).

[82] D. K. James and J. M. Tour, "Molecular Wires", in *Molecular Wires and Electronics* (Springer Science + Business Media, 2005), pp. 33–62 (cit. on p. 5).

[83] L. D. A. Siebbeles and F. C. Grozema, eds., *Charge and Exciton Transport through Molecular Wires* (Wiley-VCH Verlag GmbH & Co. KGaA, 2011) (cit. on p. 5).

[84] A. Aviram and M. A. Ratner, "Molecular Rectifiers", Chem. Phys. Lett. **29**, 277–283 (1974) (cit. on p. 5).

[85] C. Joachim, J. K. Gimzewski, and A. Aviram, "Electronics Using Hybrid-Molecular and Mono-Molecular Devices", Nature **408**, 541–548 (2000) (cit. on p. 5).

[86] P. Kornilovitch, A. Bratkovsky, and R. S. Williams, "Current Rectification by Molecules with Asymmetric Tunneling Barriers", Phys. Rev. B **66**, 165436 (2002) (cit. on p. 5).

[87] R. Liu, S.-H. Ke, W. Yang, and H. U. Baranger, "Organometallic Molecular Rectification", J. Chem. Phys. **124**, 024718 (2006) (cit. on p. 5).

[88] I. Díez-Pérez, J. Hihath, Y. Lee, L. Yu, L. Adamska, M. A. Kozhushner, I. I. Oleynik, and N. Tao, "Rectification and Stability of a Single Molecular Diode with Controlled Orientation", Nat. Chem. **1**, 635–641 (2009) (cit. on p. 5).

[89] C. A. Nijhuis, W. F. Reus, and G. M. Whitesides, "Mechanism of Rectification in Tunneling Junctions Based on Molecules with Asymmetric Potential Drops", J. Am. Chem. Soc. **132**, 18386–18401 (2010) (cit. on p. 5).

[90] S. K. Yee, J. Sun, P. Darancet, T. D. Tilley, A. Majumdar, J. B. Neaton, and R. A. Segalman, "Inverse Rectification in Donor-Acceptor Molecular Heterojunctions", ACS Nano **5**, 9256–9263 (2011) (cit. on p. 5).

[91] J. Hihath, C. Bruot, H. Nakamura, Y. Asai, I. Díez-Pérez, Y. Lee, L. Yu, and N. Tao, "Inelastic Transport and Low-Bias Rectification in a Single-Molecule Diode", ACS Nano **5**, 8331–8339 (2011) (cit. on p. 5).

[92] K. Wang, J. Zhou, J. M. Hamill, and B. Xu, "Measurement and Understanding of Single-Molecule Break Junction Rectification Caused by Asymmetric Contacts", J. Chem. Phys. **141**, 054712 (2014) (cit. on p. 5).

[93] J. Trasobares, D. Vuillaume, D. Théron, and N. Clément, "A 17 GHz Molecular Rectifier", Nat. Comm. **7**, 12850 (2016) (cit. on p. 5).

[94] K. Wang and B. Xu, "Modulation and Control of Charge Transport Through Single-Molecule Junctions", Top. Curr. Chem. **375**, 17 (2017) (cit. on p. 5).

[95] G. Reecht, F. Scheurer, V. Speisser, Y. J. Dappe, F. Mathevet, and G. Schull, "Electroluminescence of a Polythiophene Molecular Wire Suspended between a Metallic Surface and the Tip of a Scanning Tunneling Microscope", Phys. Rev. Lett. **112**, 047403 (2014) (cit. on p. 5).

[96] H. Yang, A. J. Mayne, G. Comtet, G. Dujardin, Y. Kuk, S. Nagarajan, and A. Gourdon, "Single-Molecule Light Emission at Room Temperature on a Wide-Band-Gap Semiconductor", Phys. Rev. B **90**, 125427 (2014) (cit. on p. 5).

[97] H. P. Goswami, W. Hua, Y. Zhang, S. Mukamel, and U. Harbola, "Electroluminescence in Molecular Junctions: A Diagrammatic Approach", J. Chem. Theory Comput. **11**, 4304–4315 (2015) (cit. on p. 5).

[98] K. Braun, X. Wang, A. M. Kern, H. Adler, H. Peisert, T. Chassé, D. Zhang, and A. J. Meixner, "Superluminescence from an Optically Pumped Molecular Tunneling Junction by Injection of Plasmon Induced Hot Electrons", Beilstein J. Nanotechnol. **6**, 1100–1106 (2015) (cit. on p. 5).

[99] D. Dulić, S. J. van der Molen, T. Kudernac, H. T. Jonkman, J. J. D. de Jong, T. N. Bowden, J. van Esch, B. L. Feringa, and B. J. van Wees, "One-Way Optoelectronic Switching of Photochromic Molecules on Gold", Phys. Rev. Lett. **91**, 207402–207405 (2003) (cit. on p. 5).

[100] R. Pati and S. P. Karna, "Current Switching by Conformational Change in a π-σ-π Molecular Wire", Phys. Rev. B **69**, 155419–155423 (2004) (cit. on p. 5).

[101] J. Li, G. Speyer, and O. F. Sankey, "Conduction Switching of Photochromic Molecules", Phys. Rev. Lett. **93**, 248302–248305 (2004) (cit. on p. 5).

[102] P. Mendes, A. Flood, and J. Stoddart, "Nanoelectronic Devices from Self-Organized Molecular Switches", Appl. Phys. A **80**, 1197–1209 (2005) (cit. on p. 5).

[103] B.-Y. Choi, S.-J. Kahng, S. Kim, H. Kim, H. W. Kim, Y. J. Song, J. Ihm, and Y. Kuk, "Conformational Molecular Switch of the Azobenzene Molecule: A Scanning Tunneling Microscopy Study", Phys. Rev. Lett. **96**, 156106–156109 (2006) (cit. on p. 5).

[104] M. del Valle, R. Gutiérrez, C. Tejedor, and G. Cuniberti, "Tuning the Conductance of a Molecular Switch", Nat. Nanotechnol. **2**, 176–179 (2007) (cit. on p. 5).

[105] P. Liljeroth, J. Repp, and G. Meyer, "Current-Induced Hydrogen Tautomerization and Conductance Switching of Naphthalocyanine Molecules", Science **317**, 1203–1206 (2007) (cit. on p. 5).

[106] J. Huang, Q. Li, H. Ren, H. Su, Q. W. Shi, and J. Yang, "Switching Mechanism of Photochromic Diarylethene Derivatives Molecular Junctions", J. Chem. Phys. **127**, 094705–094710 (2007) (cit. on p. 5).

[107] P. Zhao, C. feng Fang, C. juan Xia, D. sheng Liu, and S. jie Xie, "15, 16-Dinitrile DDP/CPD as a Possible Solid-State Optical Molecular Switch", Chem. Phys. Lett. **453**, 62–67 (2008) (cit. on p. 5).

[108] C. Benesch, M. F. Rode, M. Čížek, O. Rubio-Pons, M. Thoss, and A. L. Sobolewski, "Switching the Conductance of a Single Molecule by Photoinduced Hydrogen Transfer", J. Phys. Chem. C **113**, 10315–10318 (2009) (cit. on p. 5).

[109] S. Pan, Q. Fu, T. Huang, A. Zhao, B. Wang, Y. Luo, J. Yang, and J. Hou, "Design and Control of Electron Transport Properties of Single Molecules", Proc. Natl. Acad. Sci. U.S.A. **106**, 15259–15263 (2009) (cit. on p. 5).

[110] Y. Cai, A. Zhang, Y. P. Feng, and C. Zhang, "Switching and Rectification of a Single Light-Sensitive Diarylethene Molecule Sandwiched Between Graphene Nanoribbons", J. Chem. Phys. **135**, 184703–184708 (2011) (cit. on p. 5).

[111] D. Roldan, V. Kaliginedi, S. Cobo, V. Kolivoska, C. Bucher, W. Hong, G. Royal, and T. Wandlowski, "Charge Transport in Photoswitchable Dimethyldihydropyrene-Type Single-Molecule Junctions", J. Am. Chem. Soc. **135**, 5974–5977 (2013) (cit. on p. 5).

[112] B. K. Pathem, Y. B. Zheng, S. Morton, M. Å. Petersen, Y. Zhao, C.-H. Chung, Y. Yang, L. Jensen, M. B. Nielsen, and P. S. Weiss, "Photoreaction of Matrix-Isolated Dihydroazulene-Functionalized Molecules on Au{111}", Nano Lett. **13**, 337–343 (2013) (cit. on p. 5).

[113] Q.-H. Wu, P. Zhao, and D.-S. Liu, "Electronic Transport of a Molecular Photoswitch with Graphene Nanoribbon Electrodes", Chin. Phys. Lett. **31**, 057304–057307 (2014) (cit. on p. 5).

[114] F. Xie, Z.-Q. Fan, K. Liu, H.-Y. Wang, J.-H. Yu, and K.-Q. Chen, "Negative Differential Resistance and Stable Conductance Switching Behaviors of Salicylideneaniline Molecular Devices Sandwiched Between Armchair Graphene Nanoribbon Electrodes", Org. Electron. **27**, 41–45 (2015) (cit. on p. 5).

[115] W. Chen, R. Chen, B. Bian, X. ao Li, and L. Wang, "First-Principles Study of the Electronic Transport Properties of a Dihydroazulene-Based Molecular Optical Switch", Comput. Theor. Chem. **1067**, 114–118 (2015) (cit. on p. 5).

[116] T. Kumagai, "Direct Observation and Control of Hydrogen-Bond Dynamics Using Low-Temperature Scanning Tunneling Microscopy", Prog. Surf. Sci. **90**, 239–291 (2015) (cit. on p. 5).

[117] J. A. Rodríguez-Manzo, Z. J. Qi, A. Crook, J.-H. Ahn, A. T. C. Johnson, and M. Drndić, "*In Situ* Transmission Electron Microscopy Modulation of Transport in Graphene Nanoribbons", ACS Nano **10**, 4004–4010 (2016) (cit. on p. 5).

[118] C.-J. Xia, B.-Q. Zhang, Y.-H. Su, Z.-Y. Tu, and X.-A. Yan, "Electronic Transport Properties of a Single Chiroptical Molecular Switch with Graphene Nanoribbons Electrodes", Optik **127**, 4774–4777 (2016) (cit. on p. 5).

[119] T. Kumagai and L. Grill, "Direct Observation and Control of Single-Molecule Tautomerization by Low-Temperature Scanning Tunneling Microscopy", in *Tautomerism* (Wiley-Blackwell, 2016), pp. 147–174 (cit. on p. 5).

[120] N. Xin, J. Wang, C. Jia, Z. Liu, X. Zhang, C. Yu, M. Li, S. Wang, Y. Gong, H. Sun, G. Zhang, Z. Liu, G. Zhang, J. Liao, D. Zhang, and X. Guo, "Stereoelectronic Effect-Induced Conductance Switching in Aromatic Chain Single-Molecule Junctions", Nano Lett. **17**, 856–861 (2017) (cit. on p. 5).

[121] J. S. Seldenthuis, F. Prins, J. M. Thijssen, and H. S. J. van der Zant, "An All-Electric Single-Molecule Motor", ACS Nano **4**, 6681–6686 (2010) (cit. on p. 5).

[122] S. V. Aradhya and L. Venkataraman, "Single-Molecule Junctions beyond Electronic Transport", Nat. Nanotechnol. **8**, 399–410 (2013) (cit. on p. 5).

[123] H. Sadeghi, S. Sangtarash, and C. J. Lambert, "Oligoyne Molecular Junctions for Efficient Room Temperature Thermoelectric Power Generation", Nano Lett. **15**, 7467–7472 (2015) (cit. on p. 5).

[124] S. Sangtarash, C. Huang, H. Sadeghi, G. Sorohhov, J. Hauser, T. Wandlowski, W. Hong, S. Decurtins, S.-X. Liu, and C. J. Lambert, "Searching the Hearts of Graphene-Like Molecules for Simplicity, Sensitivity, and Logic", J. Am. Chem. Soc. **137**, 11425–11431 (2015) (cit. on p. 5).

[125] N. Fuentes, A. Martín-Lasanta, L. Á. de Cienfuegos, M. Ribagorda, A. Parra, and J. M. Cuerva, "Organic-Based Molecular Switches for Molecular Electronics", Nanoscale **3**, 4003–4014 (2011) (cit. on p. 5).

[126] B. K. Pathem, S. A. Claridge, Y. B. Zheng, and P. S. Weiss, "Molecular Switches and Motors on Surfaces", Annu. Rev. Phys. Chem. **64**, 605–630 (2013) (cit. on p. 5).

[127] M. L. Perrin, E. Burzurí, and H. S. J. van der Zant, "Single-Molecule Transistors", Chem. Soc. Rev. **44**, 902–919 (2015) (cit. on p. 5).

[128] J. L. Zhang, J. Q. Zhong, J. D. Lin, W. P. Hu, K. Wu, G. Q. Xu, A. T. S. Wee, and W. Chen, "Towards Single Molecule Switches", Chem. Soc. Rev. **44**, 2998–3022 (2015) (cit. on p. 5).

[129] C. Jia, A. Migliore, N. Xin, S. Huang, J. Wang, Q. Yang, S. Wang, H. Chen, D. Wang, B. Feng, Z. Liu, G. Zhang, D.-H. Qu, H. Tian, M. A. Ratner, H. Q. Xu, A. Nitzan, and X. Guo, "Covalently Bonded Single-Molecule Junctions with Stable and Reversible Photoswitched Conductivity", Science **352**, 1443–1445 (2016) (cit. on pp. 5, 6).

[130] K. Matsuda and M. Irie, "Diarylethene as a Photoswitching Unit", J. Photochem. Photobiol. C **5**, 169–182 (2004) (cit. on p. 5).

[131] C. Jia, B. Ma, N. Xin, and X. Guo, "Carbon Electrode-Molecule Junctions: A Reliable Platform for Molecular Electronics", Acc. Chem. Res. **48**, 2565–2575 (2015) (cit. on p. 5).

[132] F. Schwierz, "Graphene Transistors", Nat. Nanotechnol. **5**, 487–496 (2010) (cit. on p. 5).

[133] M. V. Fischetti, J. Kim, S. Narayanan, Z.-Y. Ong, C. Sachs, D. K. Ferry, and S. J. Aboud, "Pseudopotential-Based Studies of Electron Transport in Graphene and Graphene Nanoribbons", J. Phys.: Condens. Matter **25**, 473202–4732038 (2013) (cit. on p. 5).

[134] L. A. Agapito and H.-P. Cheng, "Ab Initio Calculation of a Graphene-Ribbon-Based Molecular Switch", J. Phys. Chem. C **111**, 14266–14273 (2007) (cit. on pp. 5, 153).

[135] Z. J. Donhauser, B. A. Mantooth, K. F. Kelly, L. A. Bumm, J. D. Monnell, J. J. Stapleton, D. W. Price, A. M. Rawlett, D. L. Allara, J. M. Tour, and P. S. Weiss, "Conductance Switching in Single Molecules Through Conformational Changes", Science **292**, 2303–2307 (2001) (cit. on p. 5).

[136] Z. J. Donhauser, B. A. Mantooth, T. P. Pearl, K. F. Kelly, S. U. Nanayakkara, and P. S. Weiss, "Matrix-Mediated Control of Stochastic Single Molecule Conductance Switching", Jpn. J. Appl. Phys. **41**, 4871–4877 (2002) (cit. on p. 5).

[137] G. K. Ramachandran, "A Bond-Fluctuation Mechanism for Stochastic Switching in Wired Molecules", Science **300**, 1413–1416 (2003) (cit. on p. 5).

[138] A. M. Moore, A. A. Dameron, B. A. Mantooth, R. K. Smith, D. J. Fuchs, J. W. Ciszek, F. Maya, Y. Yao, J. M. Tour, and P. S. Weiss, "Molecular Engineering and Measurements to Test Hypothesized Mechanisms in Single Molecule Conductance Switching", J. Am. Chem. Soc. **128**, 1959–1967 (2006) (cit. on p. 5).

[139] A. M. Moore, B. A. Mantooth, Z. J. Donhauser, Y. Yao, J. M. Tour, and P. S. Weiss, "Real-Time Measurements of Conductance Switching and Motion of Single Oligo(Phenylene Ethynylene) Molecules", J. Am. Chem. Soc. **129**, 10352–10353 (2007) (cit. on p. 5).

[140] C. D. Frisbie, "Designing a Robust Single-Molecule Switch", Science **352**, 1394–1395 (2016) (cit. on p. 6).

[141] C. G. Sánchez, M. Stamenova, S. Sanvito, D. R. Bowler, A. P. Horsfield, and T. N. Todorov, "Molecular Conduction: Do Time-Dependent Simulations Tell You More than the Landauer Approach?", J. Chem. Phys. **124**, 214708 (2006) (cit. on p. 6).

[142] J. E. Subotnik, T. Hansen, M. A. Ratner, and A. Nitzan, "Nonequilibrium Steady State Transport via the Reduced Density Matrix Operator", J. Chem. Phys. **130**, 144105 (2009) (cit. on p. 6).

[143] T. Zelovich, L. Kronik, and O. Hod, "State Representation Approach for Atomistic Time-Dependent Transport Calculations in Molecular Junctions", J. Chem. Theory Comput. **10**, 2927–2941 (2014) (cit. on pp. 6, 26, 27, 29).

[144] L. Chen, T. Hansen, and I. Franco, "Simple and Accurate Method for Time-Dependent Transport along Nanoscale Junctions", J. Phys. Chem. C **118**, 20009–20017 (2014) (cit. on pp. 6, 28, 155).

[145] T. Zelovich, L. Kronik, and O. Hod, "Molecule-Lead Coupling at Molecular Junctions: Relation between the Real- and State-Space Perspectives", J. Chem. Theory Comput. **11**, 4861–4869 (2015) (cit. on pp. 6, 27).

[146] O. Hod, C. A. Rodríguez-Rosario, T. Zelovich, and T. Frauenheim, "Driven Liouville Von Neumann Equation in Lindblad Form", J. Phys. Chem. A **120**, 3278–3285 (2016) (cit. on pp. 6, 27).

[147] T. Zelovich, L. Kronik, and O. Hod, "Driven Liouville Von Neumann Approach for Time-Dependent Electronic Transport Calculations in a Nonorthogonal Basis-Set Representation", J. Phys. Chem. C **120**, 15052–15062 (2016) (cit. on pp. 6, 27).

[148] T. Zelovich, T. Hansen, Z.-F. Liu, J. B. Neaton, L. Kronik, and O. Hod, "Parameter-Free Driven Liouville-Von Neumann Approach for Time-Dependent Electronic Transport Simulations in Open Quantum Systems", J. Chem. Phys. **146**, 092331 (2017) (cit. on pp. 6, 28).

[149] U. N. Morzan, F. F. Ramírez, M. C. G. Lebrero, and D. A. Scherlis, "Electron Transport in Real Time from First-Principles", J. Chem. Phys. **146**, 044110 (2017) (cit. on p. 6).

[150] A. Szabo and N. S. Ostlund, *Modern Quantum Chemistry* (Dover Publications, Mineola, 1996) (cit. on pp. 7, 10–12).

[151] D. Tannor, *Introduction to Quantum Mechanics: A Time-Dependent Perspective* (University Science Books, Sausalito, Calif, 2007) (cit. on pp. 7, 9).

[152] E. Schrödinger, "Quantisierung als Eigenwertproblem", Ann. Phys. (Leipzig) **81**, 109–139 (1926) (cit. on pp. 7, 32).

[153] F. Jensen, *Introduction to Computational Chemistry*, 3rd ed. (John Wiley & Sons, Chichester, Hoboken, 2017) (cit. on pp. 11–13, 16, 18).

[154] C. C. J. Roothaan, "New Developments in Molecular Orbital Theory", Rev. Mod. Phys. **23**, 69–89 (1951) (cit. on p. 12).

[155] G. G. Hall, "The Molecular Orbital Theory of Chemical Valency. VIII. A Method of Calculating Ionization Potentials", Proc. R. Soc. Lond. A **205**, 541–552 (1951) (cit. on p. 12).

[156] P. G. Szalay, T. Müller, G. Gidofalvi, H. Lischka, and R. Shepard, "Multiconfiguration Self-Consistent Field and Multireference Configuration Interaction Methods and Applications", Chem. Rev. **112**, 108–181 (2012) (cit. on p. 13).

[157] F. Neese, "Prediction of Molecular Properties and Molecular Spectroscopy with Density Functional Theory: From Fundamental Theory to Exchange-Coupling", Coordination Chemistry Reviews **253**, 526–563 (2009) (cit. on pp. 13, 15, 16, 18).

[158] P. Hohenberg and W. Kohn, "Inhomogeneous Electron Gas", Phys. Rev. **136**, B864–B871 (1964) (cit. on p. 14).

[159] W. Kohn and L. J. Sham, "Self-Consistent Equations Including Exchange and Correlation Effects", Phys. Rev. **140**, A1133–A1138 (1965) (cit. on p. 14).

[160] P. A. M. Dirac, "Note on Exchange Phenomena in the Thomas Atom", Math. Proc. Cambridge Philos. Soc. **26**, 376–385 (1930) (cit. on p. 15).

[161] J. C. Slater, "A Simplification of the Hartree-Fock Method", Phys. Rev. **81**, 385–390 (1951) (cit. on p. 15).

[162] S. H. Vosko, L. Wilk, and M. Nusair, "Accurate Spin-Dependent Electron Liquid Correlation Energies for Local Spin Density Calculations: a Critical Analysis", Can. J. Phys. **58**, 1200–1211 (1980) (cit. on p. 15).

[163] J. P. Perdew and Y. Wang, "Accurate and Simple Analytic Representation of the Electron-Gas Correlation Energy", Phys. Rev. B **45**, 13244–13249 (1992) (cit. on p. 15).

[164] T. Chachiyo, "Communication: Simple and Accurate Uniform Electron Gas Correlation Energy for the Full Range of Densities", J. Chem. Phys. **145**, 021101 (2016) (cit. on p. 15).

[165] D. M. Ceperley and B. J. Alder, "Ground State of the Electron Gas by a Stochastic Method", Phys. Rev. Lett. **45**, 566–569 (1980) (cit. on p. 15).

[166] J. P. Perdew, J. A. Chevary, S. H. Vosko, K. A. Jackson, M. R. Pederson, D. J. Singh, and C. Fiolhais, "Atoms, Molecules, Solids, and Surfaces: Applications of the Generalized Gradient Approximation for Exchange and Correlation", Phys. Rev. B **46**, 6671–6687 (1992) (cit. on p. 16).

[167] J. P. Perdew, K. Burke, and M. Ernzerhof, "Generalized Gradient Approximation Made Simple", Phys. Rev. Lett. **77**, 3865–3868 (1996) (cit. on p. 16).

[168] A. D. Becke, "A New Mixing of Hartree-Fock and Local Density-Functional Theories", J. Chem. Phys. **98**, 1372–1377 (1993) (cit. on p. 16).

[169] A. D. Becke, "Density-Functional Thermochemistry. III. The Role of Exact Exchange", J. Chem. Phys. **98**, 5648–5652 (1993) (cit. on p. 16).

[170] P. J. Stephens, F. J. Devlin, C. F. Chabalowski, and M. J. Frisch, "Ab Initio Calculation of Vibrational Absorption and Circular Dichroism Spectra Using Density Functional Force Fields", J. Phys. Chem. **98**, 11623–11627 (1994) (cit. on p. 16).

[171] C. Adamo and V. Barone, "Toward Reliable Density Functional Methods without Adjustable Parameters: The PBE0 Model", J. Chem. Phys. **110**, 6158–6170 (1999) (cit. on p. 16).

[172] C. Ullrich, *Time-Dependent Density-Functional Theory: Concepts and Applications*, 1st ed. (Oxford University Press, Oxford, New York, 2012) (cit. on pp. 16, 18).

[173] M. Marques and E. Gross, "Time-Dependent Density Functional Theory", Annu. Rev. Phys. Chem. **55**, 427–455 (2004) (cit. on pp. 16, 18).

[174] M. E. Casida, "Time-Dependent Density-Functional Theory for Molecules and Molecular Solids", J. Mol. Struct. (Theochem.) **914**, 3–18 (2009) (cit. on pp. 16, 18).

[175] E. Runge and E. K. U. Gross, "Density-Functional Theory for Time-Dependent Systems", Phys. Rev. Lett. **52**, 997–1000 (1984) (cit. on p. 16).

[176] R. van Leeuwen, "Mapping from Densities to Potentials in Time-Dependent Density-Functional Theory", Phys. Rev. Lett. **82**, 3863–3866 (1999) (cit. on p. 17).

[177] M. Ernzerhof, "Taylor-Series Expansion of Density Functionals", Phys. Rev. A **50**, 4593–4607 (1994) (cit. on p. 18).

[178] M. E. Casida, "Time-Dependent Density Functional Response Theory for Molecules", in *Recent Advances in Density Functional Methods* (WORLD SCIENTIFIC, 1995), pp. 155–192 (cit. on p. 19).

[179] S. Hirata and M. Head-Gordon, "Time-Dependent Density Functional Theory within the Tamm-Dancoff Approximation", Chem. Phys. Lett. **314**, 291–299 (1999) (cit. on p. 20).

[180] H.-P. Breuer and F. Petruccione, *The Theory of Open Quantum Systems* (Oxford University Press, Oxford, New York, 2002) (cit. on pp. 21, 22).

[181] G. Schaller, *Open Quantum Systems Far from Equilibrium*, Lecture Notes in Physics (Springer International Publishing, Cham, 2014) (cit. on pp. 21, 22).

[182] A. G. Redfield, "On the Theory of Relaxation Processes", IBM J. Res. Dev. **1**, 19–31 (1957) (cit. on p. 23).

[183] K. Blum, *Density Matrix Theory and Applications* (Plenum Press, New York, 1981) (cit. on p. 23).

[184] E. B. Davies, "Markovian Master Equations", Commun. Math. Phys. **39**, 91–110 (1974) (cit. on p. 23).

[185] R. Dümcke and H. Spohn, "The Proper Form of the Generator in the Weak Coupling Limit", Z. Phys. B **34**, 419–422 (1979) (cit. on p. 23).

[186] M. Paulsson, "Non Equilibrium Green's Functions for Dummies: Introduction to the One Particle NEGF Equations", arXiv preprint arXiv:cond-mat/0210519 (2002) (cit. on p. 29).

[187] L. E. F. Foà Torres, S. Roche, and L. Charlier, J.-C. Torres, *Introduction to Graphene-Based Nanomaterials: From Electronic Structure to Quantum Transport* (Cambridge University Press, New York, 2014) (cit. on p. 29).

[188] D. H. Lee and J. D. Joannopoulos, "Simple Scheme for Surface-Band Calculations. II. The Green's Function", Phys. Rev. B **23**, 4997–5004 (1981) (cit. on p. 29).

[189] M. P. L. Sancho, J. M. L. Sancho, and J Rubio, "Quick Iterative Scheme for the Calculation of Transfer Matrices: Application to Mo (100)", J. Phys. F **14**, 1205–1215 (1984) (cit. on p. 29).

[190] M. P. L. Sancho, J. M. L. Sancho, J. M. L. Sancho, and J Rubio, "Highly Convergent Schemes for the Calculation of Bulk and Surface Green Functions", J. Phys. F **15**, 851–858 (1985) (cit. on p. 29).

[191] M. B. Nardelli, "Electronic Transport in Extended Systems: Application to Carbon Nanotubes", Phys. Rev. B **60**, 7828–7833 (1999) (cit. on p. 29).

[192] M. B. Nardelli and J. Bernholc, "Mechanical Deformations and Coherent Transport in Carbon Nanotubes", Phys. Rev. B **60**, R16338–R16341 (1999) (cit. on p. 29).

[193] O. Hod, J. E. Peralta, and G. E. Scuseria, "First-Principles Electronic Transport Calculations in Finite Elongated Systems: A Divide and Conquer Approach", J. Chem. Phys. **125**, 114704 (2006) (cit. on p. 29).

[194] B. H. Bransden and C. J. Joachain, *Physics of Atoms and Molecules*, Pearson Education (Longman, 1983) (cit. on p. 33).

[195] J. M. Turney, A. C. Simmonett, R. M. Parrish, E. G. Hohenstein, F. A. Evangelista, J. T. Fermann, B. J. Mintz, L. A. Burns, J. J. Wilke, M. L. Abrams, N. J. Russ, M. L. Leininger, C. L. Janssen, E. T. Seidl, W. D. Allen, H. F. Schaefer, R. A. King, E. F. Valeev, C. D. Sherrill, and T. D. Crawford, "Psi4: an Open-Source Ab Initio Electronic Structure Program", WIREs Comput. Mol. Sci. **2**, 556 (2012) (cit. on p. 73).

[196] H.-J. Werner, P. J. Knowles, G. Knizia, F. R. Manby, M. Schütz, P. Celani, T. Korona, R. Lindh, A. Mitrushenkov, G. Rauhut, K. R. Shamasundar, T. B. Adler, R. D. Amos, A. Bernhardsson, A. Berning, D. L. Cooper, M. J. O. Deegan, A. J. Dobbyn, F. Eckert, E. Goll, C. Hampel, A. Hesselmann, G. Hetzer, T. Hrenar, G. Jansen, C. Köppl, Y. Liu, A. W. Lloyd, R. A. Mata, A. J. May, S. J. McNicholas, W. Meyer, M. E. Mura, A. Nicklass, D. P. O'Neill, P. Palmieri, D. Peng, K. Pflüger, R. Pitzer, M. Reiher, T. Shiozaki, H. Stoll, A. J. Stone, R. Tarroni, T. Thorsteinsson, and M. Wang, *MOLPRO, Version 2012.1, A Package of Ab Initio Programs*, see http://www.molpro.net (accessed Nov 20, 2016), 2012 (cit. on p. 73).

[197] *TURBOMOLE V6.5 2013, a Development of University of Karlsruhe and Forschungszentrum Karlsruhe GmbH, 1989-2007, TURBOMOLE GmbH, since 2007*, see http://www.turbomole.com (accessed Nov 20, 2016). (cit. on p. 89).

[198] M. W. Schmidt, K. K. Baldridge, J. A. Boatz, S. T. Elbert, M. S. Gordon, J. H. Jensen, S. Koseki, N. Matsunaga, K. A. Nguyen, S. Su, T. L. Windus, M. Dupuis, and J. A. Montgomery, "General Atomic and Molecular Electronic Structure System", J. Comput. Chem. **14**, 1347–1363 (1993) (cit. on p. 89).

[199] S. R. Bahn and K. W. Jacobsen, "An Object-Oriented Scripting Interface to a Legacy Electronic Structure Code", Comput. Sci. Eng. **4**, 56–66 (2002) (cit. on p. 129).

[200] A. H. Larsen, J. J. Mortensen, J. Blomqvist, I. E. Castelli, R. Christensen, M. Dułak, J. Friis, M. N. Groves, B. Hammer, C. Hargus, E. D. Hermes, P. C. Jennings, P. B. Jensen, J. Kermode, J. R. Kitchin, E. L. Kolsbjerg, J. Kubal, K. Kaasbjerg, S. Lysgaard, J. B. Maronsson, T. Maxson, T. Olsen, L. Pastewka, A. Peterson, C. Rostgaard, J. Schiøtz, O. Schütt, M. Strange, K. S. Thygesen, T. Vegge, L. Vilhelmsen, M. Walter, Z. Zeng, and K. W. Jacobsen, "The Atomic Simulation Environment - a Python Library for Working with Atoms", J. Phys. Condens. Matter **29**, 273002 (2017) (cit. on p. 129).

Danksagung

Am Ende dieser Dissertation möchte ich den Menschen von Herzen danken, die diese Arbeit mit ihrer Unterstützung erst ermöglicht haben.

Allen voran danke ich meinem Betreuer Jean Christophe Tremblay für die sehr intensive und angenehme Betreuung. Er zeigte großes Interesse für meine Forschung und ich konnte stets mit allen wissenschaftlichen Fragen und Problemen ein offenes Ohr bei ihm finden. Die anschließenden wissenschaftlichen Diskussionen waren sehr bereichernd und gaben meinen Projekten wichtige neue Impulse. Zudem gewährte er mir genügend Freiraum zur Entfaltung, was mir ermöglichte mein Thema zu lenken und selbstständig meinen Interessen entsprechend zu forschen.

Beate Paulus danke ich dafür, dass sie bereits während des Bachelorstudiums mein Interesse für die Theoretische Chemie geweckt hat und ich dieses dank ihrer Hilfe über die Studienjahre weiter entwickeln konnte. Außerdem hat sie mich seitdem fortwährend in vielen Belangen unterstützt. Sie hat mir ermöglicht Erfahrung in der Lehre zu sammeln, was mich in meiner persönlichen Entwicklung vorangebracht hat.

Jörn Manz möchte ich besonders dafür danken, dass er mich schon während meiner Bachelorarbeit mit seiner Begeisterungsfähigkeit für auch vermeintlich unscheinbarere Ergebnisse positiv geprägt hat. Weiterhin weckte er in mir die Freude an der wissenschaftlichen Visualisierung, was mir noch heute in meinem täglichen Schaffen zugutekommt.

Dennis J. Diestler and Jhon Fredy Pérez Torres, I would like to thank you for the numerous constructive discussions together with Jörn Manz and Jean Christophe Tremblay on electronic motion in general and the electronic flux density in particular. Since this was a main topic of doctoral studies, these discussions laid the foundation to the dissertation in its current form. I would also like to thank Jhon Fredy Pérez Torres for revealing to me the scientific pleasure on allegedly simple, small molecules during my master thesis.

Ein Projekt, das mir sehr am Herzen liegt, ist die Entwicklung des Programms ORBKIT, das ein zentraler Baustein dieser Arbeit darstellt. Dieses durfte ich zusammen mit Axel Schild und Gunter Her-

mann während meiner Tätigkeit als studentische Hilfskraft im Kooperationsprojekt mit dem Konrad-Zuse-Zentrum für Informationstechnik Berlin starten. Für die Finanzierung während der Initialisierung des Projekts danke ich Hans-Christian Hege und Beate Paulus. Großer Dank für die harmonische Zusammenarbeit in der Umsetzung des Projekts geht dabei natürlich an Axel Schild und Gunter Hermann, sowie in späteren Entwicklungsphasen an Lukas Eugen Marsoner Steinkasserer. Jean Christophe Tremblay danke ich dafür, dass er uns in diesem Vorhaben nicht nur voll unterstützt, sondern auch aktiv zu dessen Weiterentwicklung beigetragen hat.

Ich danke Gunter Hermann, Lukas Eugen Marsoner Steinkasserer, Johannes Horst Budau und Marcel Quennet für unzählige wissenschaftliche und nicht wissenschaftliche Diskussionen und das freundschaftliche Umfeld. Durch euch waren etwaige Enttäuschung über wissenschaftliche Rückschläge nur von kurzer Dauer, da ihr mich stets schnell wieder optimistisch stimmen konntet. Gunter Hermann möchte ich nochmals explizit dafür danken, dass er mir seit der Schulzeit immer zur Seite steht und wir unseren bisherigen Werdegang gemeinsam bestreiten konnten.

Den aktuellen und ehemaligen Mitgliedern der Arbeitsgruppen der Theoretischen Chemie (AG Tremblay, AG Paulus und AG Keller) spreche ich mein Dank für das sehr angenehme Arbeitsklima aus. Dem Elsa-Neumann-Stipendium des Landes Berlin und der Deutsche Forschungsgemeinschaft danke ich für die finanzielle Unterstützung während meiner Promotionszeit.

Ein besonderer Dank gilt Madlen Mattke, da sie mir immer zur Seite stand und mich in allen Belangen unterstützte. Sie hat mich fortwährend ermutigt und hatte bei etwaigen Misserfolgen stets aufbauende Worte parat.

Als letztes möchte ich meiner Familie und meinen Freunden für ihre ausdauernde Unterstützung und ihr Verständnis während der letzten Jahre einen großen Dank ausdrücken.

Danke!